AFRL-VA-WP-TR-2003-3010

CORROSION PIT TO CRACK TRANSITION

Delivery Order 0051: Task 2

Krishnan K. Sankaran
Gary E. Weaver

The Boeing Company
Mail Code S111-1041
P.O. Box 516
St. Louis, MO 63166-0516

DECEMBER 2002

Final Report for 15 May 2002 – 20 December 2002

Approved for public release; distribution is unlimited.

AIR VEHICLES DIRECTORATE
AIR FORCE RESEARCH LABORATORY
AIR FORCE MATERIEL COMMAND
WRIGHT-PATTERSON AIR FORCE BASE, OH 45433-7542

NOTICE

USING GOVERNMENT DRAWINGS, SPECIFICATIONS, OR OTHER DATA INCLUDED IN THIS DOCUMENT FOR ANY PURPOSE OTHER THAN GOVERNMENT PROCUREMENT DOES NOT IN ANY WAY OBLIGATE THE US GOVERNMENT. THE FACT THAT THE GOVERNMENT FORMULATED OR SUPPLIED THE DRAWINGS, SPECIFICATIONS, OR OTHER DATA DOES NOT LICENSE THE HOLDER OR ANY OTHER PERSON OR CORPORATION; OR CONVEY ANY RIGHTS OR PERMISSION TO MANUFACTURE, USE, OR SELL ANY PATENTED INVENTION THAT MAY RELATE TO THEM.

THIS REPORT IS RELEASABLE TO THE NATIONAL TECHNICAL INFORMATION SERVICE (NTIS). AT NTIS, IT WILL BE AVAILABLE TO THE GENERAL PUBLIC, INCLUDING FOREIGN NATIONS.

THIS TECHNICAL REPORT HAS BEEN REVIEWED AND IS APPROVED FOR PUBLICATION.

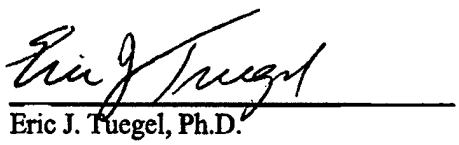

Eric J. Tuegel, Ph.D.
Engineer
Aircraft Structural Integrity

James W. Rogers, Major, USAF
Chief
Analytical Structural Mechanics Branch

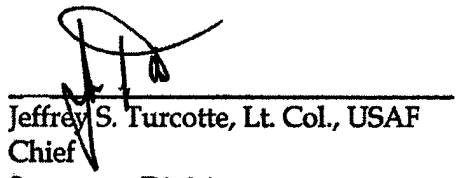

Jeffrey S. Turcotte, Lt. Col., USAF
Chief
Structures Division

Do not return copies of this report unless contractual obligations or notice on a specific document require its return.

REPORT DOCUMENTATION PAGE

Form Approved
OMB No. 0704-0188

1. REPORT DATE *(DD-MM-YY)*	2. REPORT TYPE	3. DATES COVERED *(From - To)*
December 2002	Final	05/15/2002 – 12/20/2002

4. TITLE AND SUBTITLE
CORROSION PIT TO CRACK TRANSITION
Delivery Order 0051: Task 2

5a. CONTRACT NUMBER
F33601-01-D-J001

5b. GRANT NUMBER

5c. PROGRAM ELEMENT NUMBER
62201F

6. AUTHOR(S)
Krishnan K. Sankaran
Gary E. Weaver

5d. PROJECT NUMBER
2401

5e. TASK NUMBER
00

5f. WORK UNIT NUMBER
TK

7. PERFORMING ORGANIZATION NAME(S) AND ADDRESS(ES)
The Boeing Company
Mail Code S111-1041
P.O. Box 516
St. Louis, MO 63166-0516

8. PERFORMING ORGANIZATION REPORT NUMBER

9. SPONSORING/MONITORING AGENCY NAME(S) AND ADDRESS(ES)
Air Vehicles Directorate
Air Force Research Laboratory
Air Force Materiel Command
Wright-Patterson Air Force Base, OH 45433-7542

10. SPONSORING/MONITORING AGENCY ACRONYM(S)
AFRL/VA SM

11. SPONSORING/MONITORING AGENCY REPORT NUMBER(S)
AFRL-VA-WP-TR-2003-3010

12. DISTRIBUTION/AVAILABILITY STATEMENT
Approved for public release; distribution is unlimited.

13. SUPPLEMENTARY NOTES
The majority of this report is comprised of viewgraphs.

14. ABSTRACT *(Maximum 200 Words)*
Detailed fractographic analysis was performed on corroded and then fatigued 7075-T6 specimens, available from an earlier experimental study (Contract F33615-96-D-5835, sponsored by the U.S. Air Force Office of Scientific Research and managed by Dr. K.V. Jata, AFRL Materials Directorate) to determine the characteristics of the pits from which fatigue cracks nucleated. Cracks were found to nucleate at the larger pits.

15. SUBJECT TERMS
corrosion, fatigue, damage tolerance

16. SECURITY CLASSIFICATION OF:			17. LIMITATION OF ABSTRACT:	18. NUMBER OF PAGES	19a. NAME OF RESPONSIBLE PERSON (Monitor)
a. REPORT	b. ABSTRACT	c. THIS PAGE			Dr. Eric Tuegel
Unclassified	Unclassified	Unclassified	SAR	112	19b. TELEPHONE NUMBER *(Include Area Code)* (937) 904-6772

Standard Form 298 (Rev. 8-98)
Prescribed by ANSI Std. Z39-18

Table of Contents

List of Figures

List of Figures (continued)

List of Figures (continued)

List of Figures (continued)

List of Figures (continued)

List of Tables

Acknowledgements

The "Corrosion Pit to Crack Transition" program was completed under a contract from SelectTech Services Corporation, Centerville, OH in support of Air Vehicles Directorate, Air Force Research Laboratory, WPAFB, OH. Dr. Eric Tuegel was the Air Force Technical Monitor. Dr. K. K. Sankaran was the Boeing Principal Investigator and Mr. Gary Weaver of Boeing's Physical Sciences and Systems Laboratories conducted the scanning electron microscopic investigation. Technical discussions with Dr. Eric Tuegel of the Air Vehicles Directorate are acknowledged. Permission from Dr. K. V. Jata of the Materials and Manufacturing Directorate, Air Force Research Laboratory, to use material from a previous contract is also gratefully acknowledged.

1. EXECUTIVE SUMMARY

Corrosion is an economic burden for the United States Air Force (USAF) since repair and maintenance operations undertaken to mitigate its effects on legacy aircraft are typically over-conservative due to the lack of a reliable methodology to predict the future effects of corrosion on structural performance. Therefore, a need exists for the quantitative evaluation of the effects of corrosion on such failure modes as structural fatigue. Quantitative evaluation will enable the safe and economical operations of aircraft.

Pitting is among the commonly observed type of corrosion damage in aircraft structures, as the heterogeneous microstructures of high-strength aluminum alloys such as 2024 and 7075, widely used in the construction of legacy aircraft, render them highly susceptible to this type of localized corrosion. Accordingly, quantitative modeling of corrosion damage by pitting and its effects on the fatigue behavior of aluminum alloys has received considerable attention.

In this study, the fracture surfaces of broken corrosion fatigue test specimens were examined in detail in a scanning electron microscope (SEM) to develop an understanding of the nature of the transition of the corrosion damage into fatigue cracks. The purpose was to construct a quantitative data set of the corrosion damage metrics for use in developing and validating corrosion fatigue life prediction models. Available aluminum alloy 7075-T6 specimens, which had been subjected to varying levels of pitting corrosion, systematic characterization, and fatigue testing, were used for the fractographic investigation.

The observations showed that in materials with preexisting corrosion damage, fatigue cracks nucleate at pits and start growing immediately upon the application of load in a laboratory air environment. Failure of these specimens is caused by a dominant crack, for which a single crack-nucleating pit can be found in most instances. Depending on the extent of surface pitting, secondary cracks may nucleate and grow, but have no influence on the dominant crack or the fatigue lives. The measured sizes of the crack-nucleating pits are near those of the largest pits on the precorroded specimen surface, consistent with the expectation that these pits would provide the largest initial flaws to nucleate the dominant cracks. Depending on the interaction of the various crack fronts, one of these large cracks would eventually cause the specimen failure.

Pitting corrosion causes a significant drop in the fatigue lives of aluminum alloys, even at low levels of corrosion, but reduces life very little with further increase of corrosion damage. Together with the results of other observations, the reduction of fatigue lives due to pitting damage suggests the possibility of an influential pit. Further investigations are needed to verify and refine the characteristics of such pits. The use of fractography to determine the characteristics of crack-nucleating sites has the potential to provide corrosion metrics for development and verification of life prediction models. For accurate life assessment, fatigue crack growth data at very low crack sizes of the order of pit dimensions are necessary.

2. INTRODUCTION AND BACKGROUND

2.1 Introduction

The USAF has a fleet of aging aircraft. Despite modernization plans, the average fleet age continues to increase causing increased maintenance costs and decreased mission readiness. A 1997 report by the National Research Council identified corrosion as the most costly maintenance problem for the USAF (1). For example, for the KC-135 aircraft, the majority of failures and structural repairs are caused by corrosion, which also contributes to increasingly larger share of the total maintenance cost (2).

The various forms of corrosion observed in aircraft structures include galvanic, pitting and intergranular/exfoliation corrosion, corrosion fatigue, and stress corrosion cracking. Crevice corrosion occurs when discrete areas on an alloy are physically isolated or occluded, such as in structural joints, and is characterized by the presence of pits and intergranular/exfoliation corrosion. Recent publications have reviewed the effects of the various types of corrosion and their effects on aircraft structural integrity (3). The work associated with modeling the overall effects of corrosion in USAF aging aircraft fleet has also been discussed (4).

Analytical fracture mechanics and damage tolerance methods, similar to those used for managing the effects of fatigue on structural integrity are being developed for modeling the effects of corrosion damage (5). In this context, modeling of the effects of pitting corrosion on fatigue behavior has received the most attention, partly due to the well- recognized and well-characterized effects of pitting corrosion on reducing the fatigue lives of aluminum alloys on fatigue crack nucleation and partly due to the relative ease of modeling corrosion pits as equivalent initial flaws for crack nucleation. Prior and on-going work in this area, which is relevant to the present study, is discussed in the following paragraphs.

2.2 Quantitative Assessment of the Effects of Pitting on Fatigue Behavior

The heterogeneous microstructures of high-strength aluminum alloys such as 7075, widely used in the construction of legacy aircraft, render them highly susceptible to pitting corrosion, which is a form of localized corrosion occurring on the surface of these materials. In studying the effects of localized corrosion on the fatigue behavior of aircraft structures, the influence of both preexisting corrosion as well as corrosive environments on fatigue crack initiation have been considered. For the latter case, corrosion/fatigue interactions have been modeled by the testing of pristine specimens in a corrosive environment during which fatigue and corrosion damage accumulate simultaneously. In these models, corrosion pits are considered as surface cracks whose growth rates are determined by the pitting kinetics (6-8). A fatigue crack initiates from the corrosion pit either when the pit grows to a critical size, at which the stress intensity factor reaches the threshold for fatigue cracking (6), or when the fatigue crack growth rate exceeds the pit growth rate (7). A recent study of the alloy 2024-T3 showed that both these criteria are needed for adequately describing the transition from pitting to fatigue crack growth (8).

During its service life, an aircraft structure typically experiences corrosion between flights and fatigue loading during flight, thus pointing to the need for quantifying the effects of prior corrosion on fatigue behavior. In this context, Harmsworth conducted the first quantitative study of the influence of preexisting corrosion on reducing the fatigue life of aluminum alloys (9). In this study, pit depths in alloy 2024-T4 were measured as a function of exposure time and decreasing fatigue lives were observed with increasing corrosion exposure (pit depths).

More recently, pitting corrosion/fatigue interactions have been modeled by using pit dimensions as inputs into fatigue life prediction models. Quantitative measures such as pit dimensions and surface roughness have been used as metrics to describe corrosion, and their potential feasibility in combination with crack growth analysis tools in estimating fatigue life of components subjected to corrosion has been demonstrated (10). In this study, the measured fatigue properties of etched (pitted) 2124-T851 and 7050-T7451 aluminum alloys compared reasonably well with those calculated analytically using equivalent initial flaw size assumptions. A series of criteria was also described for ranking various corrosion metrics to enable selection of the applicable parameter for structural analysis. Bray et al. (11) have also shown that prior corrosion pitting reduced the fatigue strength of aluminum alloys 2024-T3 and 2524-T3 at 10^5 cycles by approximately 40 percent. Crack growth analysis was also used in this study to predict the fatigue lives and to investigate the effects of the alloy compositions and pit morphology on the fatigue lives.

A systematic investigation was recently undertaken toward developing an integrated experimental and modeling approach to quantitatively account for the effects of prior corrosion on the fatigue behavior of structural aluminum alloys (12, 13). The effects of preexisting localized surface pitting corrosion damage on the fatigue lives of alloy 7075-T6 were measured and compared with the predicted lives using measures of corrosion (metrics) obtained from a characterization of the corrosion damage. Pit depth histograms resulting from exposing bare 7075-T6 sheets for up to 1,536 hours in a prohesion spray were determined, and the observations of damage evolution were found to be consistent with the nucleation/growth/decay nature of the pitting process. Fatigue crack growth models were used to predict the life of 7075-T6 specimens containing various levels of pitting damage and the measured lives generally agreed with the predictions using the average pit size as the initial crack size. This result was explained as due to the pit size distributions offering a significant population of pits near the average size. A continuous decrease in fatigue life with increasing pit dimensions (increasing corrosion exposure) was observed. It was also found that the data was bounded by Mil-Hdbk-5 values for 7075-T6 at Kt values of 1 and 2, perhaps suggesting a threshold for crack initiation in corroded specimens.

In several of the studies cited here, fractographic examination of broken corrosion fatigue specimens clearly showed the nucleation of dominant fatigue cracks from corrosion pits. The sizes of these crack-nucleating pits were found to be typically in the 50 – 250 μm range (9, 12, 13). None of these investigations, however, has systematically examined the fracture surface in

detail to assess the mechanisms of fatigue crack nucleation from pits and the nature of the corrosion pit to crack transition.

2.3 Corrosion Pit to Crack Transition

The fatigue damage and failure induced by pitting corrosion are composed of seven stages: pit nucleation, pit growth, transition from pit growth to short crack, short crack growth, transition from short crack to long crack, long crack growth, and fracture (14). In studying the effects of pre-existing corrosion on fatigue behavior, pit nucleation and growth are not relevant, but the nature of transition from the pit to short crack and short crack growth need to be clearly delineated. Available life prediction methods are adequate once the cracks grow beyond the short crack stage.

In polycrystalline materials, preexisting surface damage can initiate a crack immediately upon the application of load (15). This fact coupled with the observation that the fracture surfaces of aluminum alloy 2024-T3 and 2524-T3 specimens subjected to interrupted fatigue testing showed fatigue cracks emanating from pits at less than about 15 percent of the total life of corresponding noncorroded specimens and that large numbers of secondary cracks were observed in these specimens, suggests that pitting can nearly eliminate the fatigue initiation stage. The numerous cracks initiated at surface damage sites would all coalesce very quickly into one or more larger cracks and ultimately to a dominant crack.

Detailed analysis of corrosion fatigue fracture surfaces to fully delineate and understand the corrosion pit to crack transition has not been conducted. The limited amount of fractography conducted to date typically shows a very clear interface between the dominant crack and the crack-nucleating pit, suggesting that for corrosion modeling purposes, a single pit may be considered to nucleate the dominant crack immediately upon loading the specimen.

2.4 Summary

While significant progress has been made in characterizing the effects of pitting corrosion on the fatigue behavior of high-strength aluminum alloys, not enough is known about the nature of the early stages of corrosion fatigue deformation in general and the mechanism of corrosion pit to crack transition in particular. A quantitative fractographic assessment of failed and well-characterized corrosion fatigue specimens has the potential to provide an understanding of the pit to crack transition and to enable the development and validation of life prediction models.

3. PROGRAM OBJECTIVES AND APPROACH

3.1 Program Objectives

The objective of the "Corrosion Pit to Crack Transition" Program is to perform a detailed fractographic analysis of fractured, aluminum alloy corrosion fatigue specimens in which the cracks are expected to have developed at corrosion sites, generally pits. The purpose is to obtain an understanding of the corrosion pit to crack transition by identifying and documenting the

- Type, location, size, and shape of the corrosion at all identifiable crack nucleation sites
- Relevant details of how the failure progressed that could be identified from the fracture surface, especially when the cracks were small
- Dominant crack – the one that grew the largest and caused failure – for specimens with multiple crack nucleation sites.

3.2 Program Approach

The objectives of the "Corrosion Pit to Crack Transition" Program were accomplished by conducting a detailed fractographic analysis of fractured, corrosion fatigue specimens. These specimens were selected from among those available from an earlier, integrated experimental and modeling study (Contract F33615-96-D-5835, sponsored by U.S. Air Force Office of Scientific Research and managed by Dr. K.V. Jata, AFRL Materials Directorate), which quantitatively accounted for the effects of prior pitting corrosion on the fatigue behavior 7075-T6 aluminum alloy sheet material.

The planned technical approach to conducting the detailed fractographic analysis of selected corrosion fatigue specimens and documenting the corrosion pit to crack transition followed the following steps:

1) Fatigue crack documentation
2) Identification and documentation of crack nucleation sites
3) Documentation and measurement of corrosion at crack nucleation sites
4) Observation of early cracking phase.

An AMRAY 3200C variable pressure SEM with a lanthanum hexaboride source was used for specimen examination. Backscatter digital images were acquired using a Robinson detector and the secondary electron digital images were collected with a traditional Everhart-Thornly detector. The peripheral energy dispersive x-ray system contained a windowless Noran INSTRUMENTS light element detector (Beryllium) whose data was interpolated by Noran INSTRUMENT's VANTAGE Digital Microanalysis Software.

Using best laboratory practices, the fractures from the selected corrosion fatigue specimens were excised and ultrasonically cleaned. Most specimens were coated with about 0.15 nm of gold to improve the image. Some specimens in which energy dispersive analysis (EDS) was performed were not coated with gold.

The following subsections describe each of the steps in detail.

3.2.1 Fatigue Crack Documentation

The overall fracture surface was observed and photographed for each of the selected specimens. An example of this type of photograph is illustrated in Figure 1, which shows the fracture surface for a 7075-T6 specimen exposed to prohesion spray for 384 hours and fatigue tested under constant amplitude loading with a maximum stress of 35 ksi and R ratio of 0.02. The specimen life was 45,830 cycles. The fracture surface contains a dominant crack near the center of the cross section. For specimens with multiple crack nucleation sites, the dominant crack – the one that grew the largest and caused failure – was identified and its depth recorded.

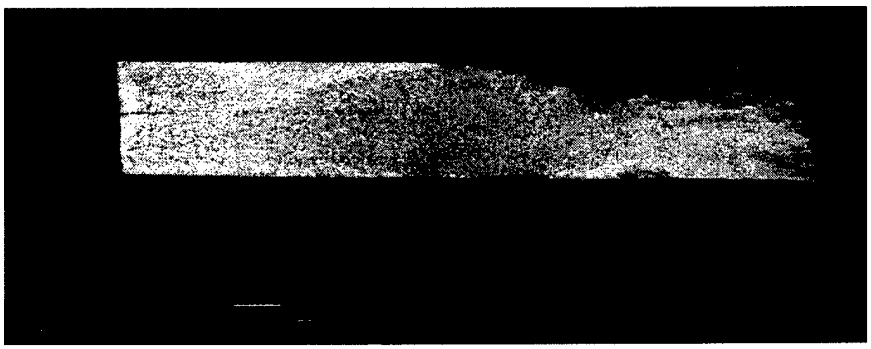

Figure 1. Sample Corrosion Fatigue Fracture Surface for 7075-T6

3.2.2 Identification and Documentation of Crack Nucleation Sites

The cracks were observed and photographed at increased SEM magnification to locate the crack nucleation sites. Identification of these crack origin regions made use of the observed crack geometry and features. For example, in the case of an independent semi-elliptical surface crack, the origin typically lies near the center of the ellipse. Higher magnification photos of this area were used to locate corrosion near or at the crack nucleation sites. If multiple adjacent cracks coalesced to form a larger dominant flaw, several crack nucleation sites may be present. The crack front for each flaw is typically separated from the other flaws by a ridgeline feature on the fracture surface. This ridge forms because of differences in the planes of the multiple cracks.

An example of a crack nucleation site is illustrated in the higher magnification photo of the fracture surface in Figure 2. Figure 3 illustrates a still higher magnification area of the same site shown in Figure 2. Evidence of corrosion can be observed at the origin of the crack.

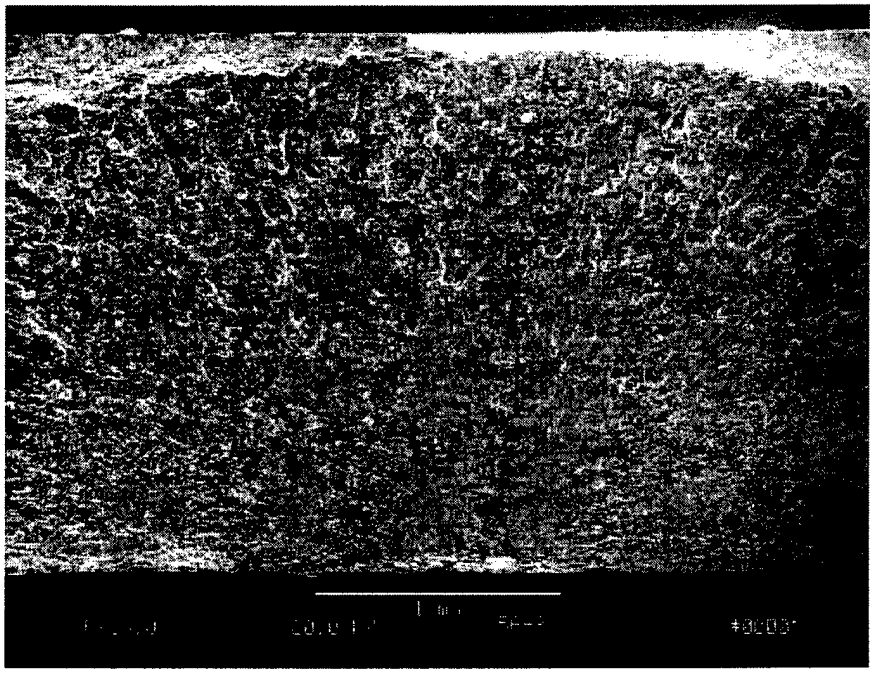

Figure 2. Crack Nucleation Site

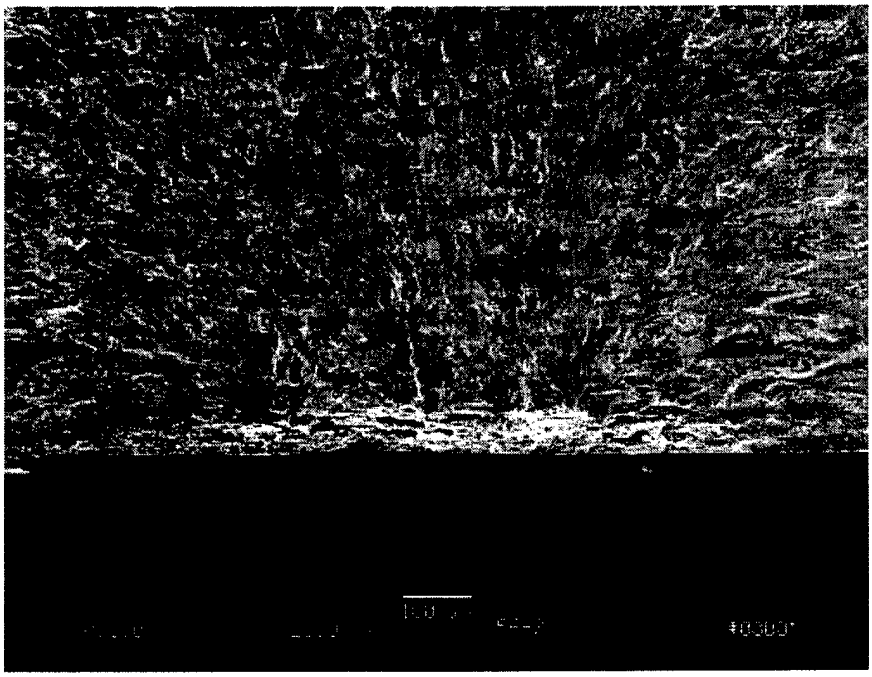

Figure 3. Crack Nucleation Site (Higher Magnification Photo)

3.2.3 Documentation and Measurement of Corrosion at Crack Nucleation Sites

Once corrosion is located at the crack nucleation sites, additional photographs were obtained at different angles to document the corrosion on the specimen front face. (The specimens were originally corroded on one side, referred to as the front face.) An example of this type of observation is illustrated in Figure 4 for the same crack origin area illustrated earlier in Figure 3. Figure 5 shows a higher magnification photo of the same region. The lighter gray region in Figures 4 and 5 is the fracture surface. The darker area is the corroded front face of the specimen.

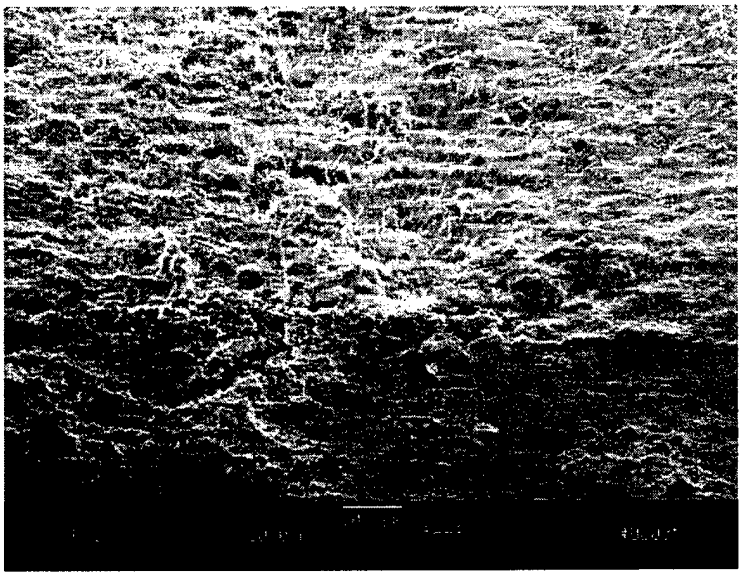

Figure 4. Corrosion at Crack Nucleation Site

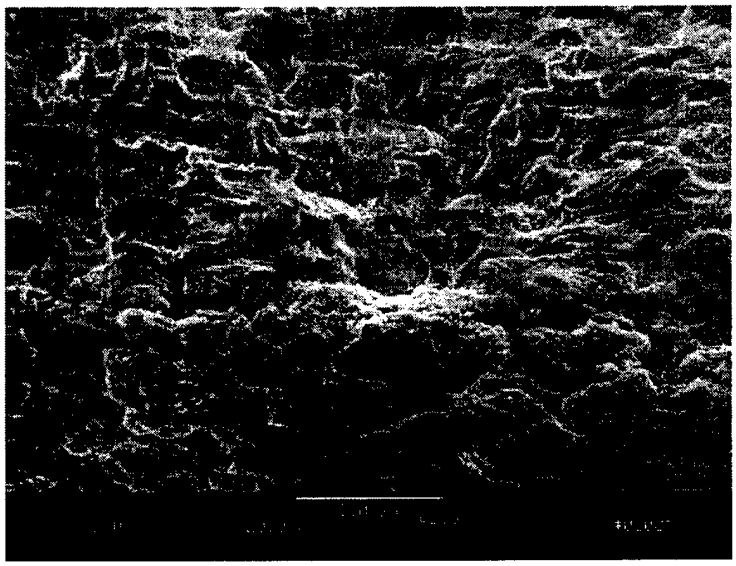

Figure 5. Corrosion at Crack Nucleation Site (Higher Magnification Photo)

Figure 6 shows the corrosion on the front face of the specimen, adjacent to the fracture surface in the vicinity of the crack nucleation zone. The fracture is directly above the specimen front face and into the page.

Figure 6. Corrosion on the Front Face of Specimen

3.2.4 Observation of Early Cracking Phase

The fracture surface surrounding the corrosion at the crack nucleation sites were photographed. Figure 7 shows an example of this type of observation. The darker area in the upper part of the photograph is the fracture surface. The lighter area near the bottom is the corrosion pit. The area contains striations and microcleavage surrounding the corrosion pit at the crack nucleation site. Other details of how the failure progressed that can be identified, especially when the cracks were small, were also documented.

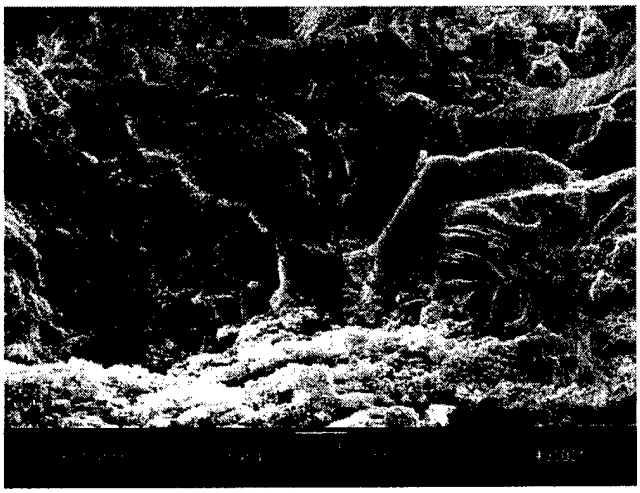

Figure 7. Fracture Surface Features Surrounding the Corrosion at the Nucleation Site

4. FRACTOGRAPHIC OBSERVATIONS

4.1 History of Specimens Used for Fractography

The specimens used in this investigation for the scanning electron microscopic observations of the fracture surfaces and the corrosion pit to crack transition were obtained from an earlier Air Force-funded investigation that studied the effects of pitting corrosion on the fatigue behavior of bare 7075-T6 aluminum alloy (12, 13). In that study, rectangular panels, 150 mm (6 inches) long and 75 mm (3 inches) wide, with the sheet rolling direction parallel to the specimen width, were prepared from 2-mm (0.080 inches)-thick, bare, aluminum alloy 7075-T6 sheet material. The panels were exposed for 24, 48, 96, 192, 384, 768 and 1,536 hours, respectively, in a prohesion spray in accordance with the ASTM G85, Annex 5, dilute electrolyte cyclic fog/dry spray test procedure. The exposure duration were chosen to obtain systematically increasing levels of corrosion that were amenable to quantitative characterization and for providing sufficient variation in the levels of corrosion for evaluating the influence on fatigue properties.

The dimensions of 200 randomly chosen pits were measured in representative panels exposed to various durations in the prohesion spray by using a metallurgical microscope with a fine focus knob calibrated to 1 μm. Pit depths were measured by focusing on the specimen surface, first at the lip of the pit and then at the bottom of the pit, with the difference in the fine focus knob reading being the pit depth. The pits were generally elongated in the sheet rolling direction, and accordingly the dimension along the rolling direction was designated as the pit length and that along the transverse direction as the pit width.

The fatigue lives of 7075-T6 specimens with various levels of pitting corrosion damage were predicted using the USAF developed fatigue crack growth software AFGROW (16). For each corrosion exposure level, fatigue lives were predicted assuming an equivalent initial flaw corresponding to pits of both average and maximum dimensions, respectively, obtained from the pit size distributions.

The fatigue lives of 7075-T6 specimens fabricated from the corroded panels were also measured by conducting constant amplitude tests at various maximum stress levels in laboratory air using an R ratio of 0.02 and a frequency of 15 Hz. Pitting corrosion decreased the fatigue lives by a factor of about 6 to 8, and the measured lives generally agreed with the predictions using the average rather than the maximum pit size as the initial flaw size. This result was explained by the pit size distributions offering a significantly larger population of pits near the average size. Following this study, additional fatigue tests were also conducted on the remaining available corroded specimens. These tests were such that a sufficiently large number of replicate fatigue tests were conducted at several different maximum stress levels for specimens with a given corrosion exposure and the results were used to develop a nondeterministic corrosion fatigue life prediction method (17).

In the present study, a total of 34 broken specimens from the previous investigations were selected for observation of the fracture surface characteristics and analysis of the corrosion pit to crack transition. Table 1 presents a list of these specimens along with the respective corrosion exposure duration and the fatigue lives, which had been measured previously. The specimen identification numbers from the previous investigations have been retained to enable unambiguous tracing of the history of these specimens as well as to maintain ease of access to specimens for any additional future evaluations.

Table 1. List of Corrosion Fatigue Specimens Selected for Fractographic Observations

Specimen Number	Specimen Identification	Corrosion Exposure (Hours)	Maximum Stress (ksi)	Fatigue Life (Cycles to Failure)
1	43-1	24	45	22,390
2	43-2	24	45	22,350
3	45-1	24	45	23,350
4	45-2	24	45	20,510
5	45-3	24	45	26,510
6	47-2	48	45	22,590
7	47-3	48	45	22,720
8	48-1	48	45	22,950
9	48-2	48	45	27,200
10	48-3	48	45	23,910
11	46-1	48	55	7,660
12	46-2	48	55	12,310
13	47-1	48	55	11,810
14	51-3	96	30	77,780
15	51-1	96	35	52,530
16	50-3	96	40	37,940
17	49-2	96	45	39,340
18	50-2	96	45	20,350
19	49-3	96	50	18,250
20	50-1	96	50	14,500
21	58-2	768	30	179,820
22	58-3	768	35	77,710
23	60-1	768	35	37,620
24	58-1	768	40	39,940
25	59-3	768	45	19,310
26	60-2	768	45	17,670
27	59-2	768	50	17,320
28	61-3	1,536	35	39,380
29	62-1	1,536	35	30,950
30	62-2	1,536	40	22,950
31	61-2	1,536	45	15,130
32	63-3	1,536	45	18,830
33	61-1	1,536	55	6,550
34	63-2	1,536	55	6,040

4.2 Fracture Surface Characteristics

4.2.1 Pits and Fatigue Crack Nucleation

Detailed views of the various aspects of the fracture surfaces of the 34 broken specimens are presented in the collection of fractographs in this section and in the Appendix. These photographs, with a few exceptions noted later, identify the pits that nucleated the dominant cracks and their growth to the critical size. Each of the fracture surfaces of the broken specimens is characterized by a single dominant crack that grew to critical size and caused the catastrophic failure. Except in one specimen (number 59-3), these cracks all nucleated from pits on the corroded surface of the broken specimens.

In our prior modeling studies of the fatigue crack nucleation in corroded specimens, we assumed pits were distributed randomly on the corroded surface (12, 13). As shown in Figure 8, a single semi-elliptic surface crack is assumed to develop at a pit somewhere on the corroded surface. The model independently computes crack growth on the surface (using pit length as twice the initial crack length) as well as through the thickness (using the pit depth as the initial crack length). Fatigue life is defined as the number of load cycles for the crack to reach the critical size.

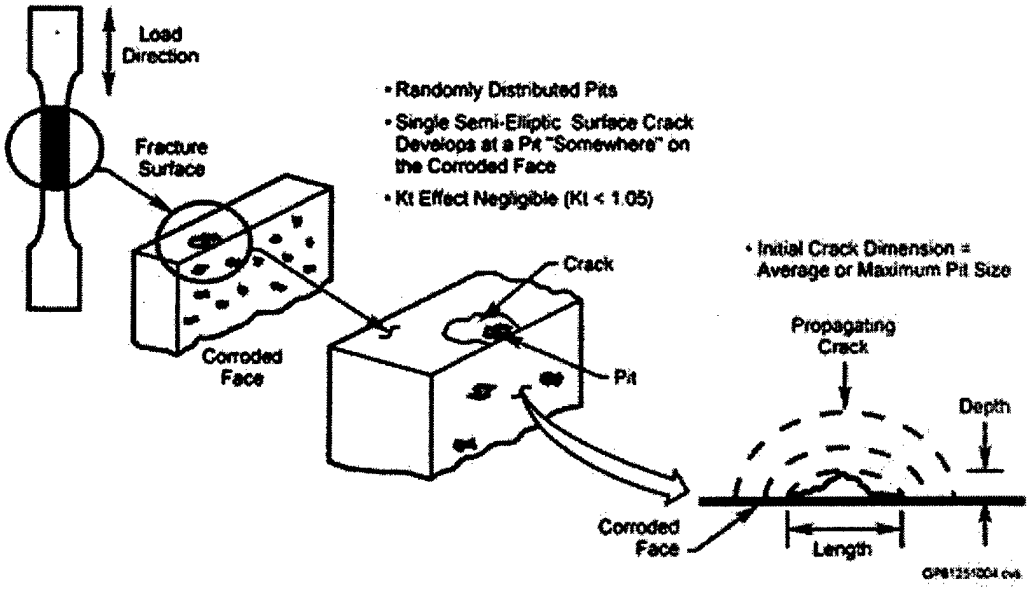

Figure 8. Schematic of the Model Used for Fatigue Life Prediction of Corroded 7075-T6 Specimens

The range of sizes of the pits on the corroded surface of the 7075-T6 specimens would include pits too small to nucleate fatigue cracks, those that nucleate cracks exhibiting small crack behavior, and those that nucleate larger cracks. However, upon continued loading, most of the nucleated cracks rapidly coalesce into one or a few larger cracks, which eventually leads to one dominant crack. Nucleation of multiple cracks was observable in some of the examined specimens. Depending upon the number of observable crack-nucleating pits, the 34 specimens are classified as follows:

- In about half of the specimens examined, shown for example in Figure 9 for specimen 43-1, a single pit is identified to nucleate the dominant crack.

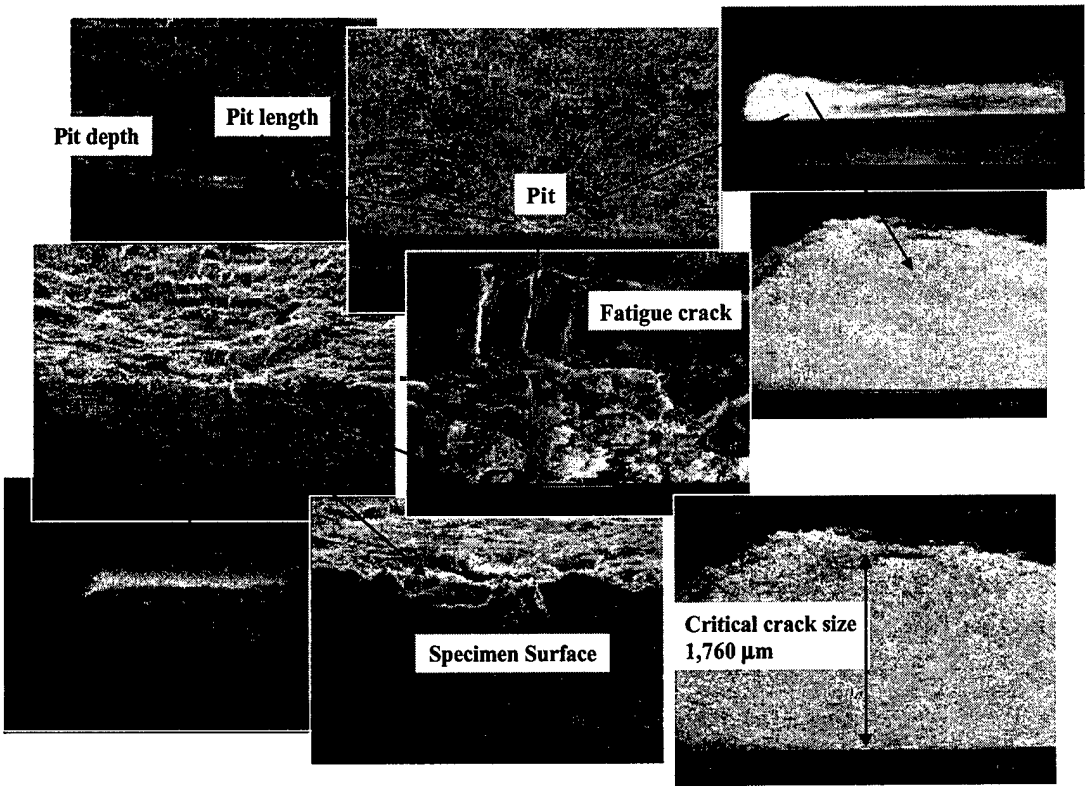

Figure 9. Fracture Surface of Specimen 43-1 Showing Single Crack-Nucleating Pit and the Critical Crack

- In some cases, shown for example in Figure 10 for specimen 51-3, cracks nucleated from two adjacent pits and coalesced, as evidenced by the ridge in the fracture surface. However, it is difficult to distinguish the two pits clearly, as they appear to have joined just as the corrosion exposure ended. While there is only one dominant crack, the length of the crack-nucleating pit is considered the sum of the length of both the pits.

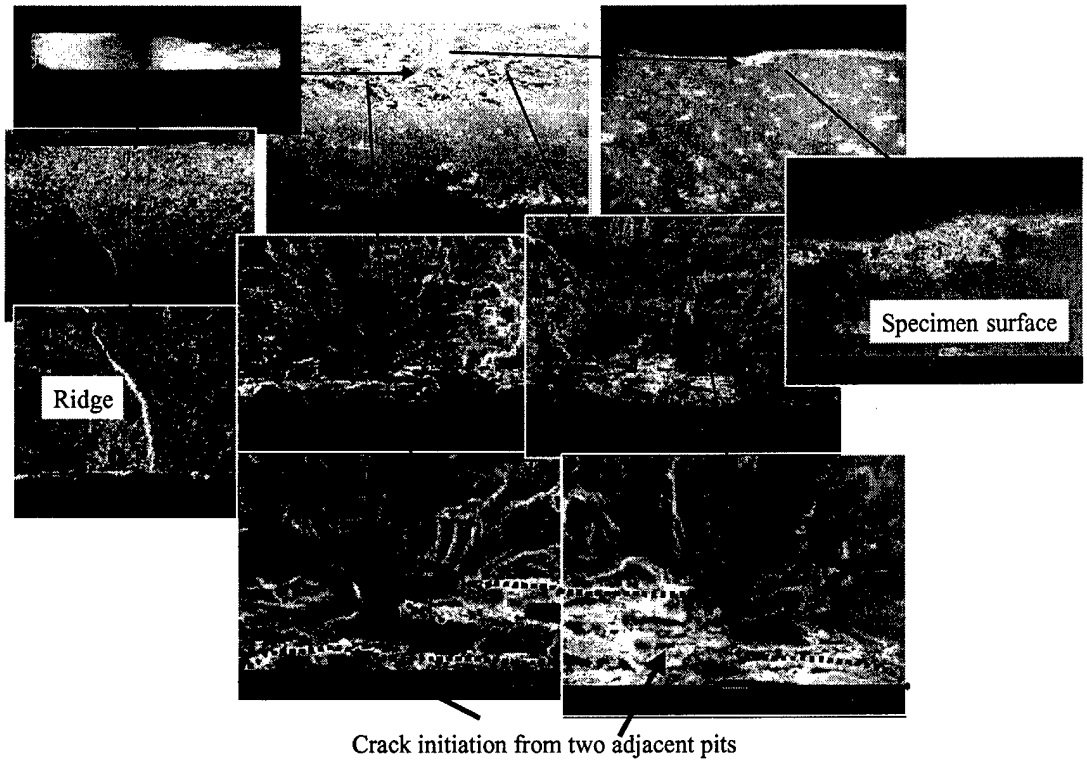

Figure 10. Fracture Surface of Specimen 51-3 Showing Cracks Nucleating From Adjacent Pits and Coalescing Into Single Crack

- In a few cases, shown for example in Figure 11 for specimen 48-3, several cracks are observed to nucleate from the fracture surface. These all rapidly coalesced to a single crack for which a nucleating pit can be identified.

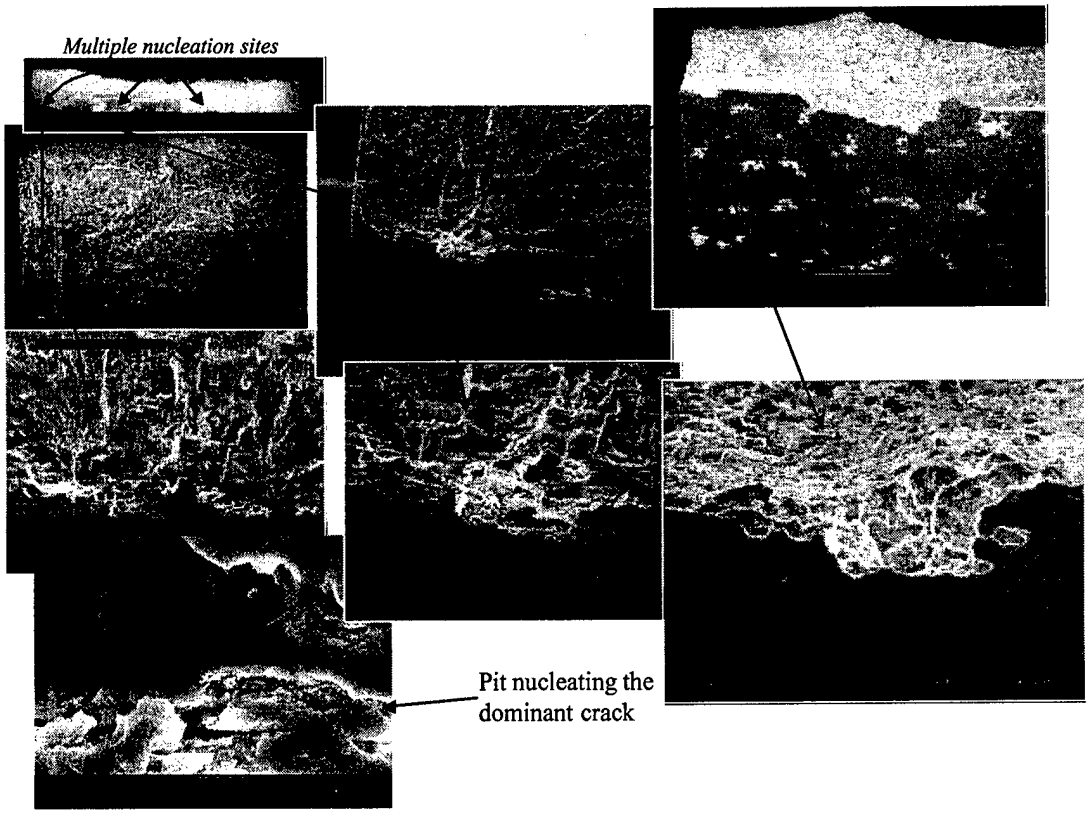

Figure 11. Fracture Surface of Specimen 48-3 Showing Cracks Nucleating From Multiple Pits and Coalescing Into Single Crack

- In a few cases, shown for example in Figure 12 for specimen 45-1, no pits could be identified because of the nature of surface corrosion, even though one dominant crack still caused the failure.

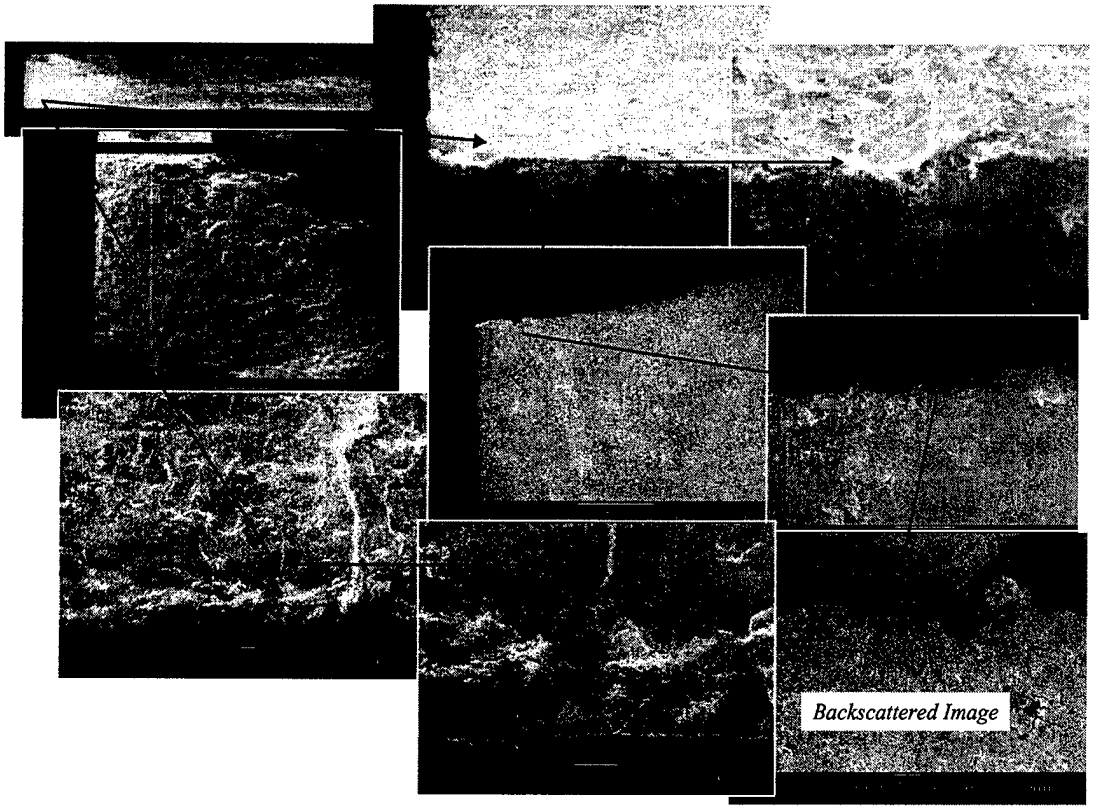

Figure 12. Fracture Surface of Specimen 45-1 Showing a Dominant Crack But No Discernible Pits

The above observations are summarized in Table 2. It should be pointed out that, despite these differences, a dominant crack was always observed in all the specimens. Except in those cases where pits could not be clearly delineated, the pit that nucleated the dominant crack could be identified. While the depth of the pit (the dimension perpendicular to the corroded surface) could be measured reasonably accurately, measurement of the length of the pit was subject to the uncertainty resulting from coalescence of adjacent pits on the corroded specimen surface. In addition, no correlation is obvious between the corrosion exposure duration or the maximum stress level and the number of crack-nucleating pits.

Table 2. Summary of Observed Crack-Nucleating Pits

Specimen Identification	Corrosion Exposure (Hours)	Maximum Stress (ksi)	Fatigue Life (Cycles to Failure)
Dominant crack nucleating from single pit			
43-1	24	45	22,390
45-2	24	45	20,510
47-3	48	45	22,720
48-2	48	45	27,200
46-1	48	55	7,660
51-1	96	35	52,530
49-2	96	45	39,340
50-2	96	45	20,350
49-3	96	50	18,250
50-1	96	50	14,500
58-2	768	30	179,820
58-3	768	35	77,710
58-1	768	40	39,940
61-3	1,536	35	39,380
62-1	1,536	35	30,950
62-2	1,536	40	22,950
63-3	1,536	45	18,830
Dominant crack nucleating from two adjacent pits			
43-2	24	45	22,350
51-3	96	30	77,780
50-3	96	40	37,940
60-1	768	35	37,620
Dominant crack nucleating from multiple pits			
45-3	24	45	26,510
48-1	48	45	22,950
48-3	48	45	23,910
46-2	48	55	12,310
47-1	48	55	11,810
60-2	768	45	17,670
61-2	1,536	45	15,130
61-1	1,536	55	6,550
Crack nucleating pit not discernible			
45-1	24	45	23,350
47-2	48	45	22,590
59-2	768	50	17,320
63-2	1,536	55	6,040
Crack nucleation from the noncorroded face			
59-3	768	45	19,310

4.2.2 Characterization of Fatigue Crack Nucleation Sites and Crack Growth

The depth and length of the crack nucleating pits, measured from the fracture surfaces, are shown in Table 3. Also listed in this table are the mean and the maximum values of the pit depth and length obtained from a distribution of 200 measurements on corroded panels exposed to the various duration (12, 13). It is interesting to note that the measured pit dimensions are in many cases higher than even the maximum dimensions from the pit size distributions. The possible reasons for this observation are discussed in detail in the following section.

For selected specimens, an energy-dispersive x-ray spectroscopic analysis of the material in the vicinity of the pit and the base material was performed. An example of such observation is shown in Figure 13 for specimen 60-1. While all of the corroded specimens had been cleaned using American Society for Testing and Materials (ASTM) standard procedures to remove the corrosion products, it is impossible to remove them completely. The EDS traces shown in Figure 13 are as expected. The area of the pit shows traces of oxygen consistent with the nature of the corrosion product. The base material adjacent to the pit shows primarily aluminum with signals from the alloying elements, zinc, magnesium and copper. Similar observations are shown for selected specimens in the figures in the appendix.

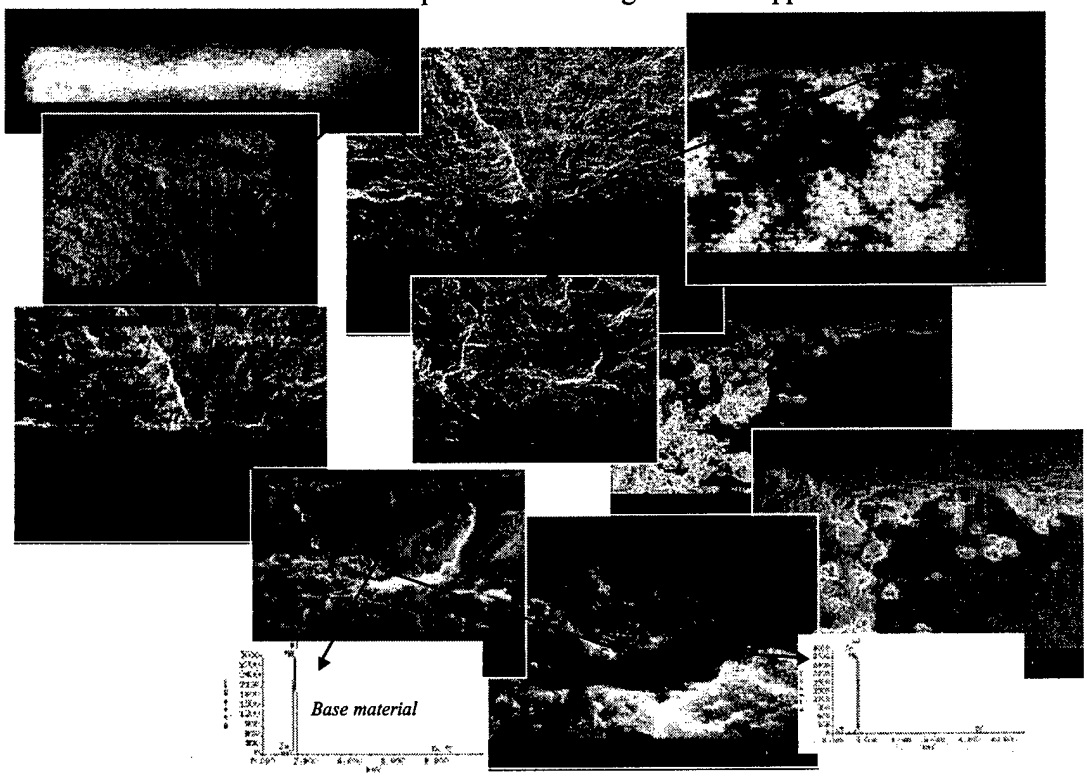

Figure 13. Fracture Surface of Specimen 60-1 Showing EDS Traces

During fatigue crack growth, aluminum alloys such as 7075-T6 exhibit ductile striations, which represent successive positions of the fatigue crack front during crack propagation. For each of

the 34 specimens, an examination of striations was made at three locations – close to the origin of the crack in the vicinity of the pit/crack interface (site 1), about midway from the origin (site 2), and close to the critical crack depth (site 3). An example of such observation is shown in Figure 14 for sample 43-2. Similar results for the remaining specimens are included in the appendix. As expected, the number of striations per unit length decreases with increasing distance from the origin due to increasing crack growth rate with increasing crack length and stress intensity. However, for all the specimens, fatigue life estimated from the observed striations was significantly lower than that measured. While there is one dominant crack, local variations in crack growth rates are expected due to multiple crack fronts, which renders estimation of life from striations meaningless.

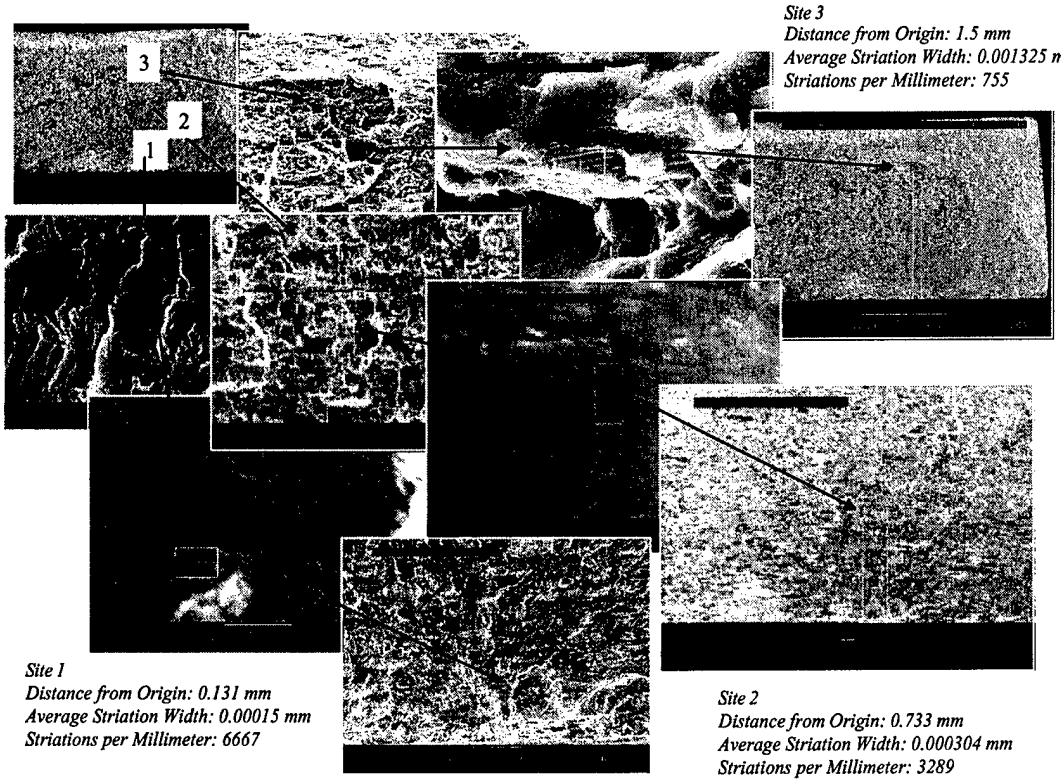

Figure 14. Fracture Surface of Specimen 43-2 Showing Fatigue Striations

Table 3 also lists the size (perpendicular to the corroded surface) of the dominant crack at failure. In almost all cases, the fatigue crack has propagated through a significant part of the 2-mm-thick test specimens, before reaching critical size.

TABLE 3. Comparison of Measured Pit Dimensions With the Values From the Size Distributions (All Pit and Crack Dimensions in μm)

Specimen Identification	Corrosion Exposure (Hours)	Meas Pit Depth	Meas Pit Length	Aspect ratio	Max Pit Depth	Mean Pit Depth	Max Pit Length	Mean Pit Length	Critical Crack Depth
43-1	24	38	173	4.6	36	9.3	240	36.2	1,760
43-2	24	46	699	15.2	36	9.3	240	36.2	1,570
45-1	24	Pits not discernible			36	9.3	240	36.2	1,770
45-2	24	32	82	2.6	36	9.3	240	36.2	1,760
45-3	24	25	226	9.0	36	9.3	240	36.2	1,610
47-2	48	13	36	2.8	35	12.1	500	115	1,790
47-3	48	38	899	23.7	35	12.1	500	115	1,430
48-1	48	33	311	9.4	35	12.1	500	115	1,670
48-2	48	39	314	8.1	35	12.1	500	115	1,180
48-3	48	73	334	4.6	35	12.1	500	115	1,890
46-1	48	50	1,049	21.0	35	12.1	500	115	1,828
46-2	48	51	402	7.9	35	12.1	500	115	1,090
47-1	48	44	615	14.0	35	12.1	500	115	1,660
51-3	96	55	1,150	20.9	29	13.9	300	107	1,940
51-1	96	48	365	7.6	29	13.9	300	107	1,790
50-3	96	22	485	22.0	29	13.9	300	107	1,760
49-2	96	36	154	4.3	29	13.9	300	107	1,890
50-2	96	48	429	8.9	29	13.9	300	107	1,310
49-3	96	20	191	9.6	29	13.9	300	107	1,500
50-1	96	58	528	9.1	29	13.9	300	107	1,630
58-2	768	48	456	9.5	37	23.5	600	163	1,880
58-3	768	21	151	7.2	37	23.5	600	163	1,620
60-1	768	25	520	20.8	37	23.5	600	163	1,660
58-1	768	77	178	2.3	37	23.5	600	163	1,870
59-3	768	23	467	20.3	37	23.5	600	163	1,670
60-2	768	42	312	7.4	37	23.5	600	163	1,560
59-2	768	Pits not discernible			37	23.5	600	163	1,370
61-3	1,536	71	665	9.4	83	50.5	1,300	426	1,660
62-1	1,536	Pits not discernible			83	50.5	1,300	426	1,550
62-2	1,536	46	503	10.9	83	50.5	1,300	426	1,760
61-2	1,536	86	116	1.3	83	50.5	1,300	426	1,830
63-3	1,536	51	598	11.7	83	50.5	1,300	426	1,370
61-1	1,536	28	220	7.9	83	50.5	1,300	426	137
63-2	1,536	Pits not discernible			83	50.5	1,300	426	1,200

5. DISCUSSION OF CORROSION PIT TO CRACK TRANSITION

5.1 Effects of Corrosion Damage on Fatigue Crack Nucleation

Section 2, Introduction and Background, reviewed the results of a number of prior investigations, which all showed that in specimens containing localized surface corrosion damage such as pitting, fatigue always initiates at these preexisting damage sites. In addition, individual fatigue cracks would also be expected to nucleate from all the pits present on the corroded surface, because in polycrystalline materials, preexisting surface damage can initiate a crack immediately upon application of a load (15). However, all these cracks would coalesce early into one or few larger cracks, which would eventually lead to a dominant crack, as observed in all of the specimens investigated. Smaller secondary cracks, when observed such as in specimen 48-3 (Figure 11), probably initiated later in the test.

In 30 of the 34 specimens examined, a single pit could be identified as the site of nucleation of the dominant crack and the length and depth of this crack-nucleating pit could be measured from the fracture surface. The width of this pit cannot be determined from only one-half of the broken specimen. As shown in Table 3, the measured dimensions of the crack-nucleating pit, particularly the length and to a lesser extent the depth, vary over a wide range, which is somewhat to be expected from the varying corrosion exposure in the specimens.

In general, the measured length and depth of the pits are closer to the corresponding maximum values obtained from the pit size distributions, which is consistent with the expectation that the larger pits would provide larger initial flaws that would initiate the dominant cracks. However, this observation is not consistent with the results of the earlier study in which the measured lives of the corroded specimens were in general closer to the lives predicted by using the average rather than the maximum pit dimensions as the sizes of the equivalent initial flaw (12, 13). A possible reason for this could be that for life prediction, crack growth data for cracks of the size of the pit dimensions were not available. Data available in the AFGROW materials databases were then modified to account for early growth behavior by extending the middle part of the curve (the Paris regime) below the threshold stress intensity. This approach would effectively increase the growth rates during the early stages of fatigue crack growth and would predict lower lives for a given pit size than if the true crack growth rates near the threshold region had been available and used. Thus, the measured fatigue lives would agree with those predicted using pit sizes less than the maximum sizes and perhaps closer to the average sizes.

It is important to discuss the technical challenges inherent in measuring the crack-nucleating pit sizes from the fracture surfaces and comparing them with the statistical distributions obtained from measurement of the pit sizes in the corroded panels. The size distributions of the pits on the corroded surfaces of the panels were obtained from pit size measurements using optical metallography. A disadvantage of this technique is that it is a line-of-sight method that does not allow observation of undercutting by the pits. Thus, the pit depth values measured in the corroded panels could be lower than the actual sizes. Secondly, the pit size measurements did

not account for the surface density of the pits, i.e., the number of pits per unit area. In addition to the length, width, and depth of the pits, the surface density also increases with increasing corrosion exposure. This renders unambiguous distinction of pits very difficult in both the corroded panels and the fracture surfaces. Two or more adjacent pits may then appear to nucleate the same crack, as shown in Figure 10. Due to the interaction of adjacent pits, the dimensions of the crack-nucleating pit measured from the fracture surfaces would then be higher than its intrinsic dimensions. This uncertainty would appear to increase with increasing corrosion exposure and the correspondingly increasing surface density of the pits, as illustrated in Figure 15. It should also be noted that one (specimen 59-2) of the four specimens for which pits could not be clearly measured in the fracture surface was exposed for 768 hours, and two (specimens 61-2 and 63-2) of these four specimens were exposed for 1,536 hours.

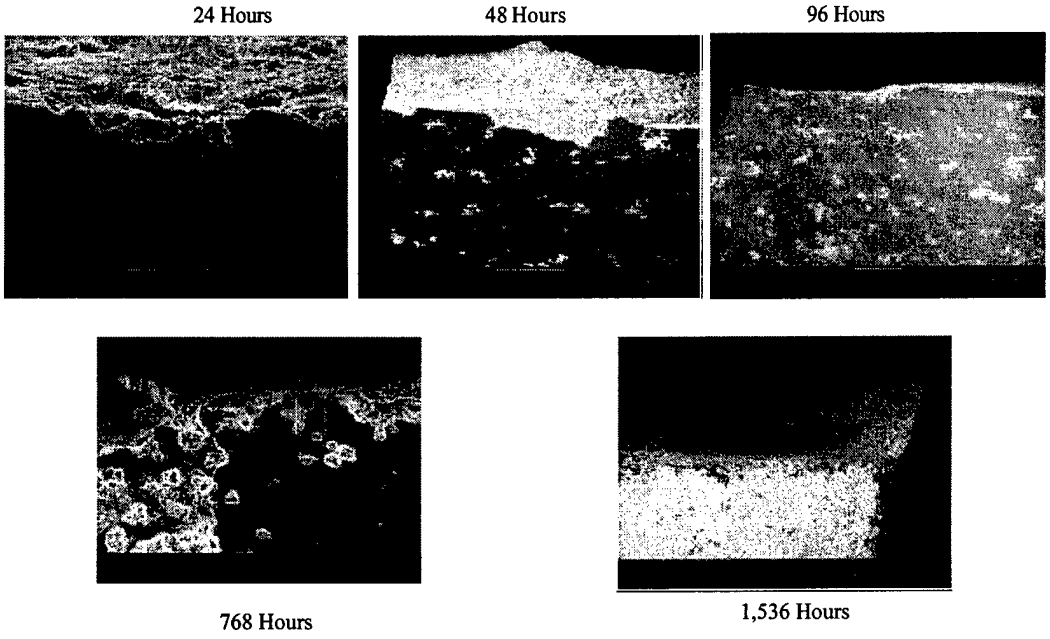

Figure 15. Corroded Surface of Specimen Showing Increasing Surface Density of Pits With Increasing Corrosion Exposure

It is interesting to note that the pit depth values measured from the fracture surfaces, which vary between 13 and 86 μm with a mean of 43 μm, are in the range of 10- to 300- μm pit depth measured in 2024-T4 specimens corroded in an aggressive 20 wt% neutral salt spray by Harmsworth (9) and are close to the 75- to 100- μm pit depth measured in naturally corroded specimens by Tuegel and Mills (18). The implications of these observations for predicting the effects of corrosion pitting on fatigue lives are discussed in the next section.

5.2 Effects of Corrosion Damage on Fatigue Life

The measured fatigue lives of the 34 corroded specimens examined in this investigation are shown in Figure 16. The measured lives of bare, noncorroded baseline 7075-T6 specimens are also shown. The life of the noncorroded 7075-T6 specimen at a maximum stress level of 45 ksi, shown as 200,000 cycles, was obtained from Mil-HdBk-5. Consistent with the results of all earlier studies, fatigue life of 7075-T6 is reduced drastically once corrosion damage is present in the specimen surface, as evidenced by the large reduction in life following only 24 hours exposure. After this initial reduction, further corrosion exposure appears to reduce life only little.

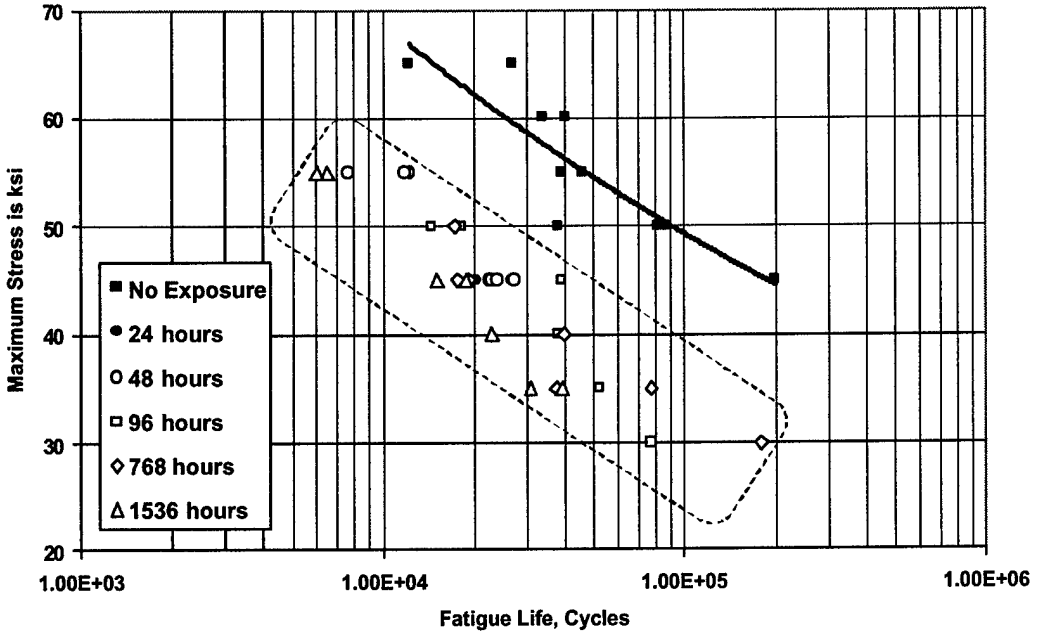

Figure 16. Fatigue Lives of Corroded and Baseline 7075-T6 Specimens

In the investigation by Harmsworth reported by Cole et al. (3), the fatigue lives of 2024-T4 dropped to 30 percent of the life for noncorroded specimens following exposure in a 20 percent neutral salt fog for 4 hours (corresponding to a pit depth of about 25 μm), to less than 20 percent of the life for non-corroded specimens following exposure for 8 hours (corresponding to a pit depth of about 50 μm) and finally to less than 10 percent of the life for noncorroded specimens following exposure for 32 days (corresponding to a pit depth of about 250 μm). Also, as reported by Cole et al. (3), a significant drop in the fatigue life was observed for a lightly pitted 7075-T73 sheet compared with the noncorroded samples, which was further reduced only slightly in heavily pitted specimens.

In the more recent investigation by Tuegel and Mills (18), the fatigue life of 7075-T6 specimens were reduced significantly after natural corrosion exposure for 3 months, with little further reduction upon exposure up to 12 months. These authors attributed the initial reduction of fatigue lives to the formation of an influential pit following which further exposure had only a minor effect on fatigue life. SEM examination of the fracture surface showed that the pits at crack origin were 75 to 100 μm deep, and based on a holistic life assessment, it was suggested that the influential pit should be 100 to 150 μm deep with an aspect ratio of 3:1. The present investigation and that by Harmsworth (9) also show a large reduction of fatigue lives at corrosion damage levels corresponding to much lower measured pit dimensions. Further systematic investigations are necessary to verify and refine the life assessment methods.

6. CONCLUSIONS

The following conclusions can be drawn from the results of the fractographic examination and analysis of broken corrosion fatigue specimens:

- In aluminum alloys with preexisting corrosion pits, fatigue cracks nucleate at pits and start growing immediately upon the application of load in a laboratory air environment. Failure of these specimens is caused by a dominant crack, for which a single crack-nucleating pit can be found in most instances.

- Depending on the extent of surface pitting, secondary cracks may nucleate and grow, but have no influence on the dominant crack or the fatigue lives.

- The measured sizes of the crack-nucleating pits are near those of the largest pits on the precorroded specimen surface, consistent with the expectation that the largest pits would provide the largest initial flaws, which would nucleate the dominant cracks. Depending on the interaction of the various crack fronts, one of these would eventually cause the specimen failure.

- In the range of corrosion exposure levels examined, pitting corrosion causes a significant drop in the fatigue lives of aluminum alloys, even at low levels of corrosion, but reduces life very little with further increase of corrosion damage.

- The nature and rate of reduction of fatigue lives due to pitting damage suggests the possibility of an influential pit. Further investigations are needed to verify and refine the characteristics of such pits.

- The use of fractography to determine the characteristics of crack-nucleating sites has the potential to provide corrosion metrics for development and verification of life-prediction models. For accurate life assessment, fatigue crack growth data at very low crack sizes (about 50 μm) are necessary.

7. REFERENCES

1. "Aging of U.S. Air Force Aircraft," Final Report, Committee on Aging of U.S. Air Force Aircraft, National Materials Advisory Board Commission on Engineering and Technical Systems, National Research Council, National Materials Advisory Board Publication NMAB-488-2, National Academy Press, Washington, D.C., 1997.

2. F. Grimsley, "A Case Study in Corrosion," *Proceedings of the 2001 USAF Aircraft Structural Integrity Program Conference*, December 2001, Williamsburg, VA.

3. G. K. Cole, G. Clark, and P. K. Sharp, "The Implications of Corrosion with Respect to Aircraft Structural Integrity," Aeronautical and Maritime Research Laboratory, Melbourne, Australia, Research Report DSTO-RR-0102, AR-010-199, March 1997.

4. R. Kinzie, "Corrosion in USAF Aging Aircraft Fleets," Paper 16-1, NATO Research and Technology Organization, Applied Vehicle technology Workshop, Corfu, Greece, October 1998.

5. J. N. Scheuring and A. F. Grandt, "Quantification of Corrosion damage Utilizing a Fracture Mechanics Based Methodology," *Proceedings of the 2001 USAF Aircraft Structural Integrity Program Conference*, December 2001, Williamsburg, VA.

6. Y. Kondo, Prediction of Fatigue Crack Initiation Life Based on Pit Growth, Corrosion, 45 (1989) pp 7-11.

7. D. W. Hoeppner, "Model for Prediction of Fatigue Lives based Upon a Pitting Corrosion Fatigue Process," in **Fatigue Mechanisms**, ASTM STP 675, *ASTM*, Philadelphia (1979) pp 841-870.

8. G. C. Chen, K. C. Wan, M. Gao, R. P. Wei, and T. H. Flournoy, "Transition from Pitting to Fatigue Crack Growth - Modeling of Corrosion Fatigue Nucleation in 2024-T3 Aluminum Alloy," *Mat. Sci. Eng.*, A219, 126 (1996) pp 126-132.

9. C.L. Harmsworth, "Effect of Corrosion on the Fatigue Behavior of 2024-t4 Aluminum Alloy," US Air Force Aeronautical Systems Division Technical Report 61-131, July 1961.

10. R. Perez, "Metrics Exploration and Transformation Development for Corrosion/Fatigue," Final Report, Delivery Order 0005, USAF Contract F33615-95-D-3216, November 1996.

11. G. H. Bray, R. J. Bucci, E. L. Colvin, and M. Kulak, "Effects of Prior Corrosion on the S/N Fatigue Performance of Aluminum Alloys 2024-T3 and 2524-T3," **Effects of**

Environment on the Initiation of Crack Growth, ASTM STP 1298, *ASTM*, Philadelphia (1997) pp 89-103.

12. K.K. Sankaran, "Validation of Accelerated Corrosion Tests for Aging Aircraft Life Prediction: Effects of Pitting Corrosion on the Mechanical Behavior of 7075-T6 Aluminum Alloys," Final Report, Air Force Contract F33615-96-D-5835, Delivery Order 0026-02, 1998.

13. K. K. Sankaran, R. Perez, and K. V. Jata, "Effects of Pitting Corrosion on the Fatigue Behavior of Aluminum Alloy 7075-T6: Modeling and Experimental Studies," *Mat. Sci. and Eng.*, A297 (2001) pp. 223-229.

14. P. Shi and S. Mahadevan, "Probabilistic Estimation of Pitting Corrosion Fatigue Life," 41st AIAA/ASME/ASCE/ASC Structures, Structural Dynamics, and Materials Conference, April 2000, Atlanta, GA.

15. K. J. Miller, "Materials Science Perspective of Metal Fatigue Resistance," *Mat. Sci. Tech.*, 9 (1993) pp 453-462.

16. J. A. Harter, "AFGROW Users Guide and Technical Manual," Report AFRL-VA-WP-TR-1999-3016, US Air Force, WPAFB, Ohio (1999).

17. H. Smith, Jr., R. Perez, K. K. Sankaran, P. Hoffman, and M. Hoffman, "The Effects of Corrosion on Fatigue Life – A Non-Deterministic Approach," American Institute Of Aeronautics And Astronautics (2001) Paper 2001-1376.

18. E. J. Tuegel and T. B. Mills, "Correlation of Holistic Structural Assessment Method with Corrosion-Fatigue Experiments," *Proceedings of the 6th Joint FAA/DoD/NASA Conference on Aging Aircraft*, September 2002, San Francisco, CA.

APPENDIX

Photographs documenting the detailed fractographic evaluation of the 34 specimens are shown in Figures A-1 through A-68. Each specimen has two corresponding figures, one describing the crack nucleation site and the other showing the crack growth and striations.

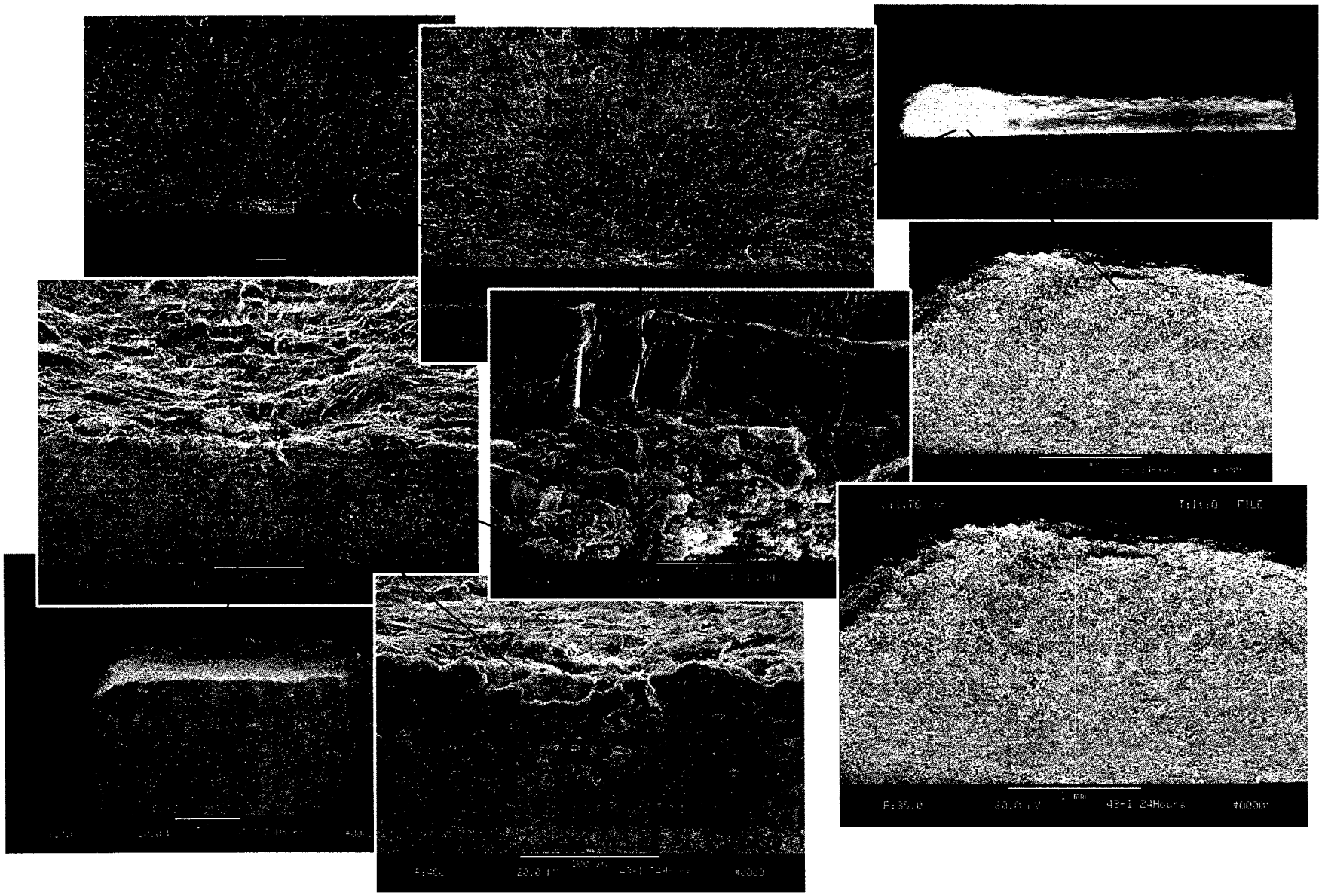

Figure A-1. Specimen 43-1

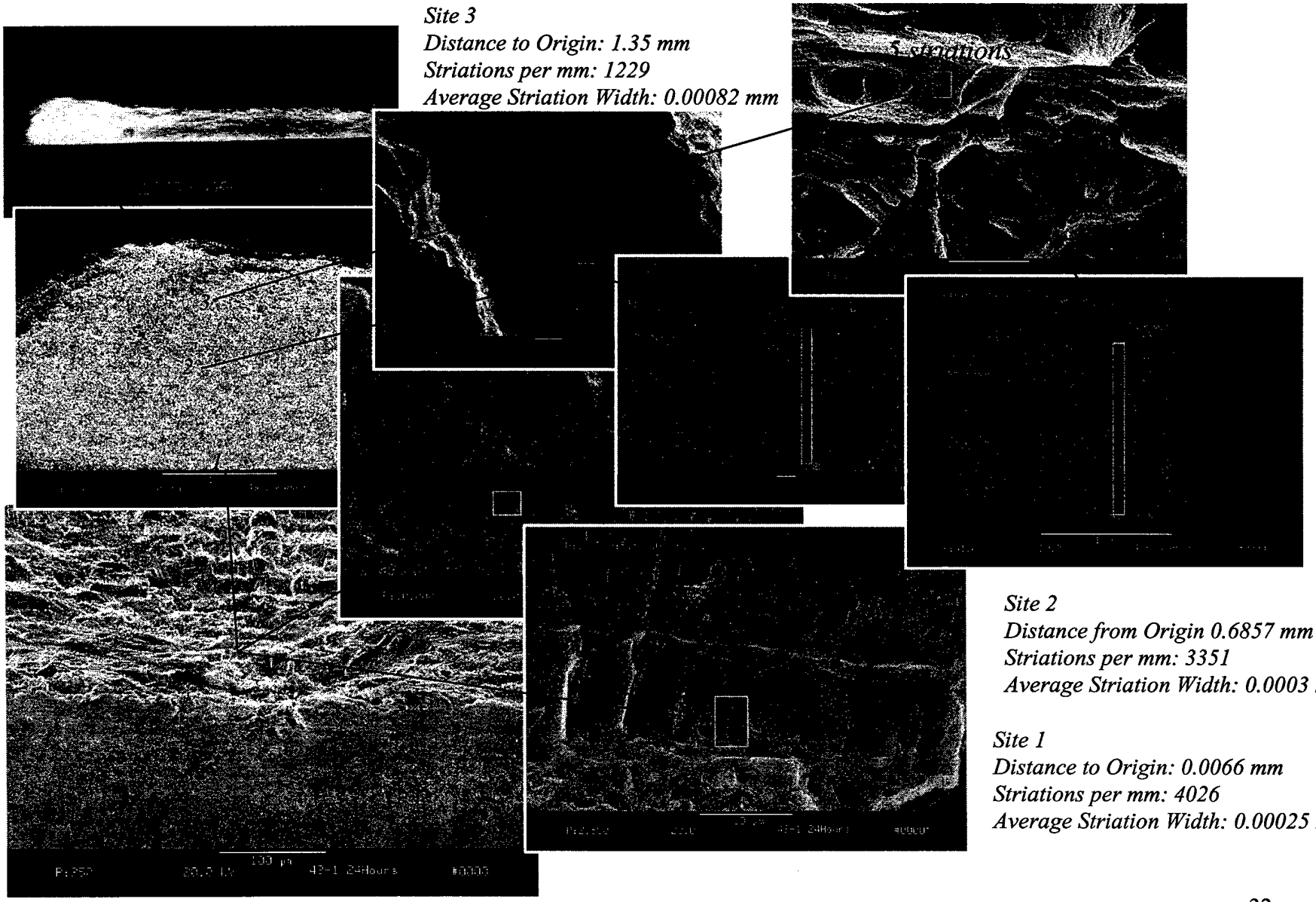

Site 3
Distance to Origin: 1.35 mm
Striations per mm: 1229
Average Striation Width: 0.00082 mm

Site 2
Distance from Origin 0.6857 mm
Striations per mm: 3351
Average Striation Width: 0.0003 mm

Site 1
Distance to Origin: 0.0066 mm
Striations per mm: 4026
Average Striation Width: 0.00025 mm

Figure A-2. Specimen 43-1

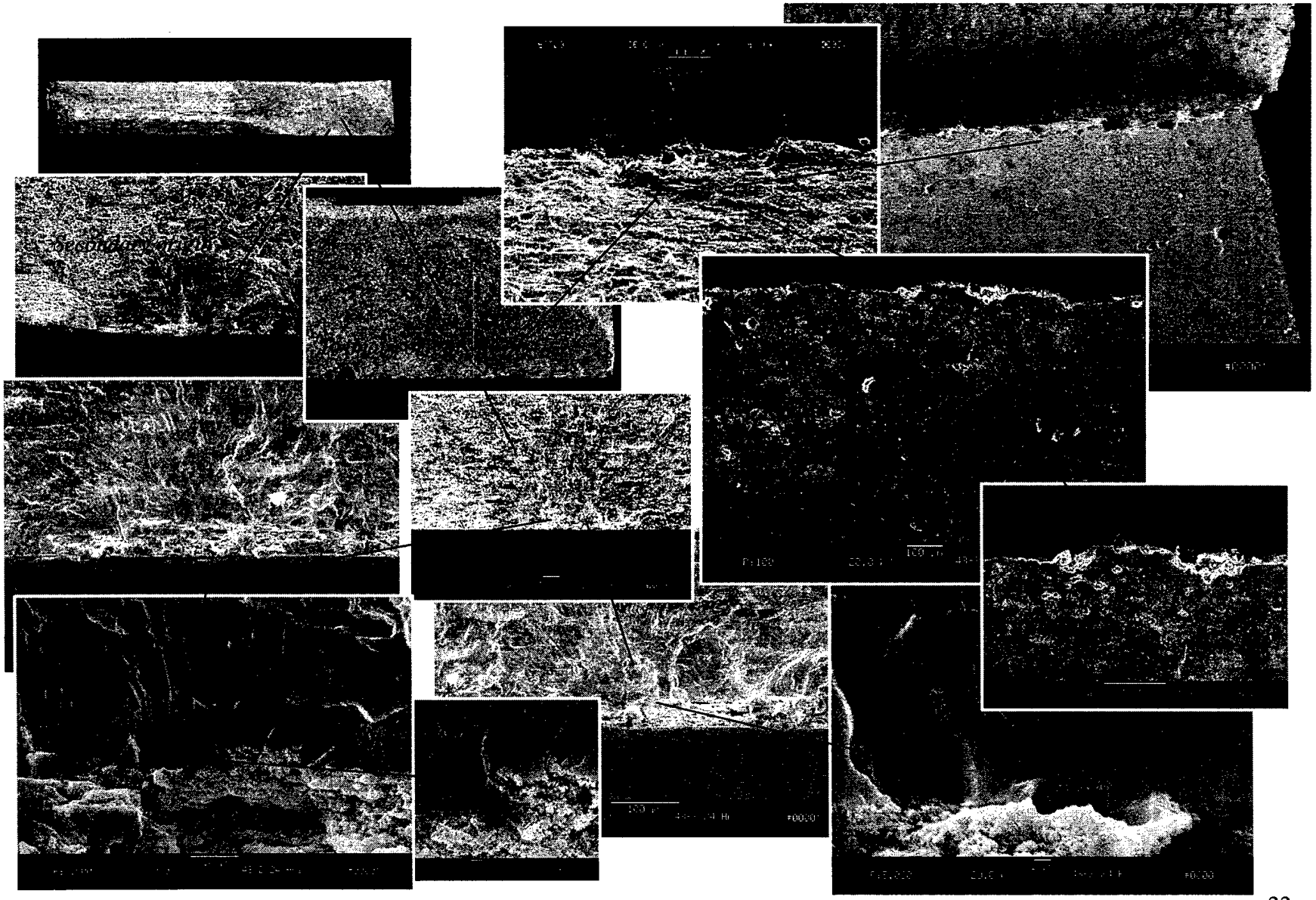

Figure A-3. Specimen 43-2

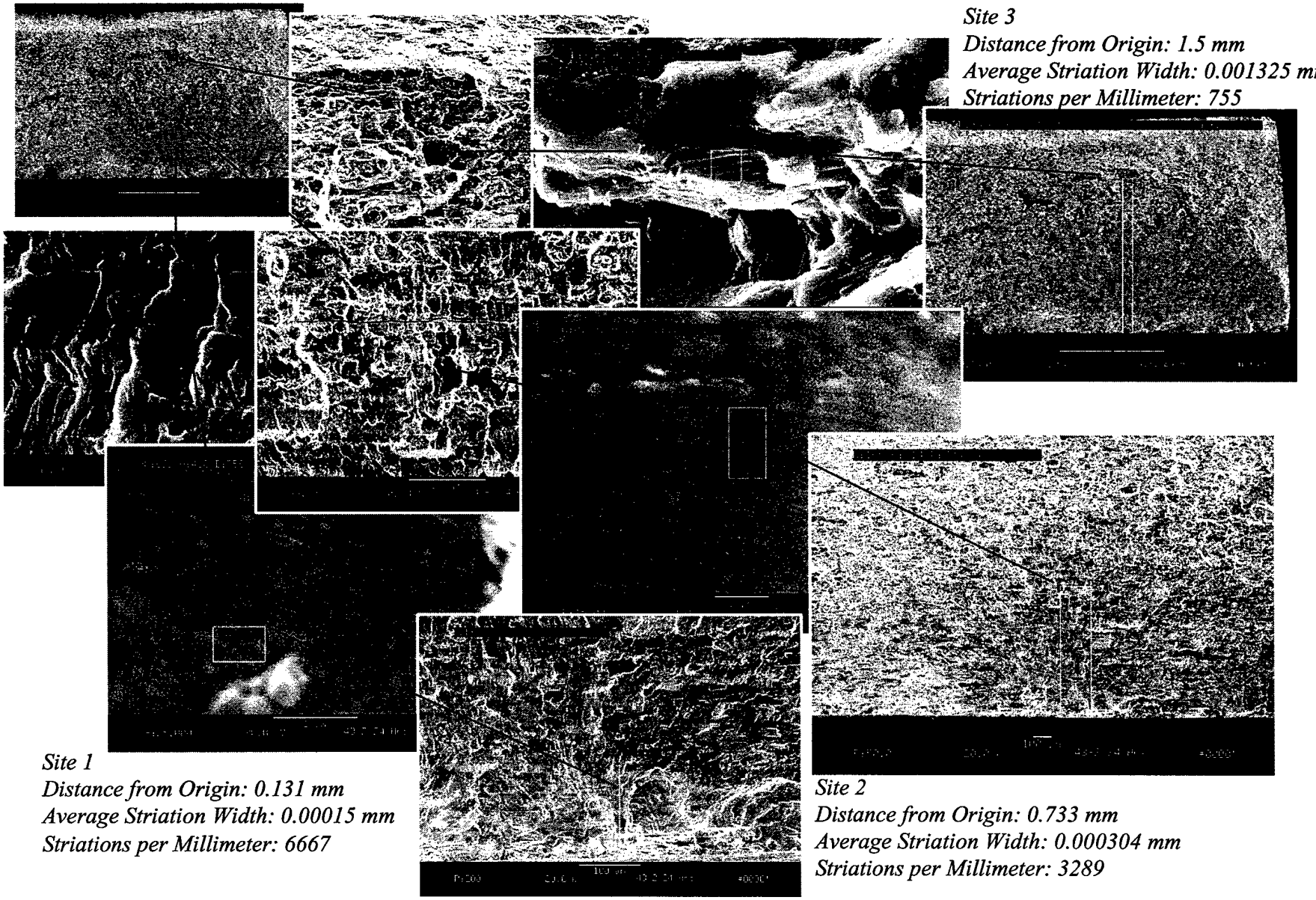

Site 3
Distance from Origin: 1.5 mm
Average Striation Width: 0.001325 mm
Striations per Millimeter: 755

Site 1
Distance from Origin: 0.131 mm
Average Striation Width: 0.00015 mm
Striations per Millimeter: 6667

Site 2
Distance from Origin: 0.733 mm
Average Striation Width: 0.000304 mm
Striations per Millimeter: 3289

Figure A-4. Specimen 43-2

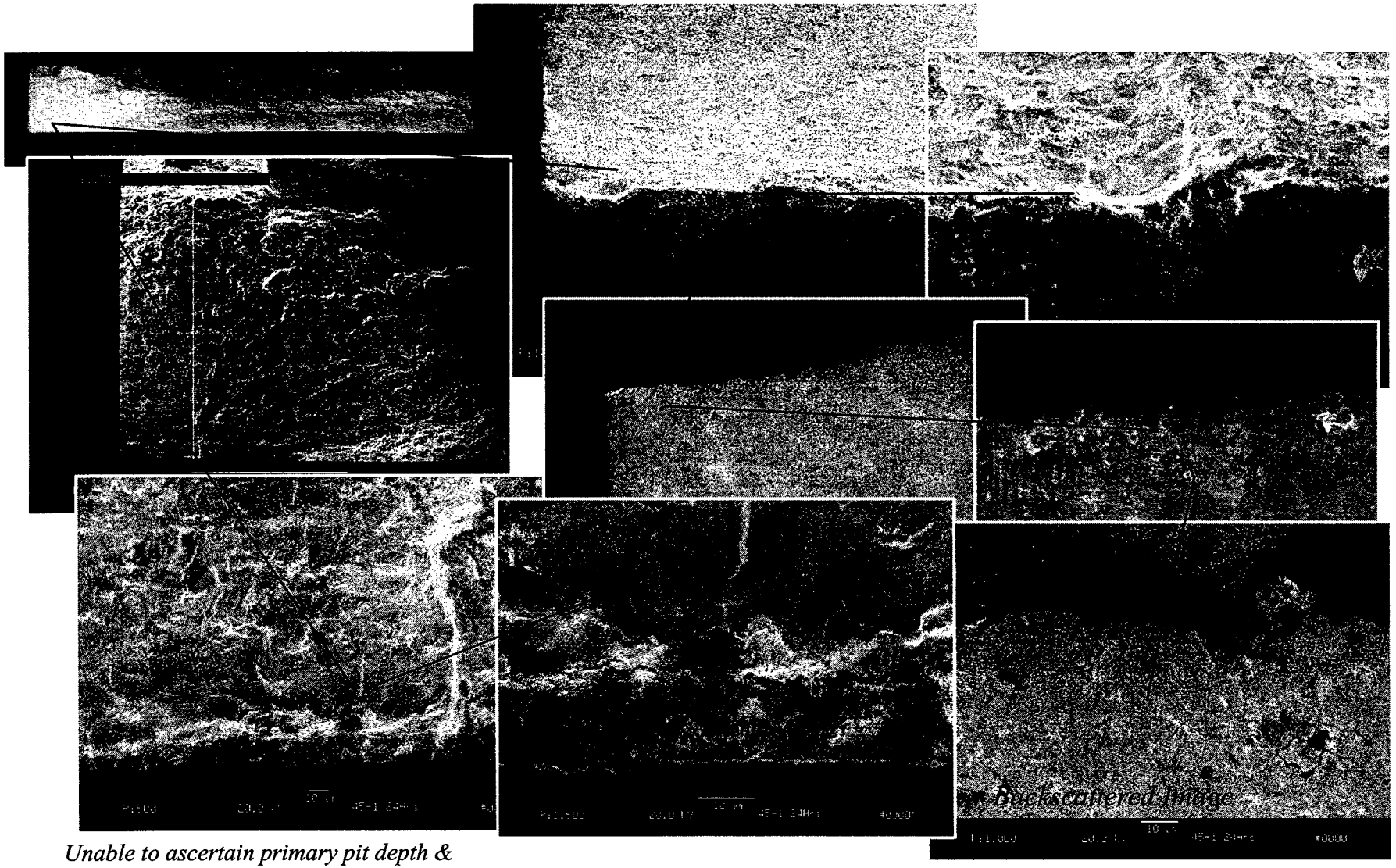

Unable to ascertain primary pit depth & primary pit length. Minimal corrosion at origin.

Figure A-5. Specimen 45-1

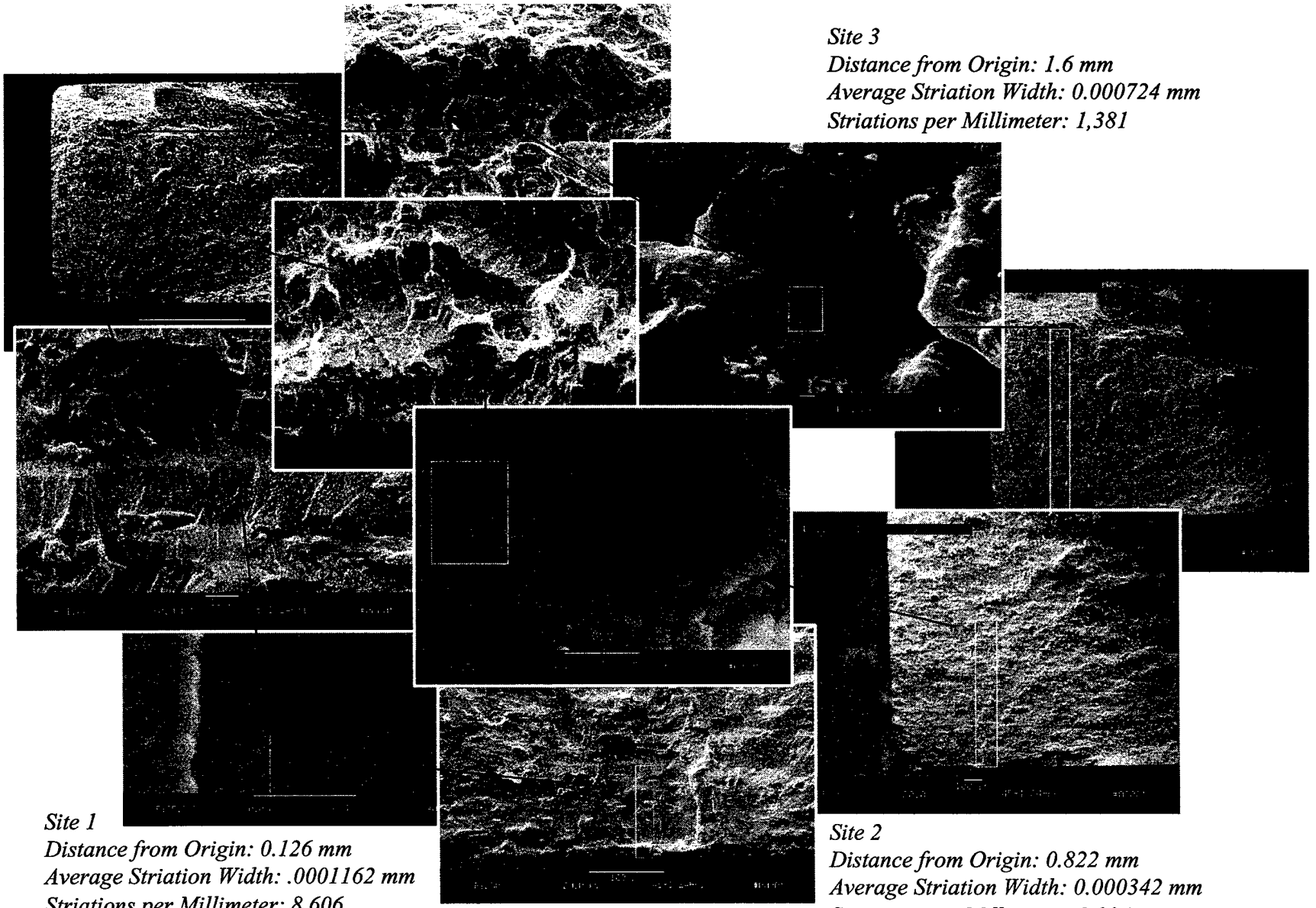

Site 3
Distance from Origin: 1.6 mm
Average Striation Width: 0.000724 mm
Striations per Millimeter: 1,381

Site 1
Distance from Origin: 0.126 mm
Average Striation Width: .0001162 mm
Striations per Millimeter: 8,606

Site 2
Distance from Origin: 0.822 mm
Average Striation Width: 0.000342 mm
Striations per Millimeter: 2,924

Figure A-6. Specimen 45-1

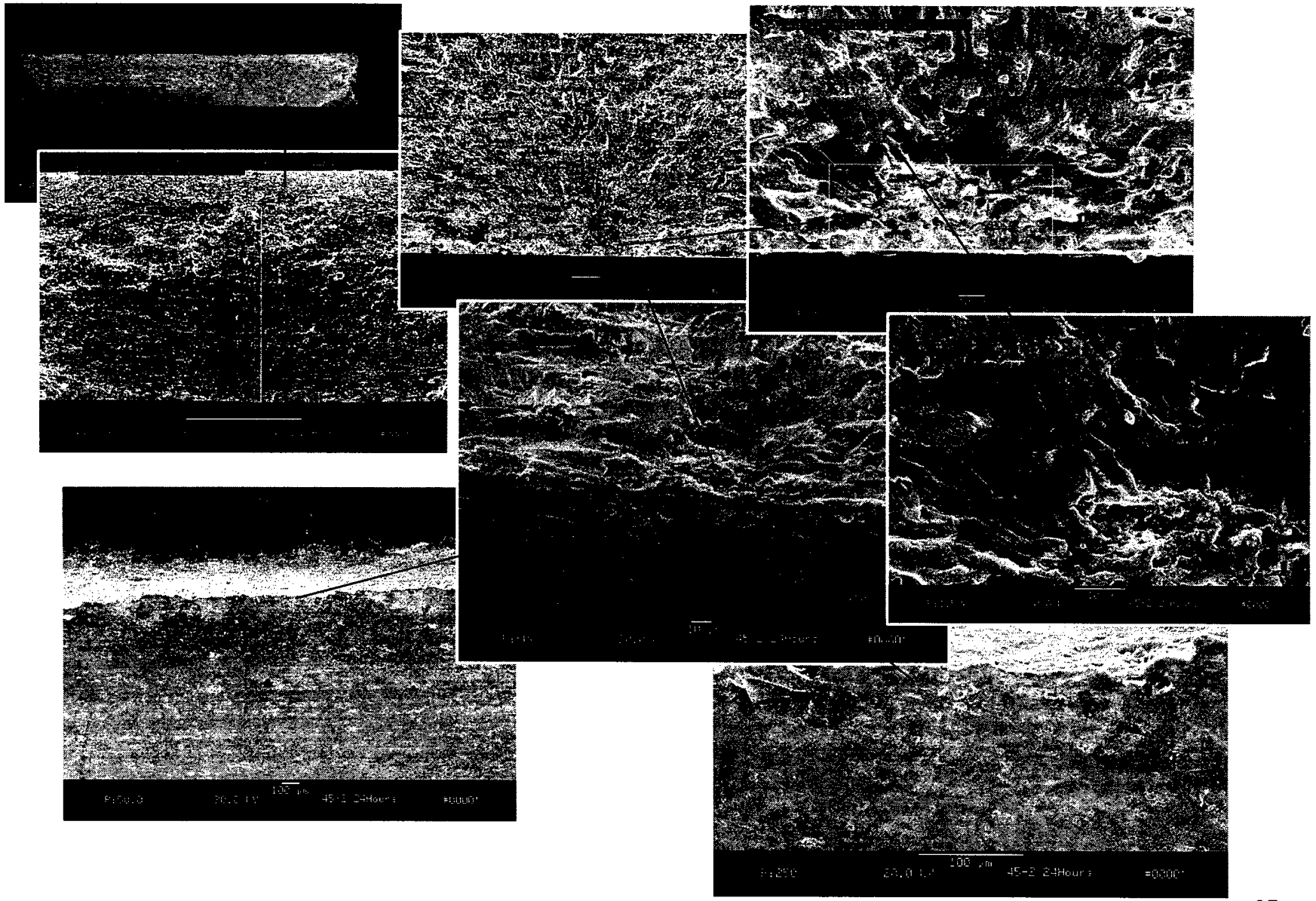

Figure A-7. Specimen 45-2

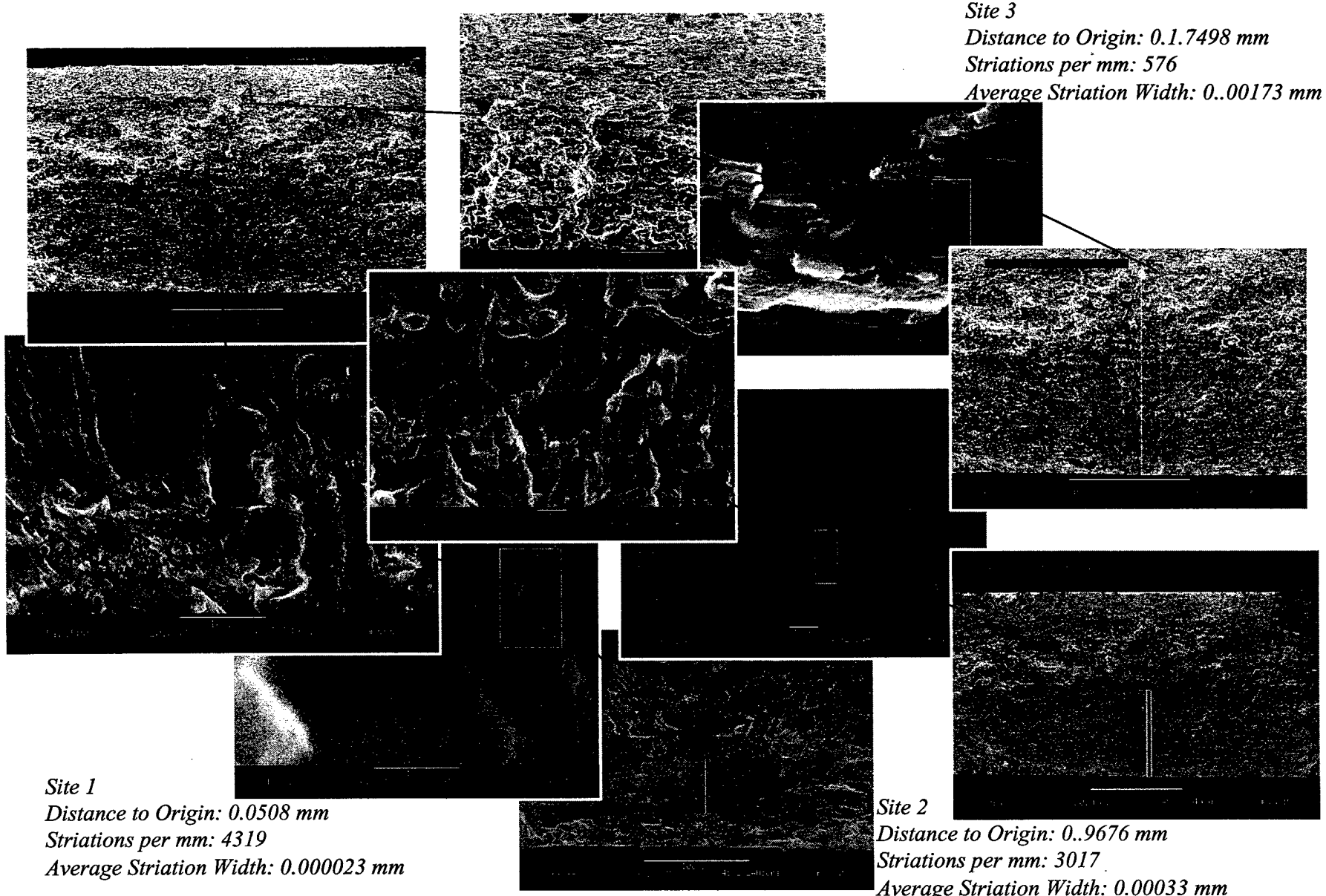

Site 3
Distance to Origin: 0.1.7498 mm
Striations per mm: 576
Average Striation Width: 0..00173 mm

Site 1
Distance to Origin: 0.0508 mm
Striations per mm: 4319
Average Striation Width: 0.000023 mm

Site 2
Distance to Origin: 0..9676 mm
Striations per mm: 3017
Average Striation Width: 0.00033 mm

Figure A-8. Specimen 45-2

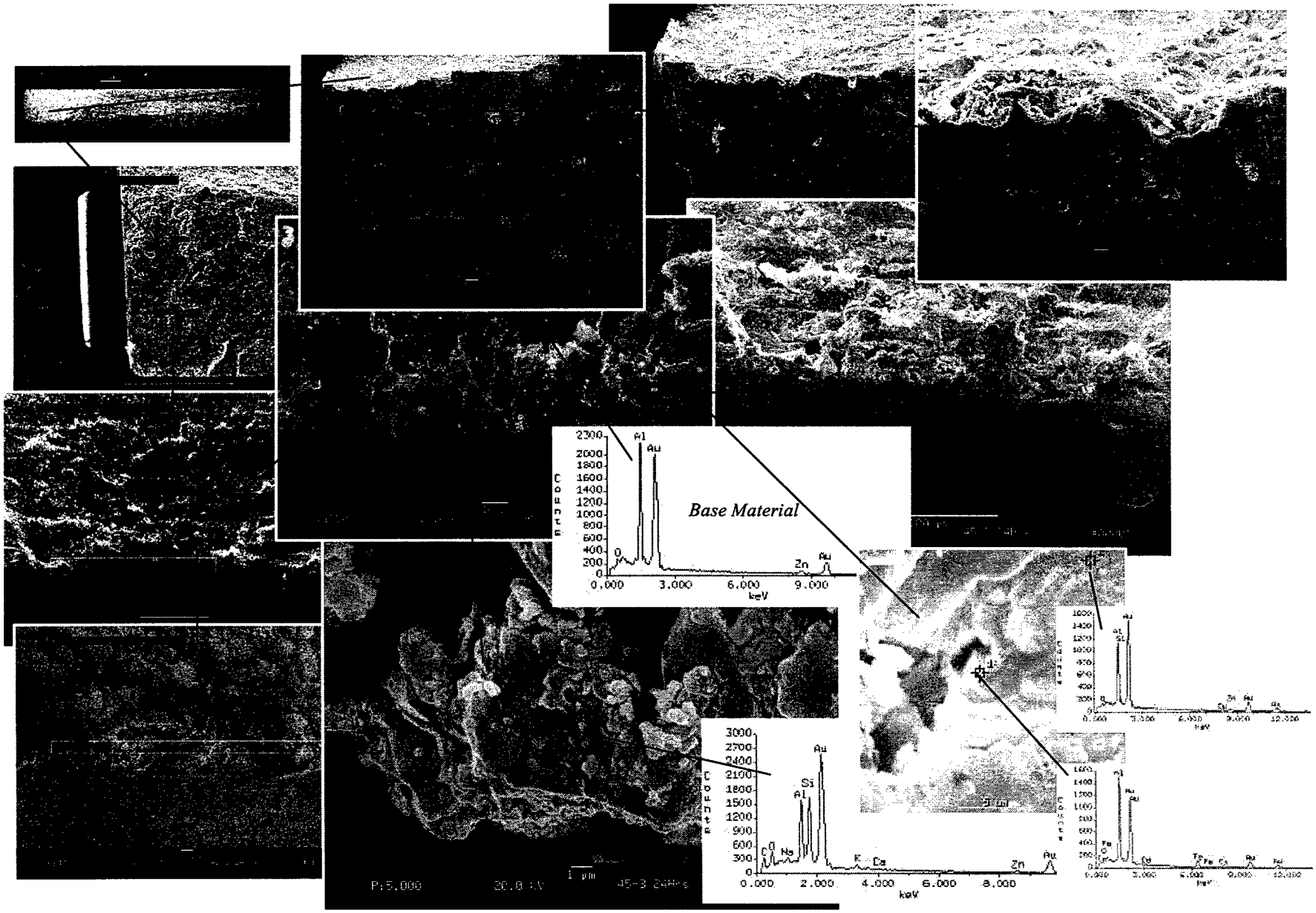

Figure A-9. Specimen 45-3

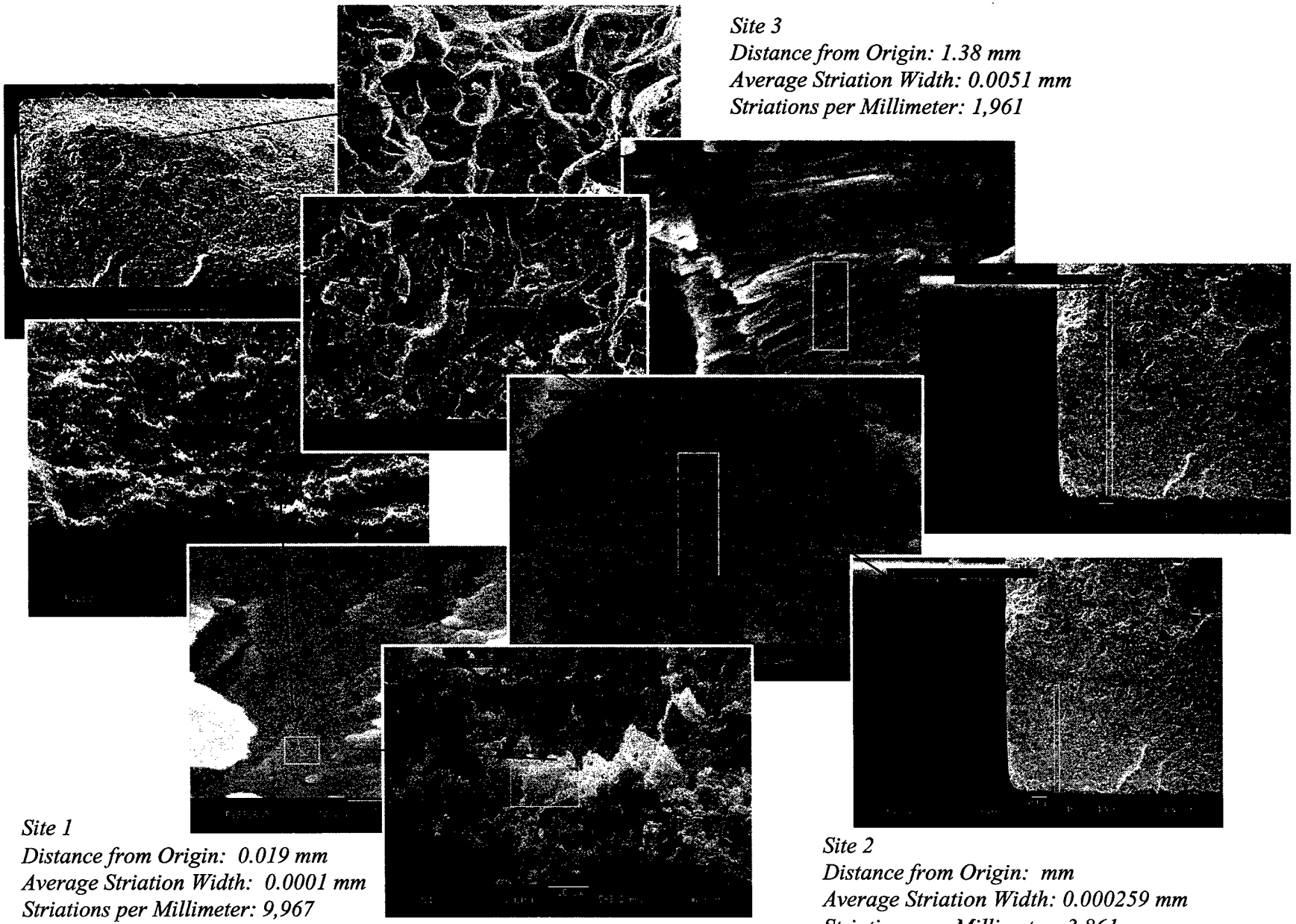

Site 3
Distance from Origin: 1.38 mm
Average Striation Width: 0.0051 mm
Striations per Millimeter: 1,961

Site 1
Distance from Origin: 0.019 mm
Average Striation Width: 0.0001 mm
Striations per Millimeter: 9,967

Site 2
Distance from Origin: mm
Average Striation Width: 0.000259 mm
Striations per Millimeter: 3,861

Figure A-10. Specimen 45-3

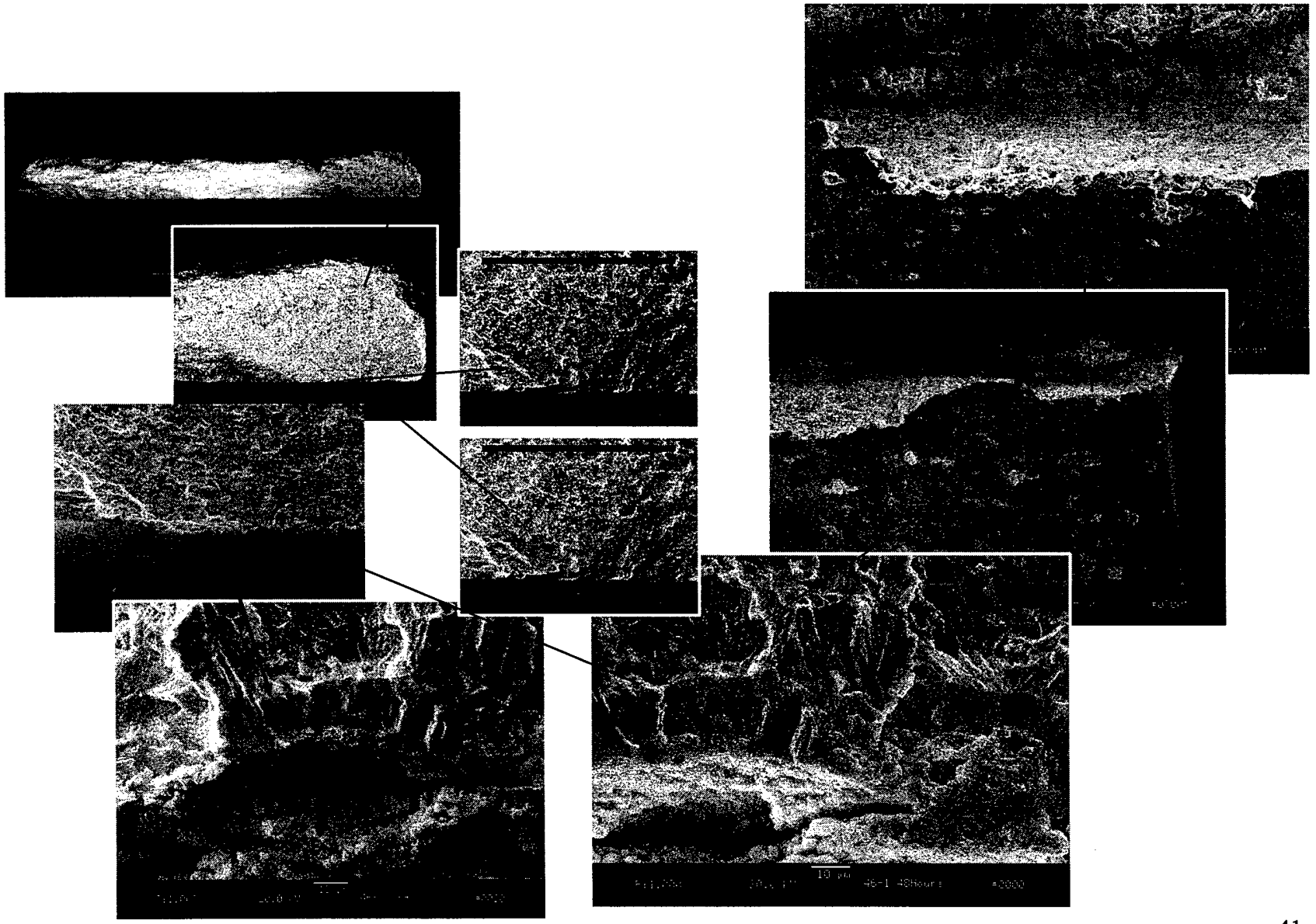

Figure A-11. Specimen 46-1

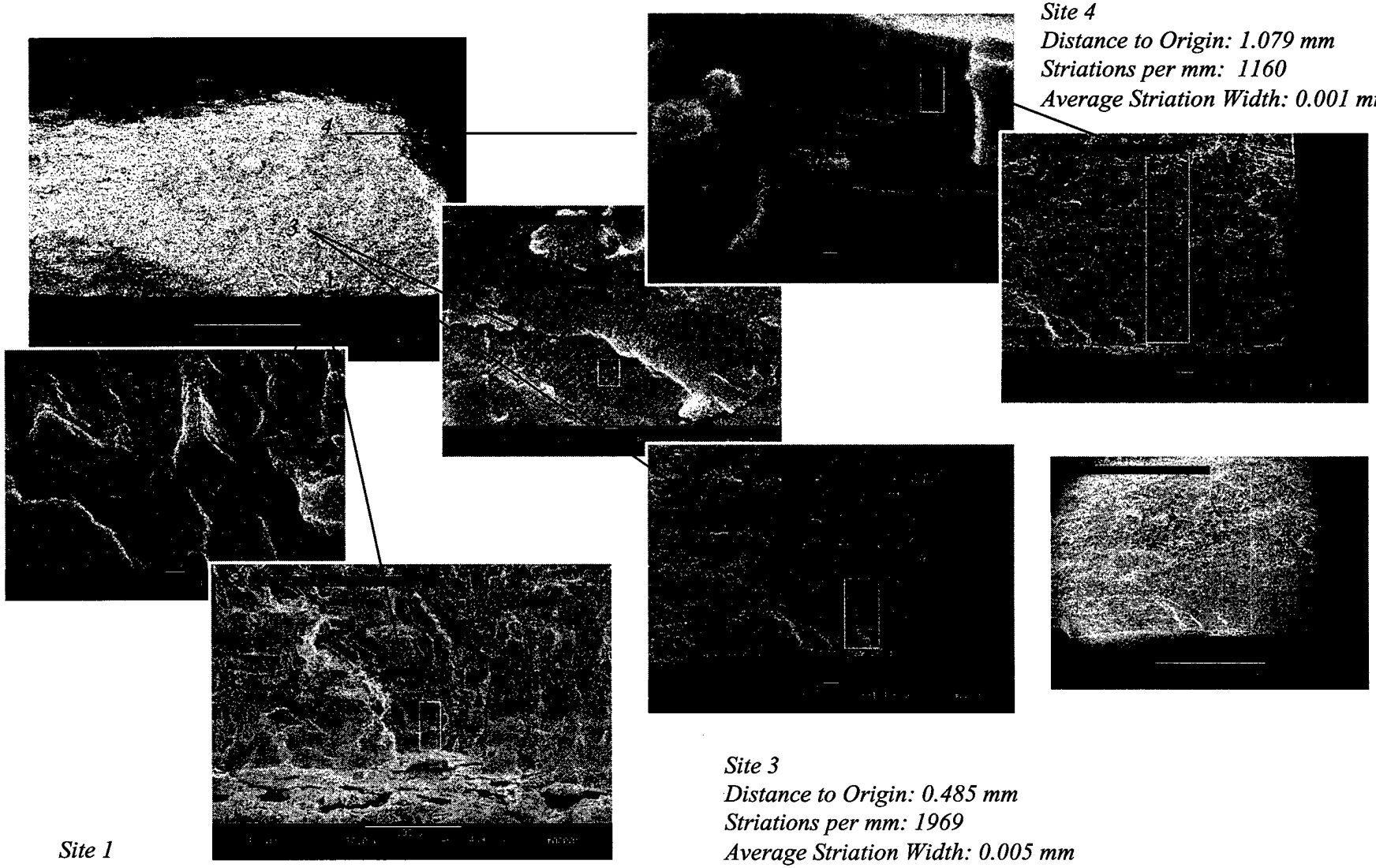

Site 4
Distance to Origin: 1.079 mm
Striations per mm: 1160
Average Striation Width: 0.001 mm

Site 3
Distance to Origin: 0.485 mm
Striations per mm: 1969
Average Striation Width: 0.005 mm

Site 1
Distance to Origin: 0.00558 mm
Striations per mm: 3706
Average Striation Width: 0.00027 mm

Figure A-12. Specimen 46-1

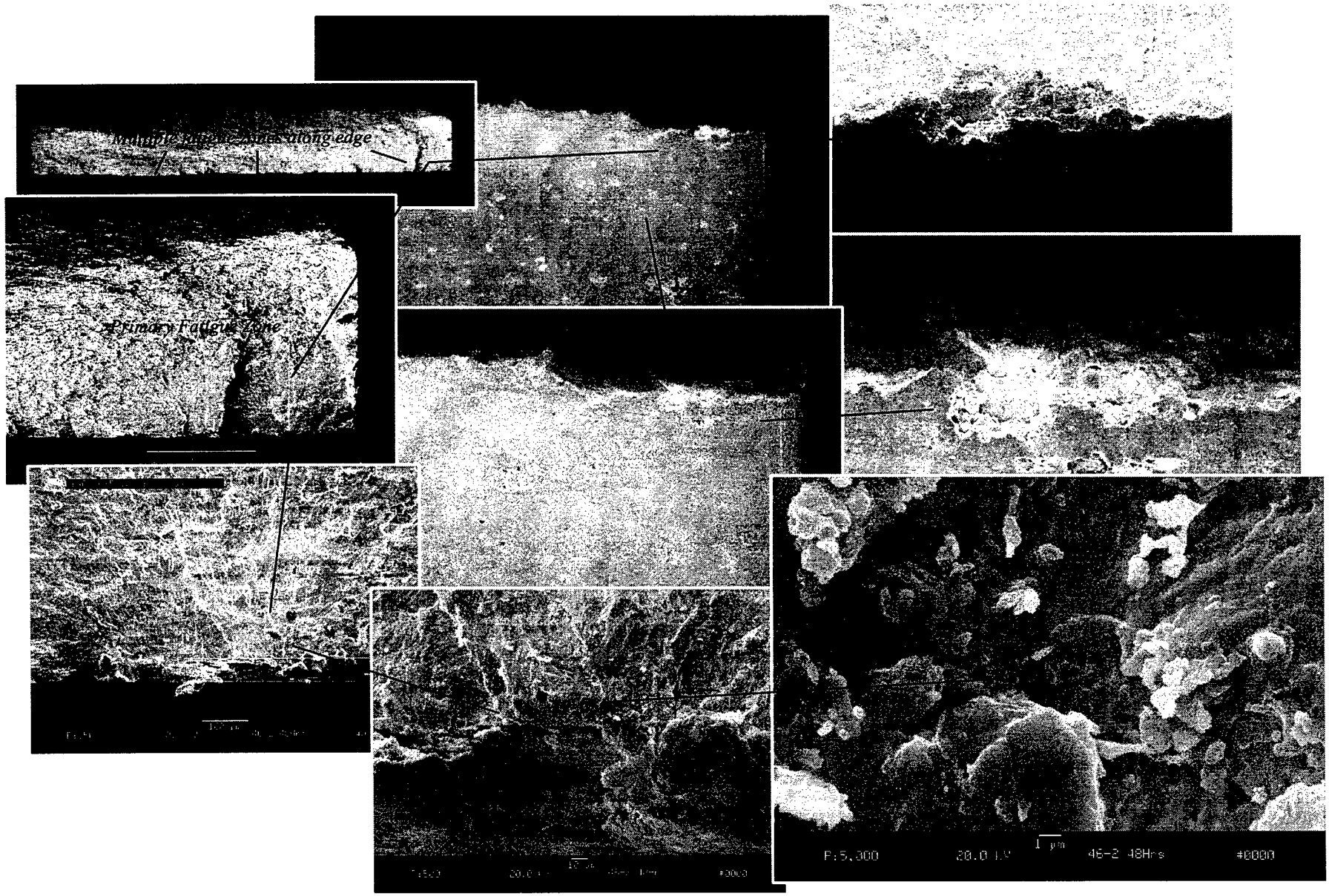

Figure A-13. Specimen 46-2

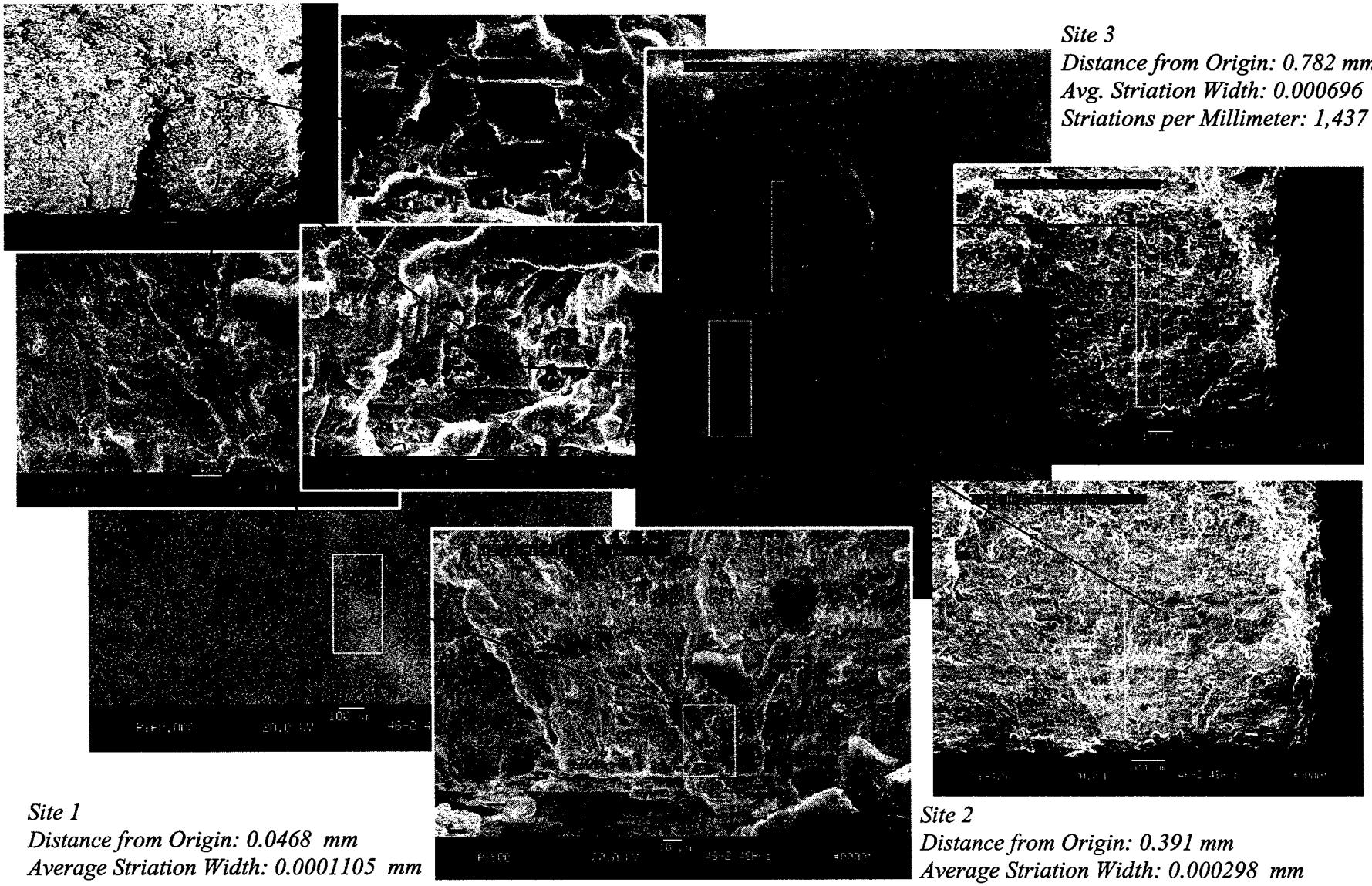

Site 3
Distance from Origin: 0.782 mm
Avg. Striation Width: 0.000696 mm
Striations per Millimeter: 1,437

Site 1
Distance from Origin: 0.0468 mm
Average Striation Width: 0.0001105 mm
Striations per Millimeter: 9,050

Site 2
Distance from Origin: 0.391 mm
Average Striation Width: 0.000298 mm
Striations per Millimeter: 3,356

Figure A-14. Specimen 46-2

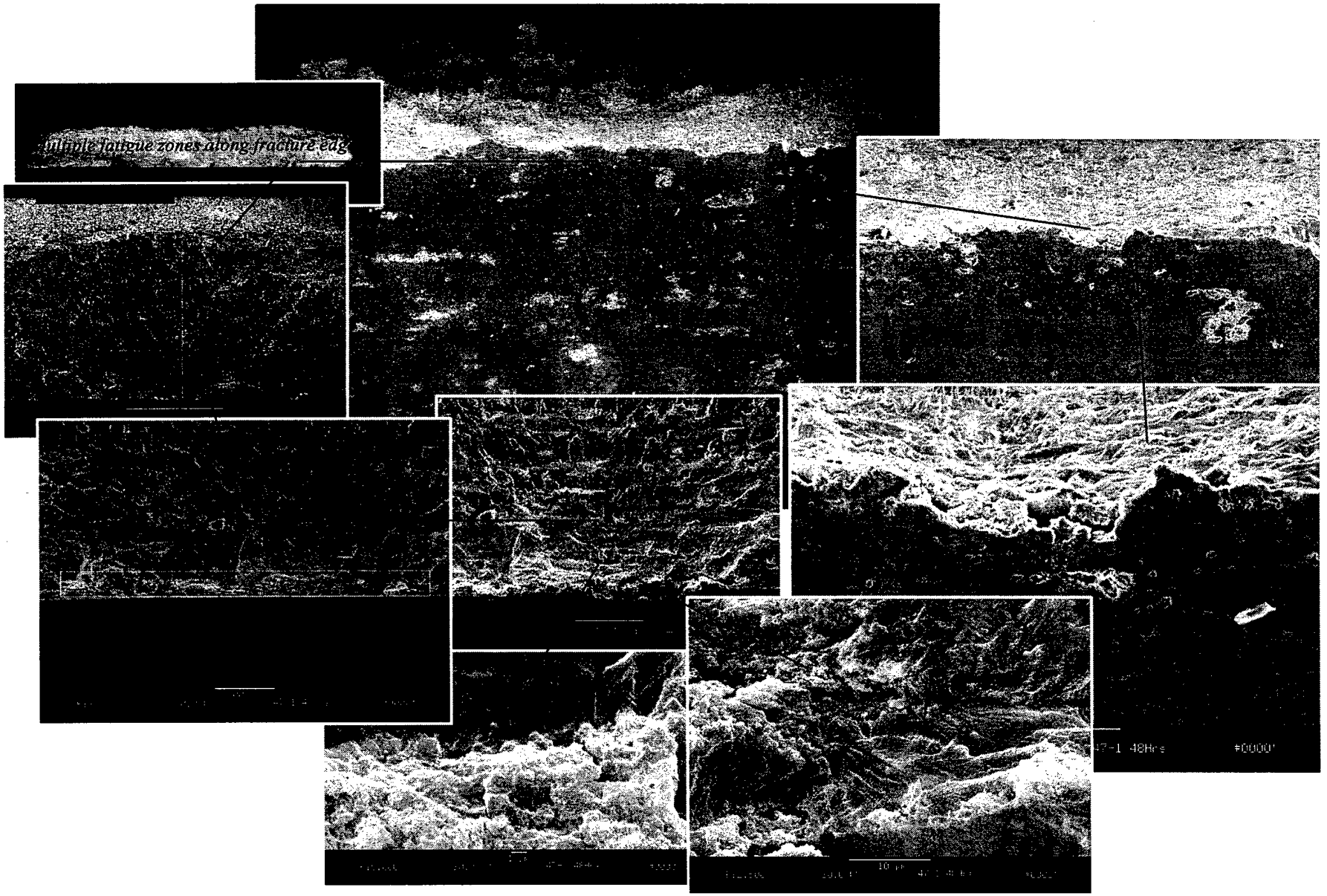

Figure A-15. Specimen 47-1

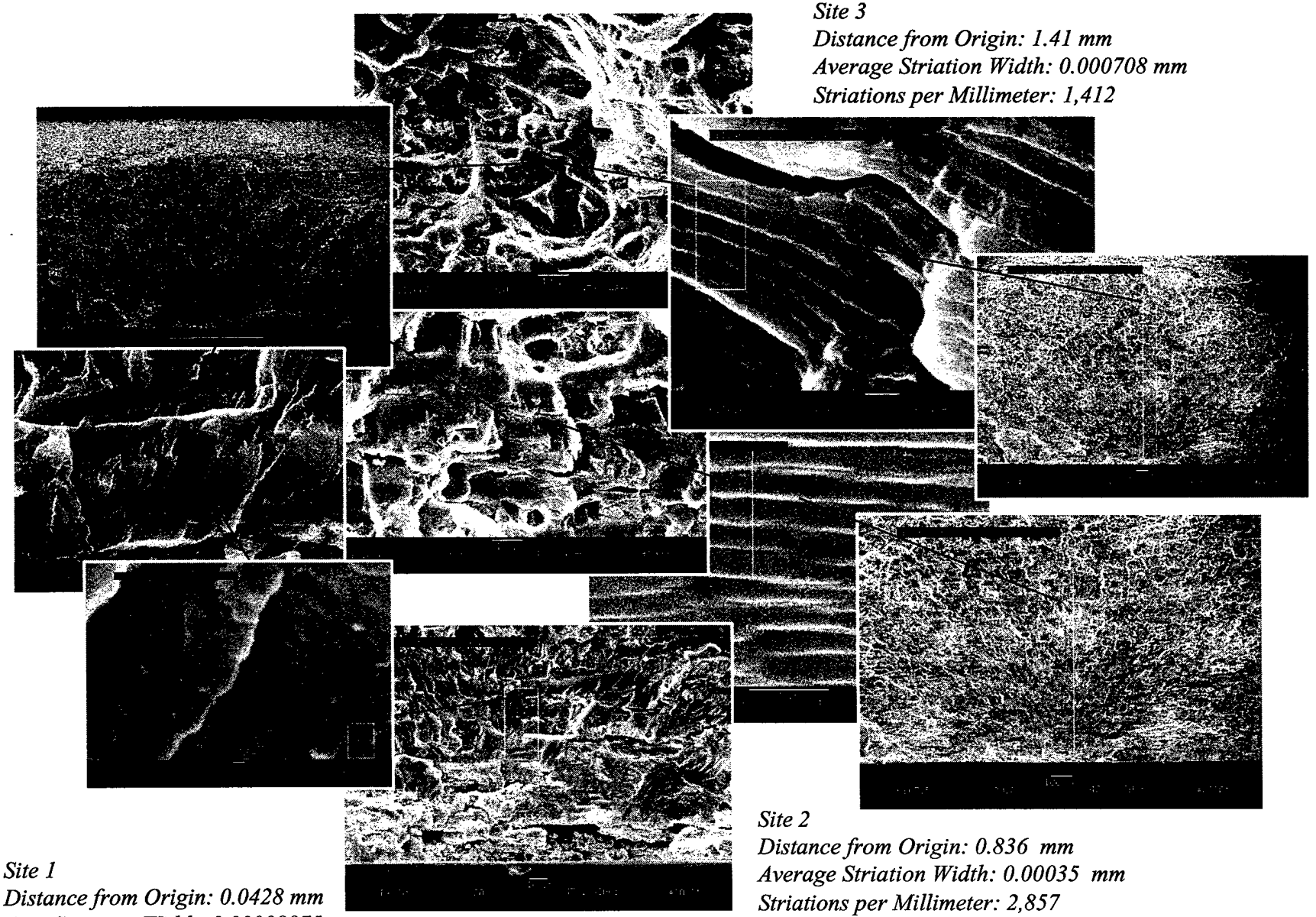

Site 3
Distance from Origin: 1.41 mm
Average Striation Width: 0.000708 mm
Striations per Millimeter: 1,412

Site 2
Distance from Origin: 0.836 mm
Average Striation Width: 0.00035 mm
Striations per Millimeter: 2,857

Site 1
Distance from Origin: 0.0428 mm
Avg. Striation Width: 0.00008975 mm
Striations per Millimeter: 11,142

Figure A-16. Specimen 47-1

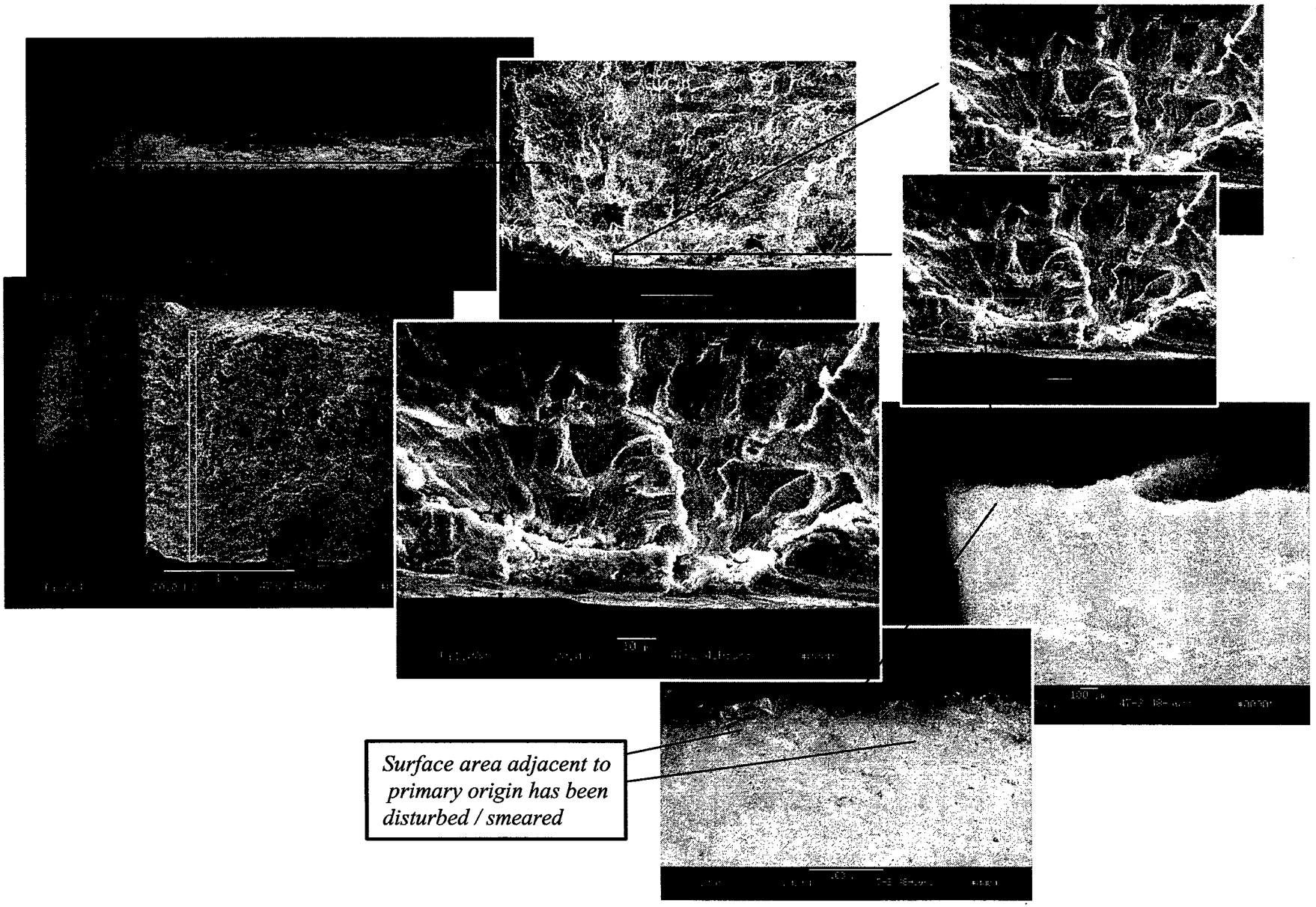

Figure A-17. Specimen 47-2

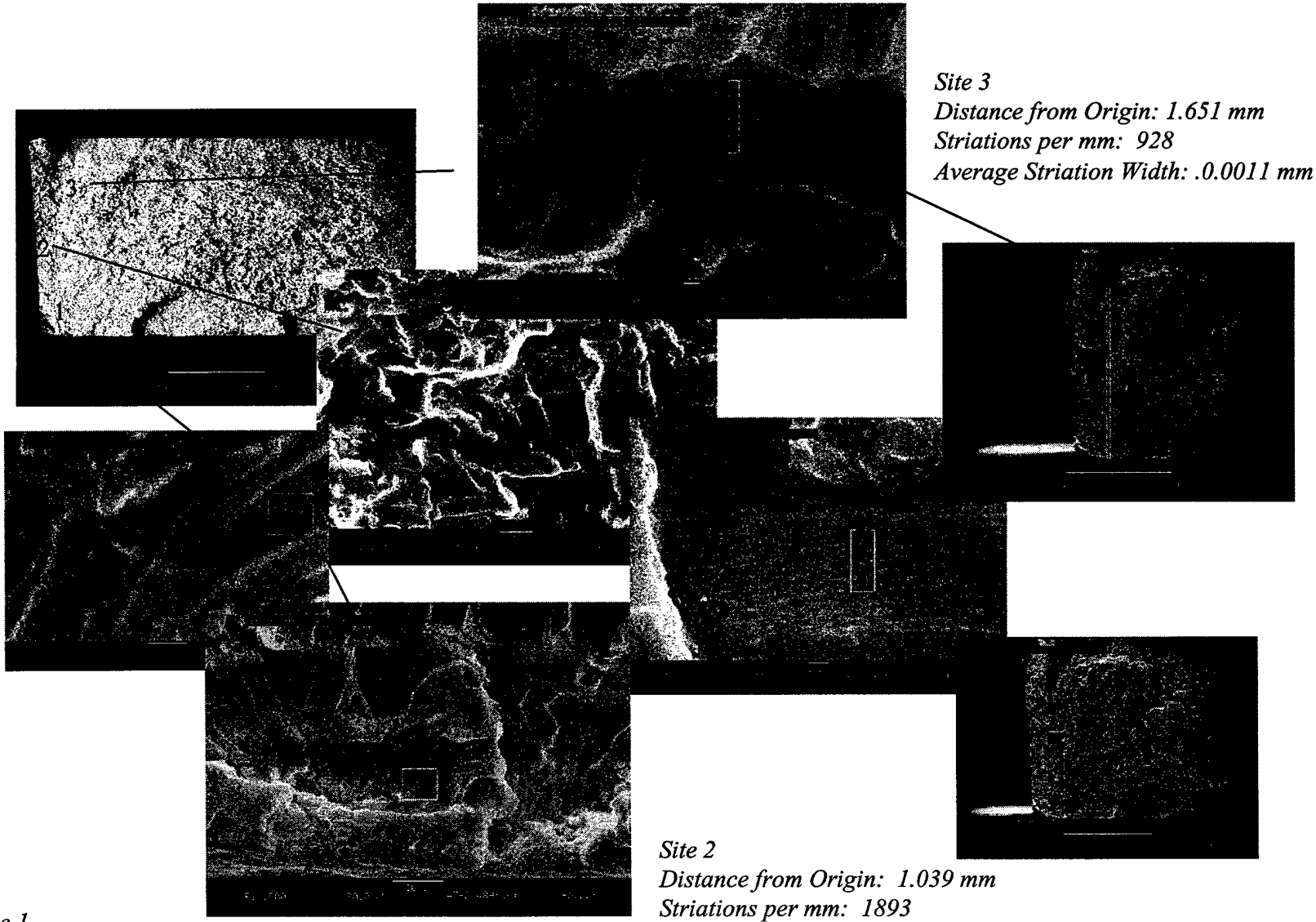

Site 3
Distance from Origin: 1.651 mm
Striations per mm: 928
Average Striation Width: .0.0011 mm

Site 2
Distance from Origin: 1.039 mm
Striations per mm: 1893
Average Striation Width: 0.00052 mm

Site 1
Distance to Origin: 0.0102 mm
Striations per mm: 3186
Average Striation Width: 0.0003 mm

Figure A-18. Specimen 47-2

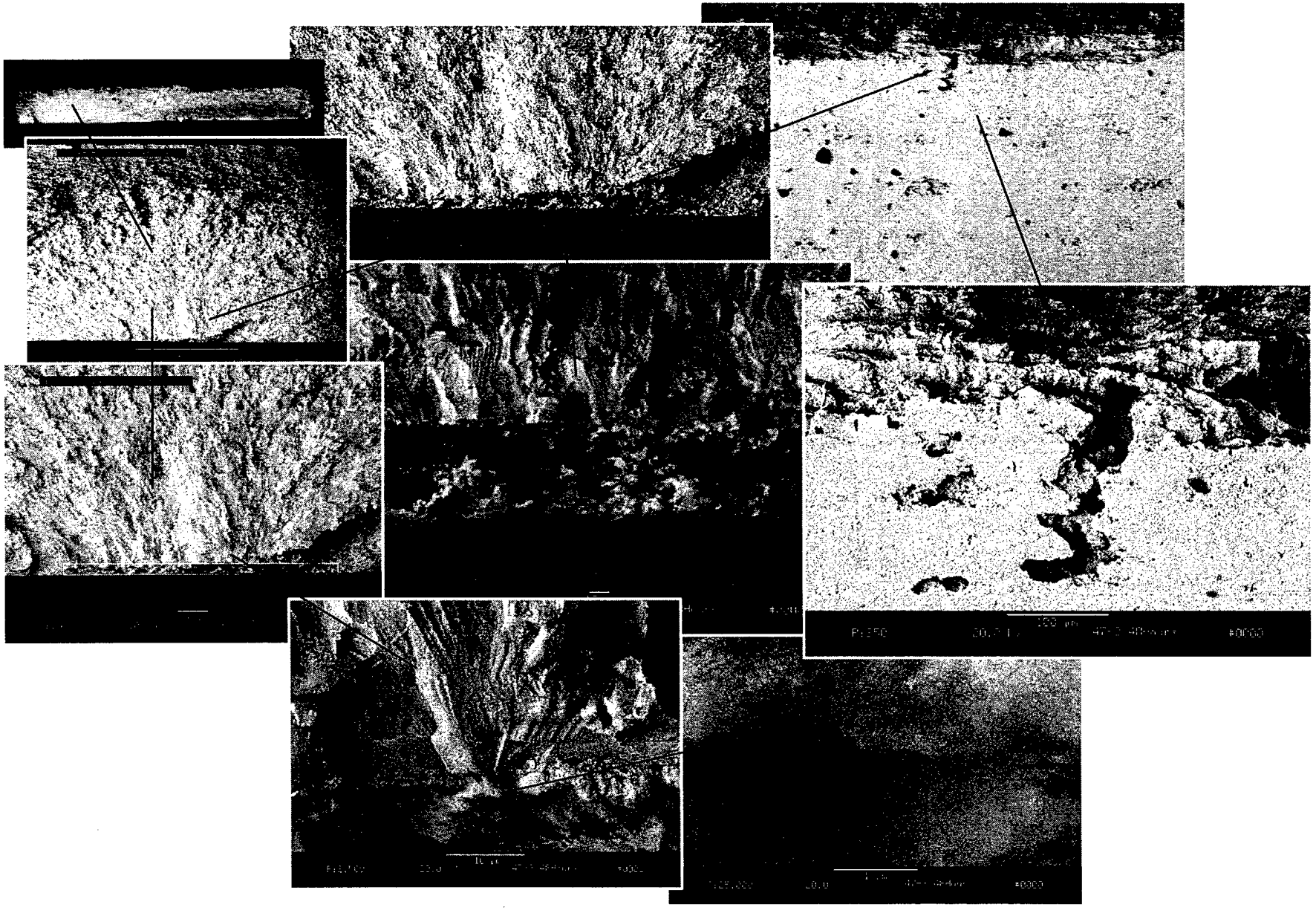

Figure A-19. Specimen 47-3

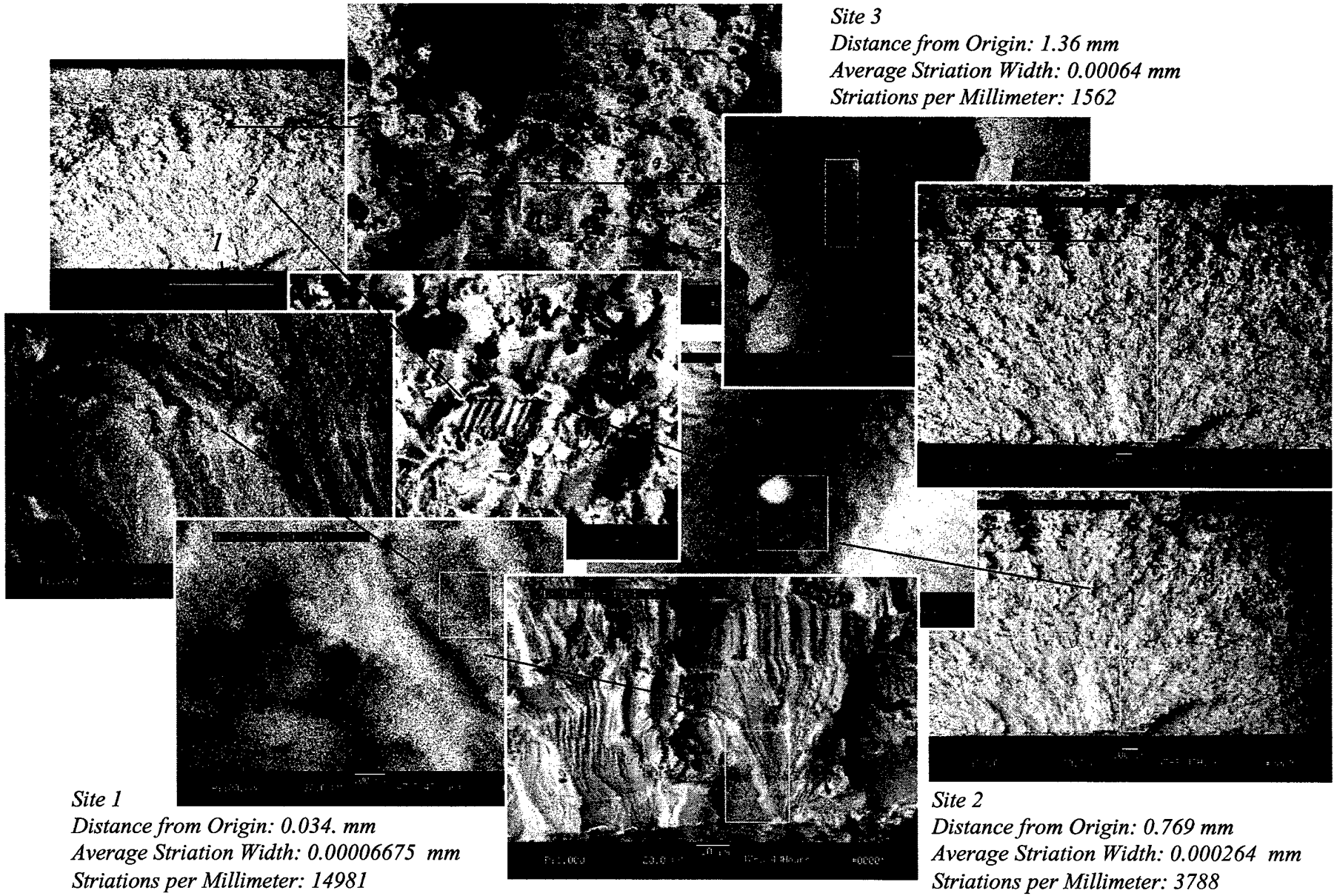

Site 3
Distance from Origin: 1.36 mm
Average Striation Width: 0.00064 mm
Striations per Millimeter: 1562

Site 1
Distance from Origin: 0.034. mm
Average Striation Width: 0.00006675 mm
Striations per Millimeter: 14981

Site 2
Distance from Origin: 0.769 mm
Average Striation Width: 0.000264 mm
Striations per Millimeter: 3788

Figure A-20. Specimen 47-3

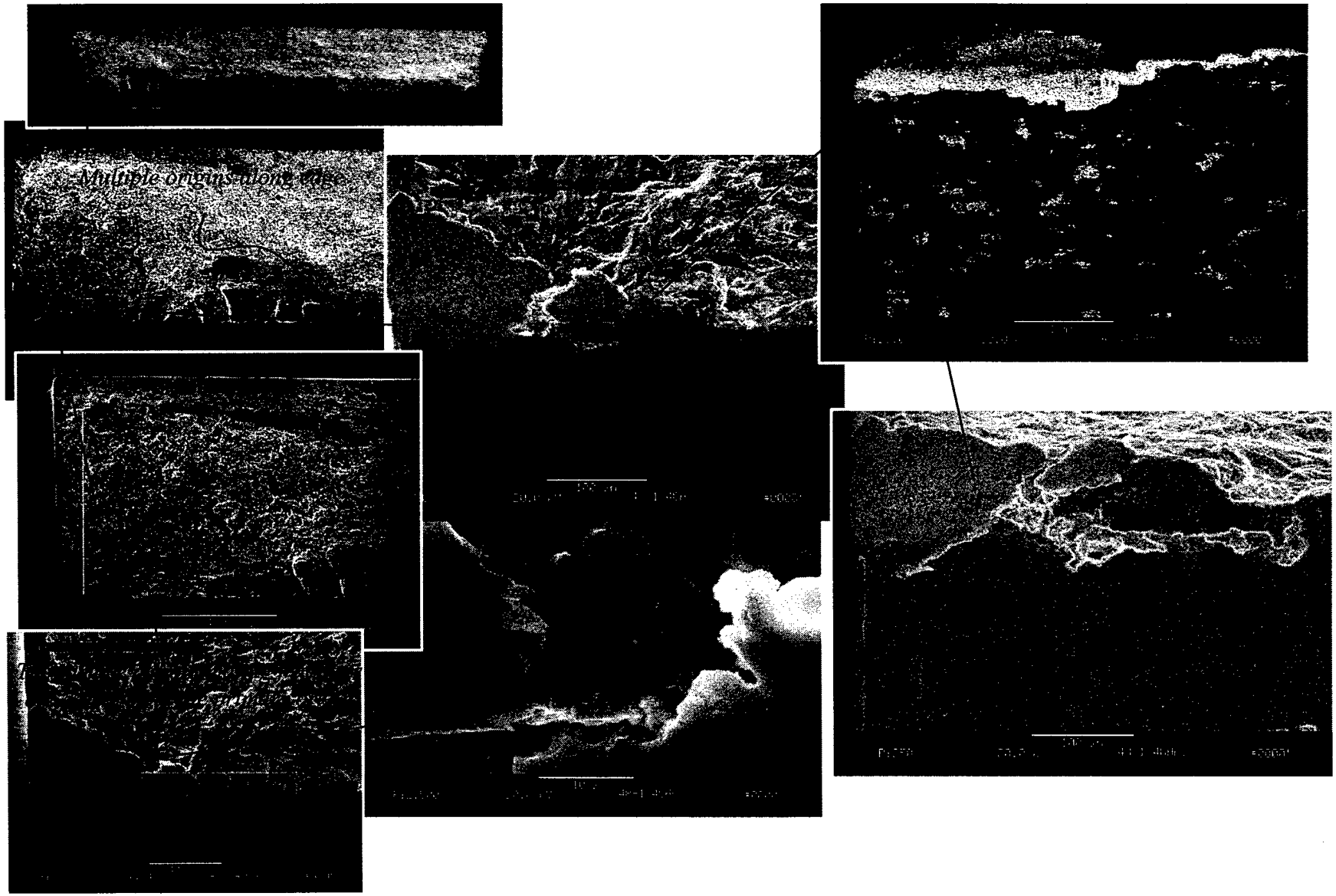

Note: Due to damage at origin, only visible section of pit was used to determine it 's length.

Figure A-21. Specimen 48-1

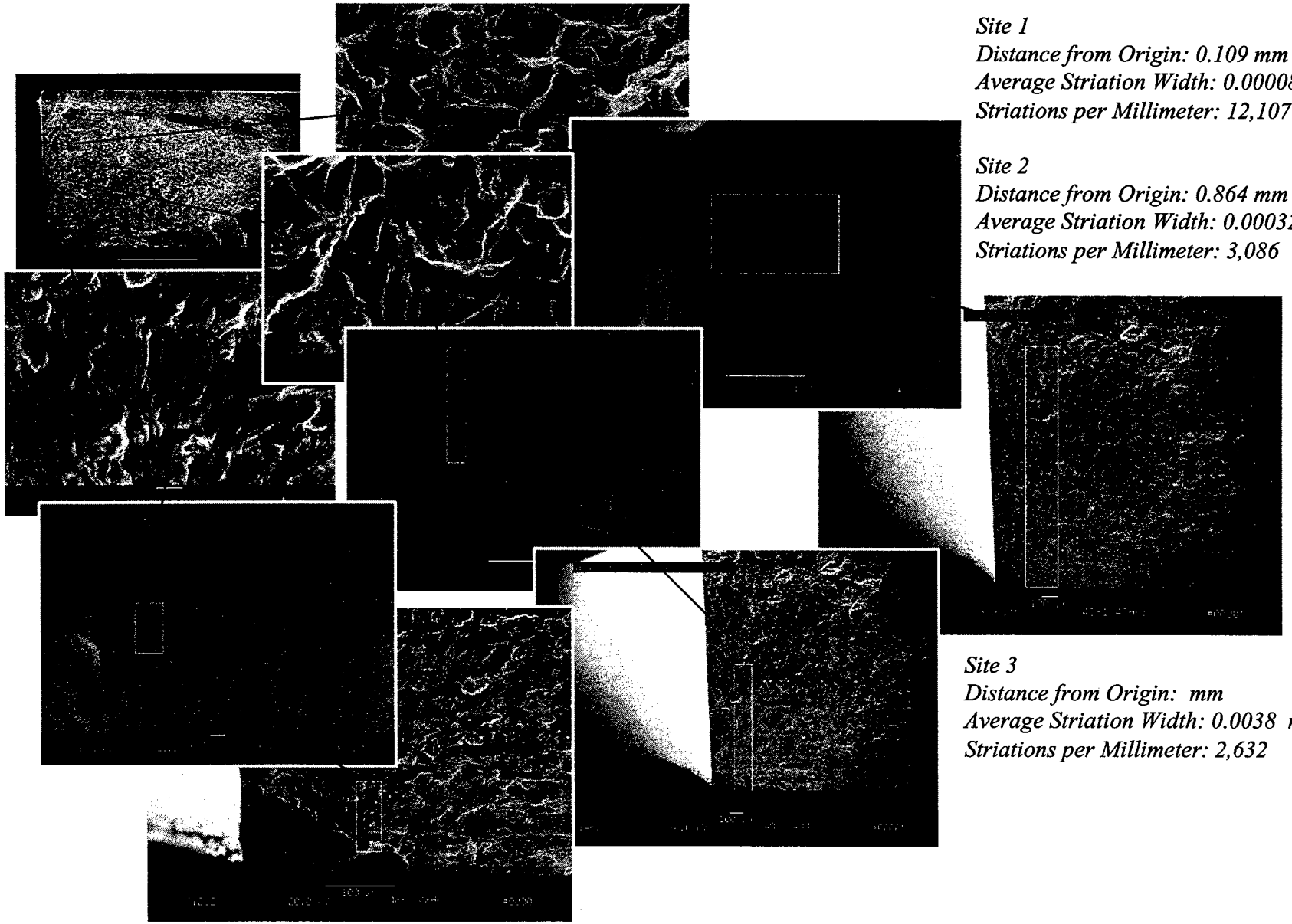

Site 1
Distance from Origin: 0.109 mm
Average Striation Width: 0.0000826 mm
Striations per Millimeter: 12,107

Site 2
Distance from Origin: 0.864 mm
Average Striation Width: 0.000324 mm
Striations per Millimeter: 3,086

Site 3
Distance from Origin: mm
Average Striation Width: 0.0038 mm
Striations per Millimeter: 2,632

Figure A-22. Specimen 48-1

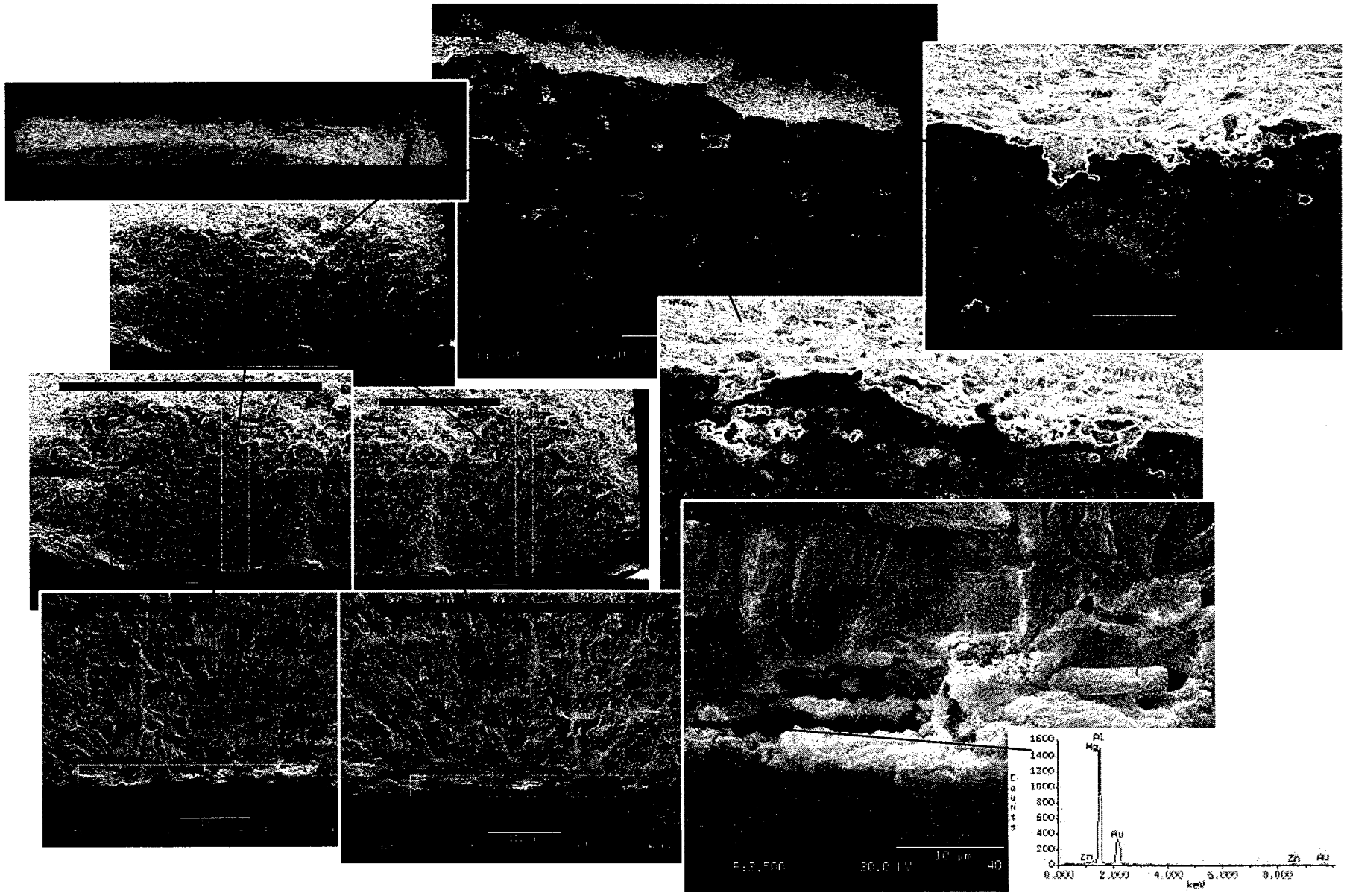

Figure A-23. Specimen 48-2

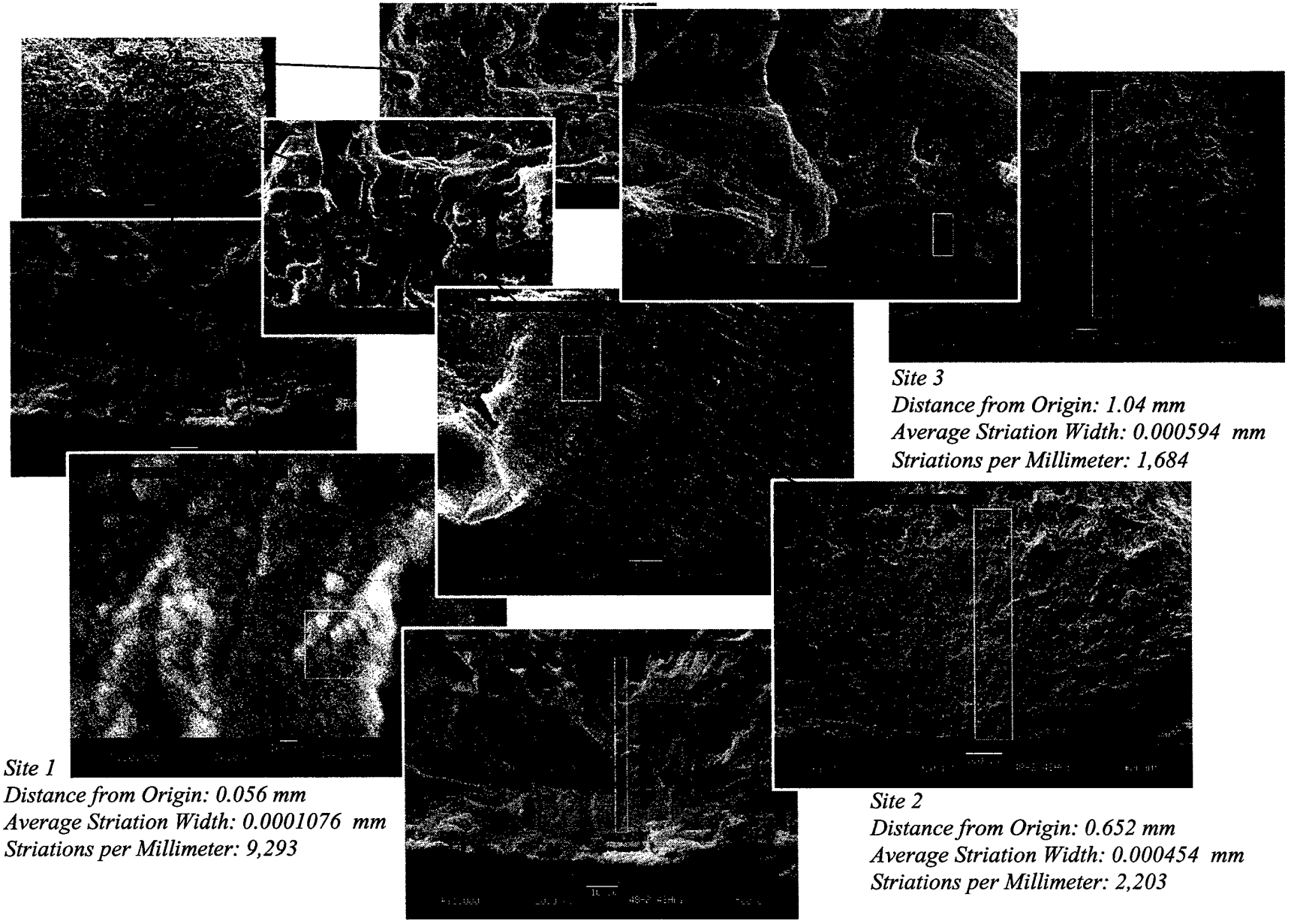

Site 3
Distance from Origin: 1.04 mm
Average Striation Width: 0.000594 mm
Striations per Millimeter: 1,684

Site 1
Distance from Origin: 0.056 mm
Average Striation Width: 0.0001076 mm
Striations per Millimeter: 9,293

Site 2
Distance from Origin: 0.652 mm
Average Striation Width: 0.000454 mm
Striations per Millimeter: 2,203

Figure A-24. Specimen 48-2

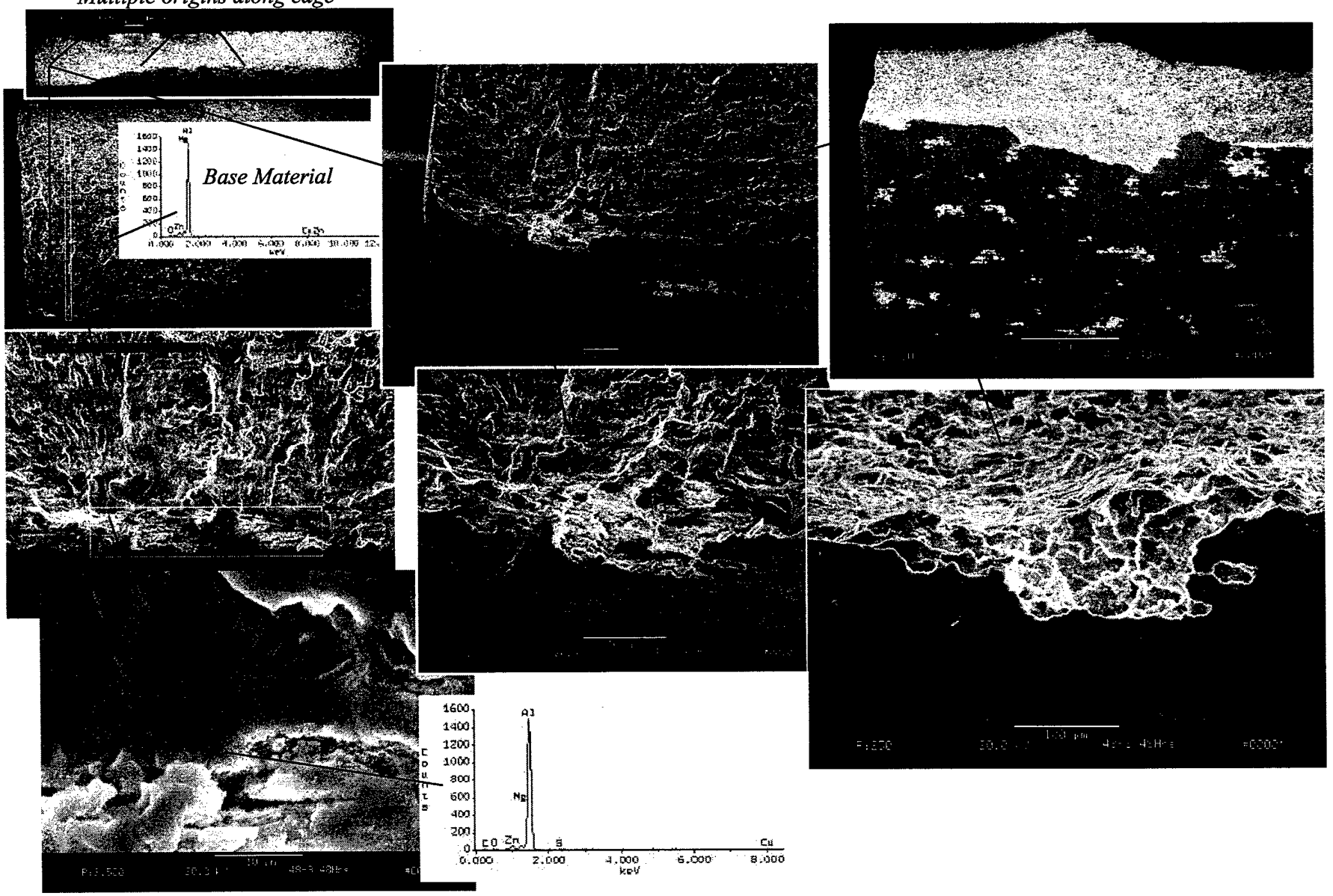

Figure A-25. Specimen 48-3

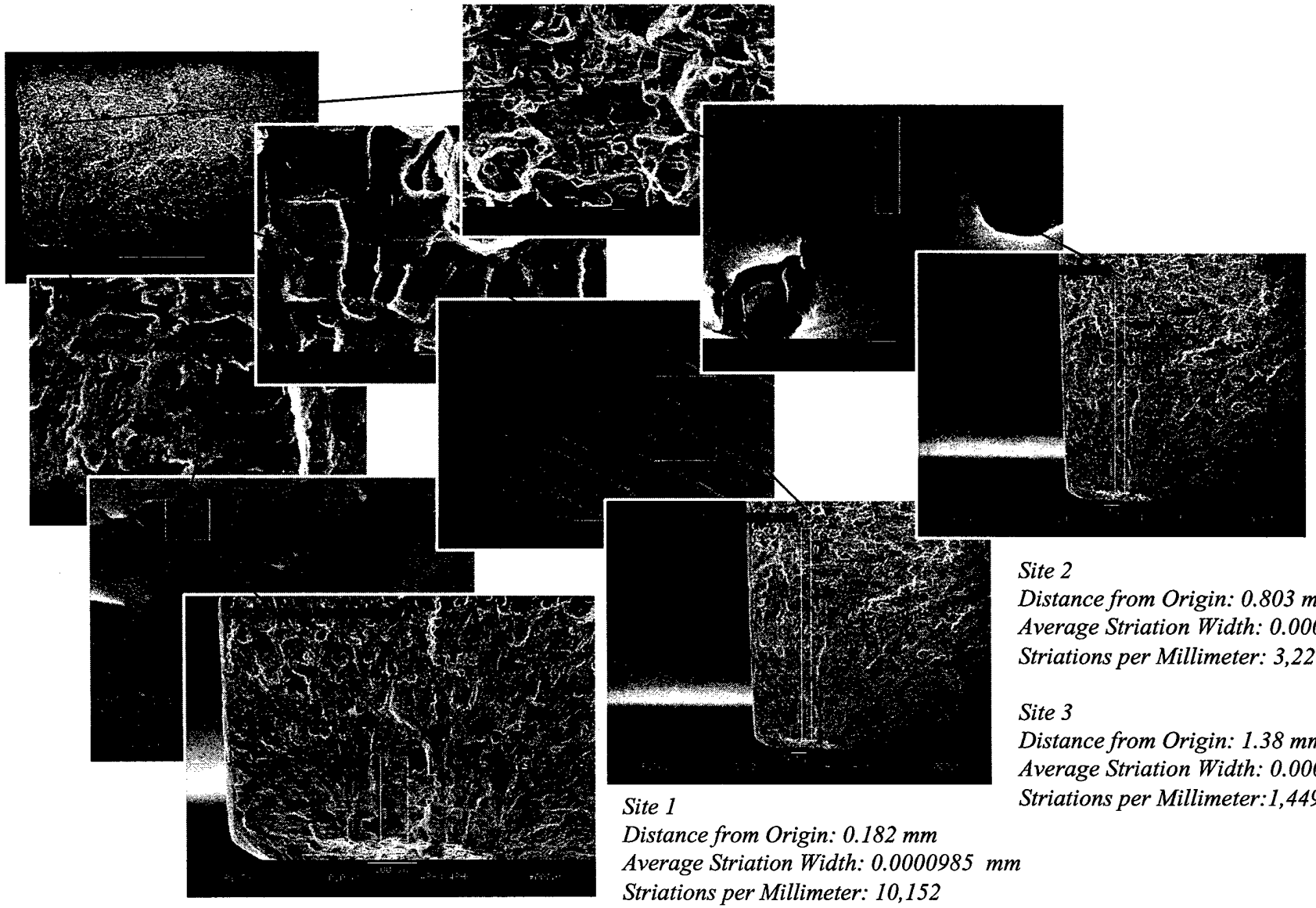

Site 2
Distance from Origin: 0.803 mm
Average Striation Width: 0.00031 mm
Striations per Millimeter: 3,226

Site 3
Distance from Origin: 1.38 mm
Average Striation Width: 0.00069 mm
Striations per Millimeter:1,449

Site 1
Distance from Origin: 0.182 mm
Average Striation Width: 0.0000985 mm
Striations per Millimeter: 10,152

Figure A-26. Specimen 48-3

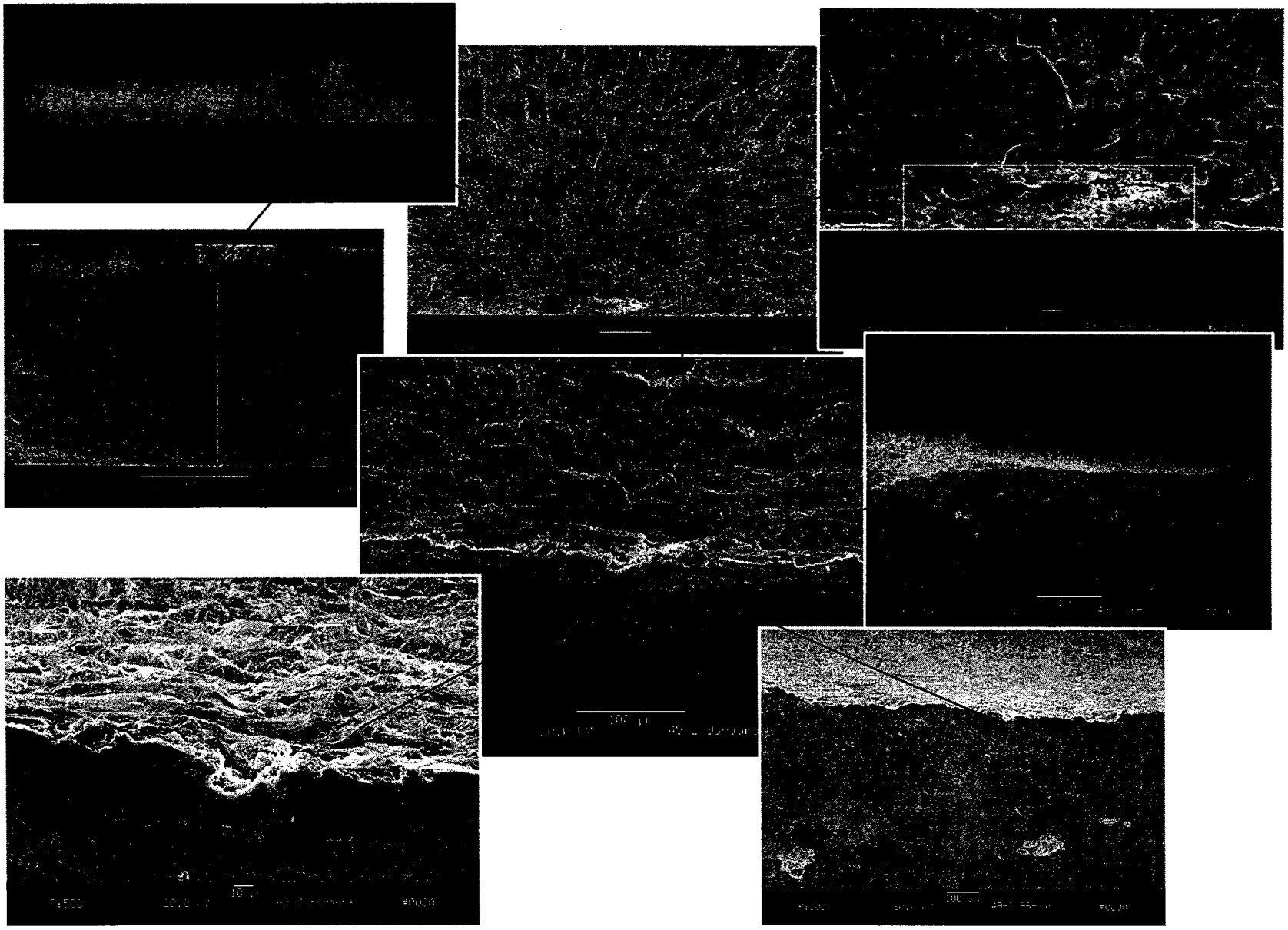

Figure A-27. Specimen 49-2

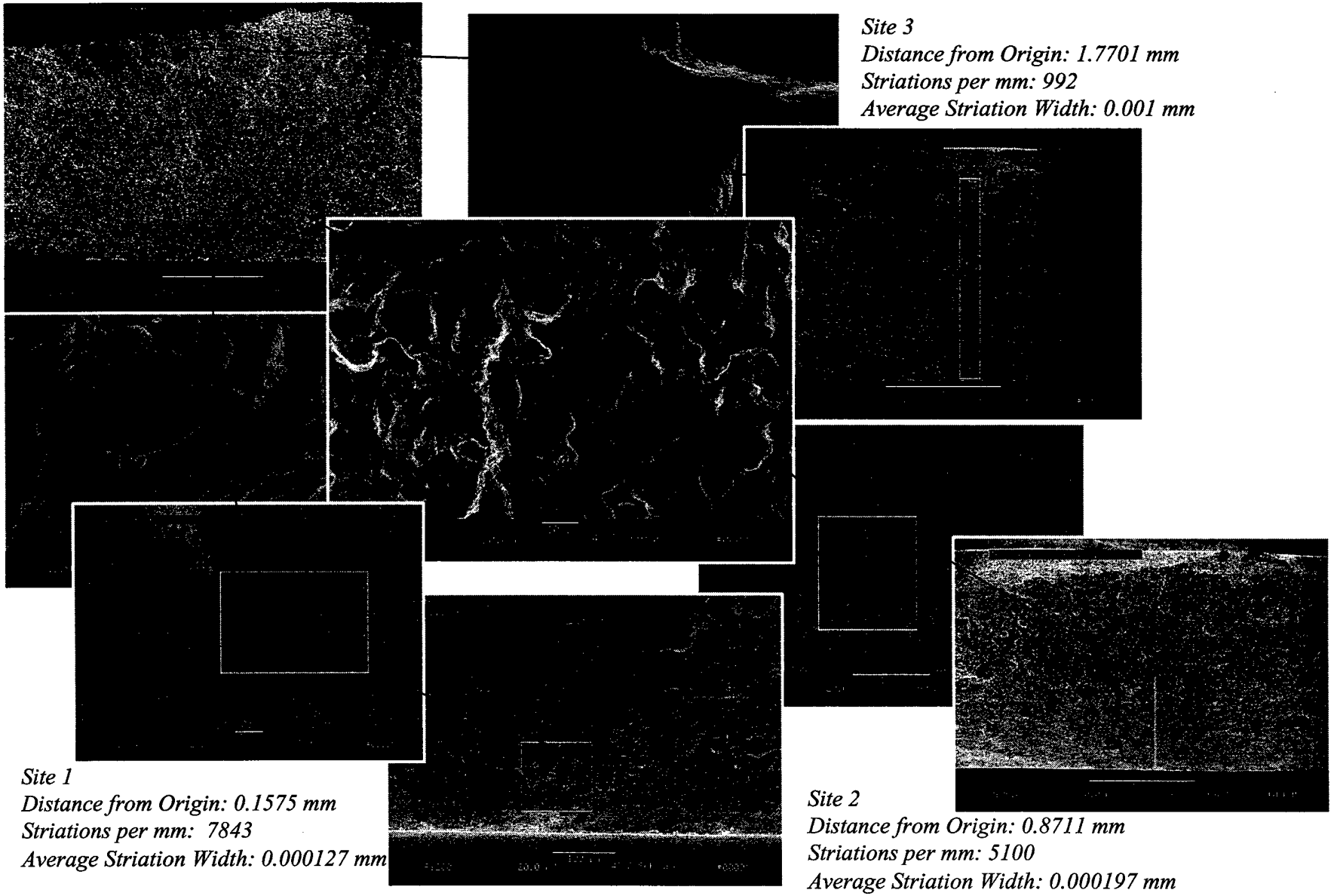

Site 3
Distance from Origin: 1.7701 mm
Striations per mm: 992
Average Striation Width: 0.001 mm

Site 1
Distance from Origin: 0.1575 mm
Striations per mm: 7843
Average Striation Width: 0.000127 mm

Site 2
Distance from Origin: 0.8711 mm
Striations per mm: 5100
Average Striation Width: 0.000197 mm

Figure A-28. Specimen 49-2

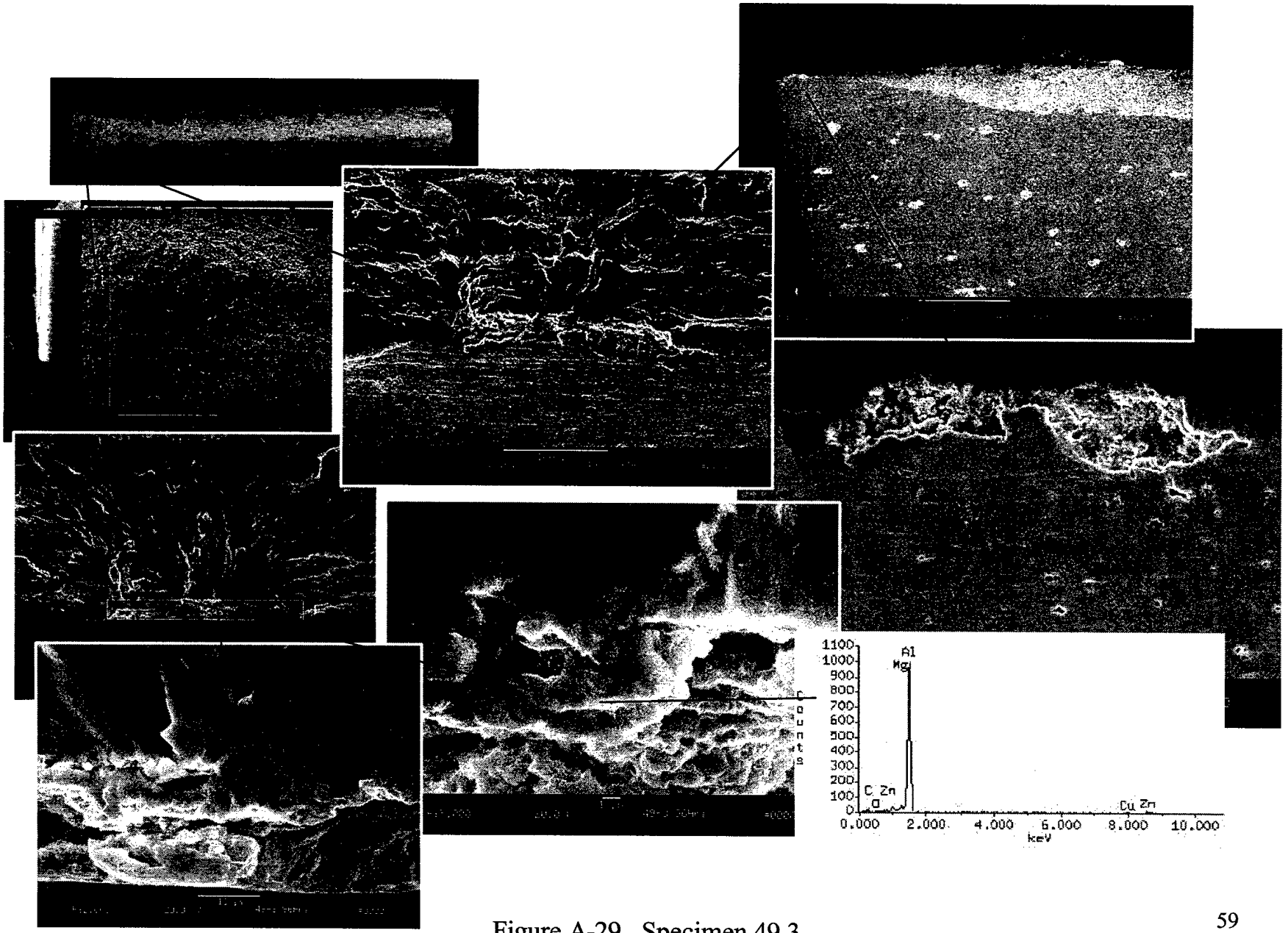

Figure A-29. Specimen 49-3

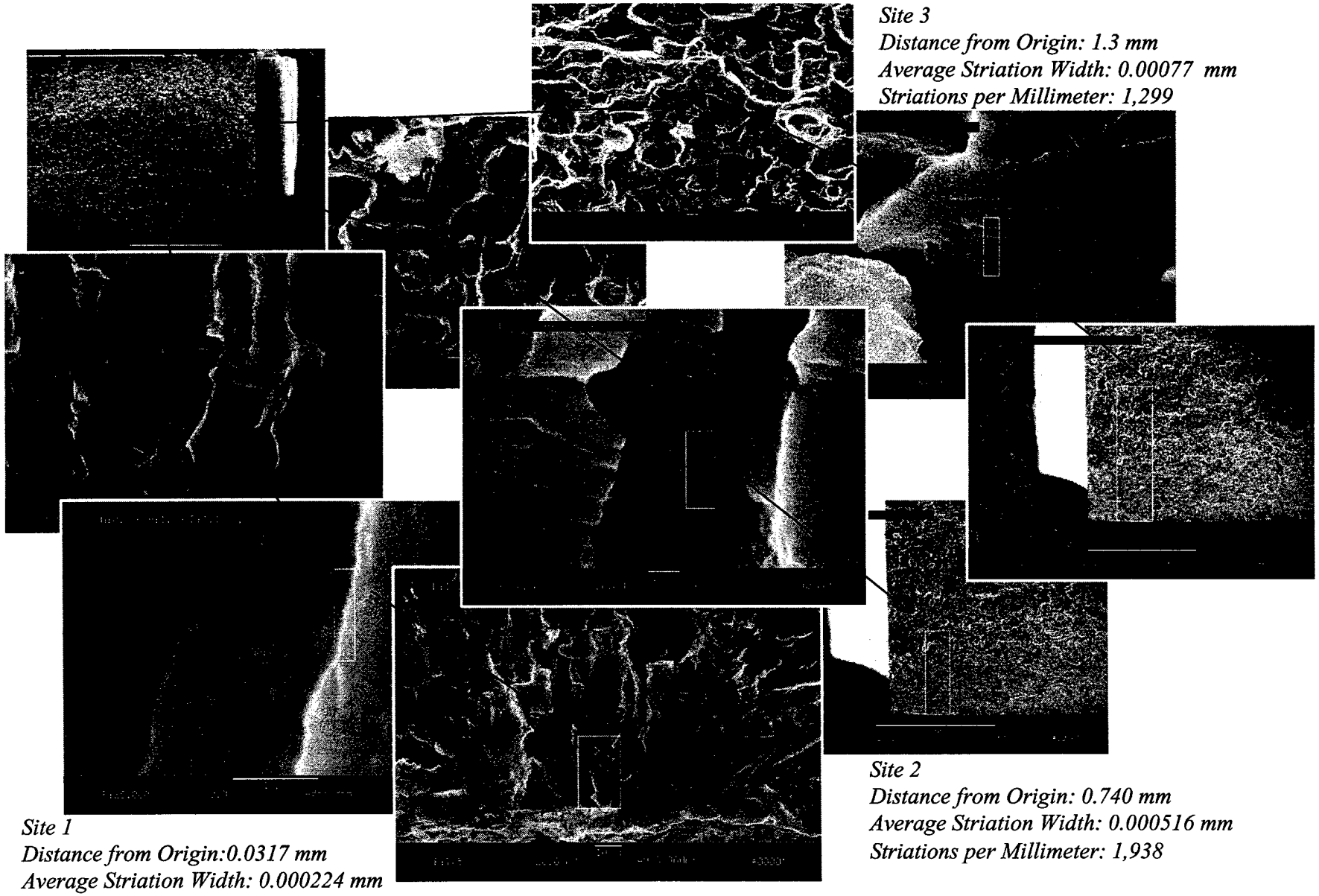

Site 3
Distance from Origin: 1.3 mm
Average Striation Width: 0.00077 mm
Striations per Millimeter: 1,299

Site 2
Distance from Origin: 0.740 mm
Average Striation Width: 0.000516 mm
Striations per Millimeter: 1,938

Site 1
Distance from Origin:0.0317 mm
Average Striation Width: 0.000224 mm
Striations per Millimeter: 4,464

Figure A-30. Specimen 49-3

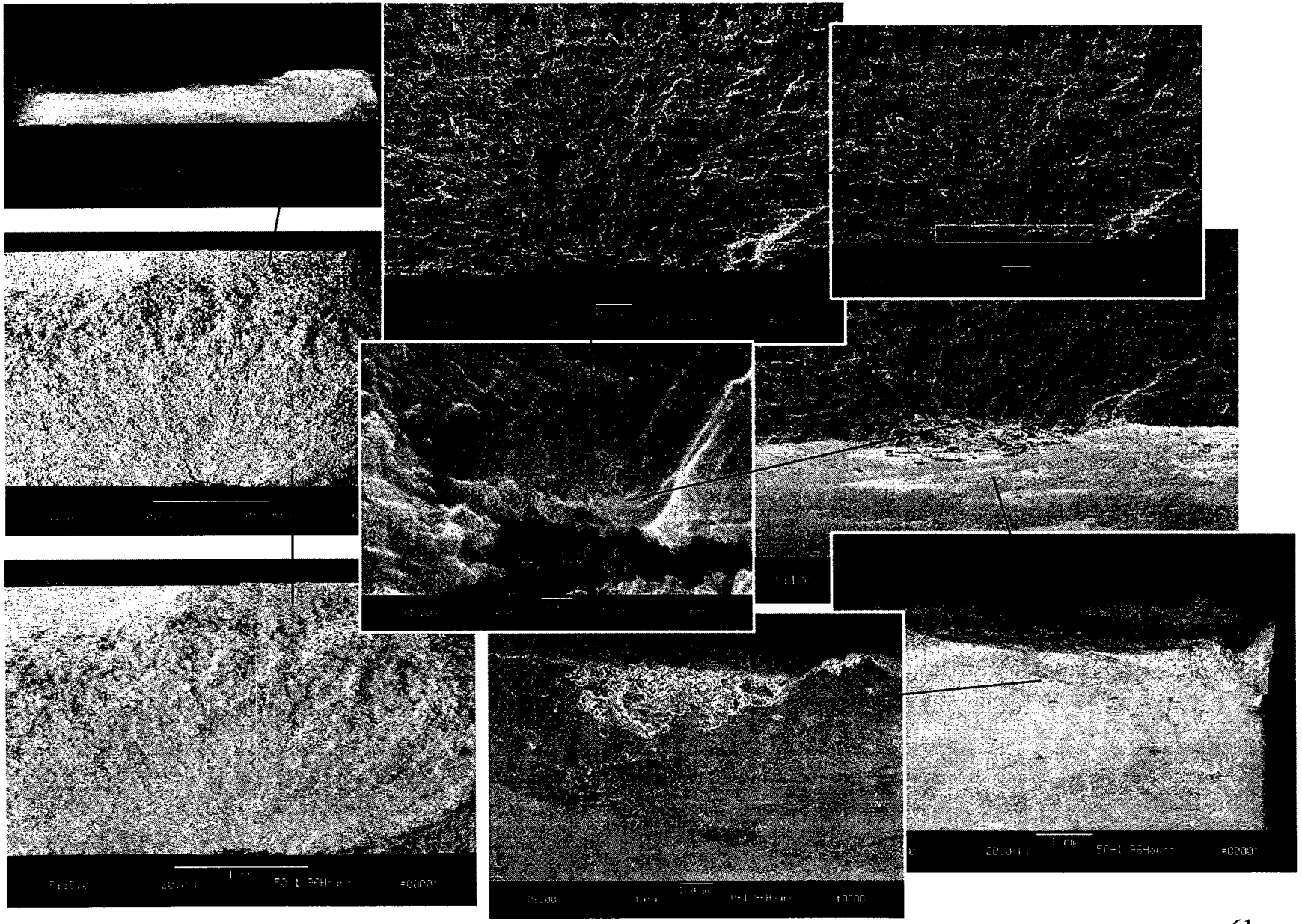

Figure A-31. Specimen 50-1

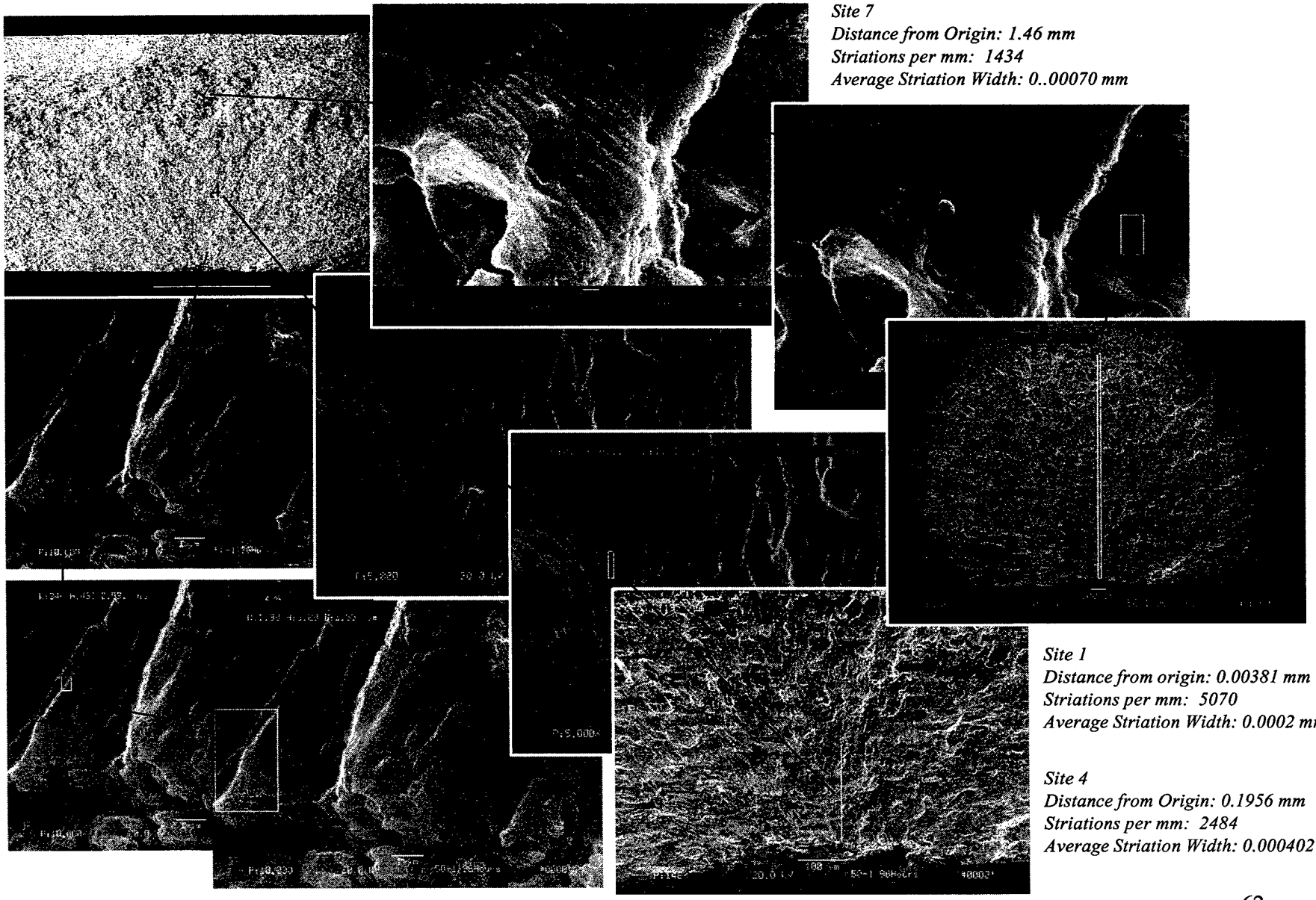

Site 7
Distance from Origin: 1.46 mm
Striations per mm: 1434
Average Striation Width: 0..00070 mm

Site 1
Distance from origin: 0.00381 mm
Striations per mm: 5070
Average Striation Width: 0.0002 mm

Site 4
Distance from Origin: 0.1956 mm
Striations per mm: 2484
Average Striation Width: 0.000402 mm

Figure A-32. Specimen 50-1

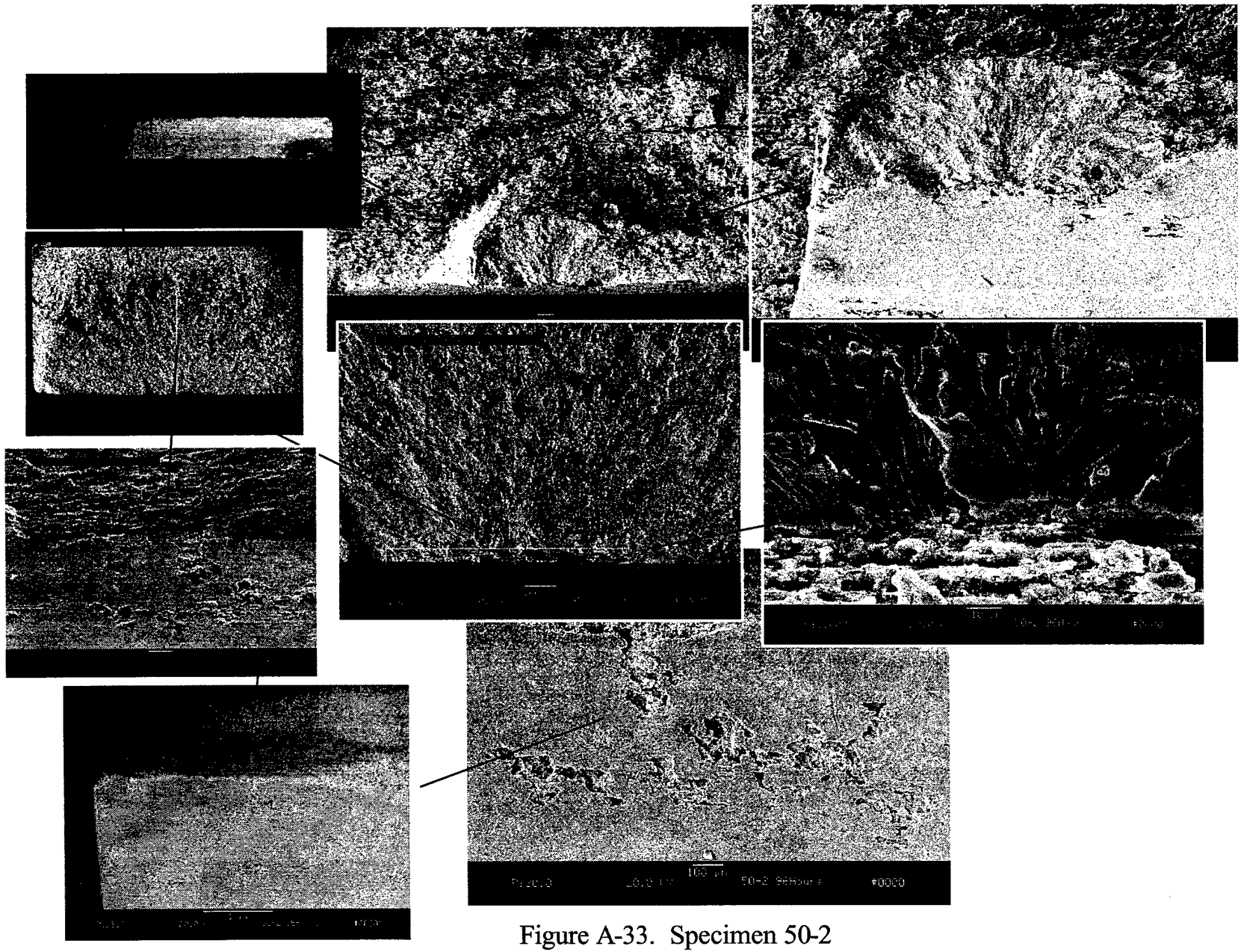

Figure A-33. Specimen 50-2

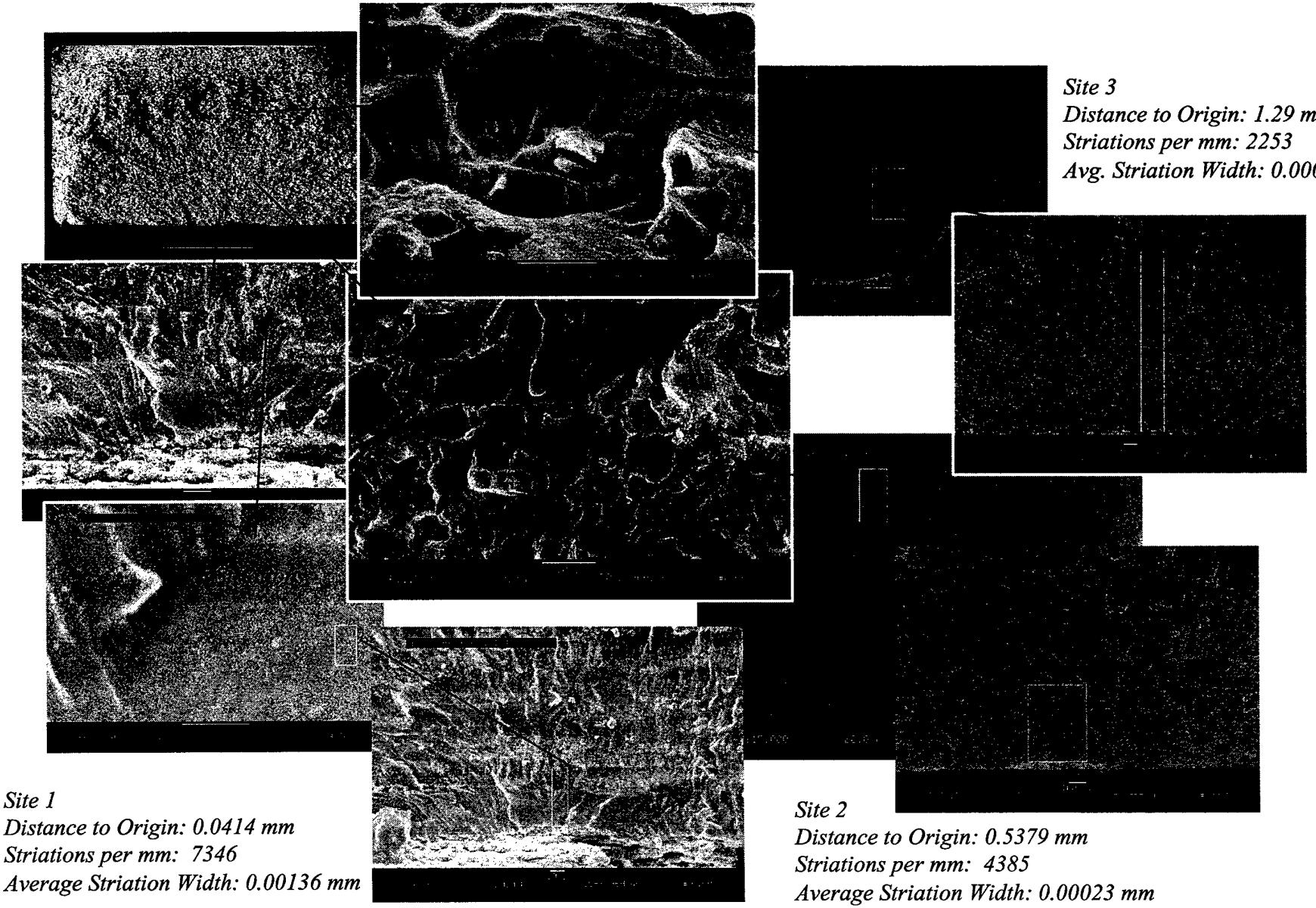

Site 3
Distance to Origin: 1.29 mm
Striations per mm: 2253
Avg. Striation Width: 0.00044 mm

Site 1
Distance to Origin: 0.0414 mm
Striations per mm: 7346
Average Striation Width: 0.00136 mm

Site 2
Distance to Origin: 0.5379 mm
Striations per mm: 4385
Average Striation Width: 0.00023 mm

Figure A-34. Specimen 50-2

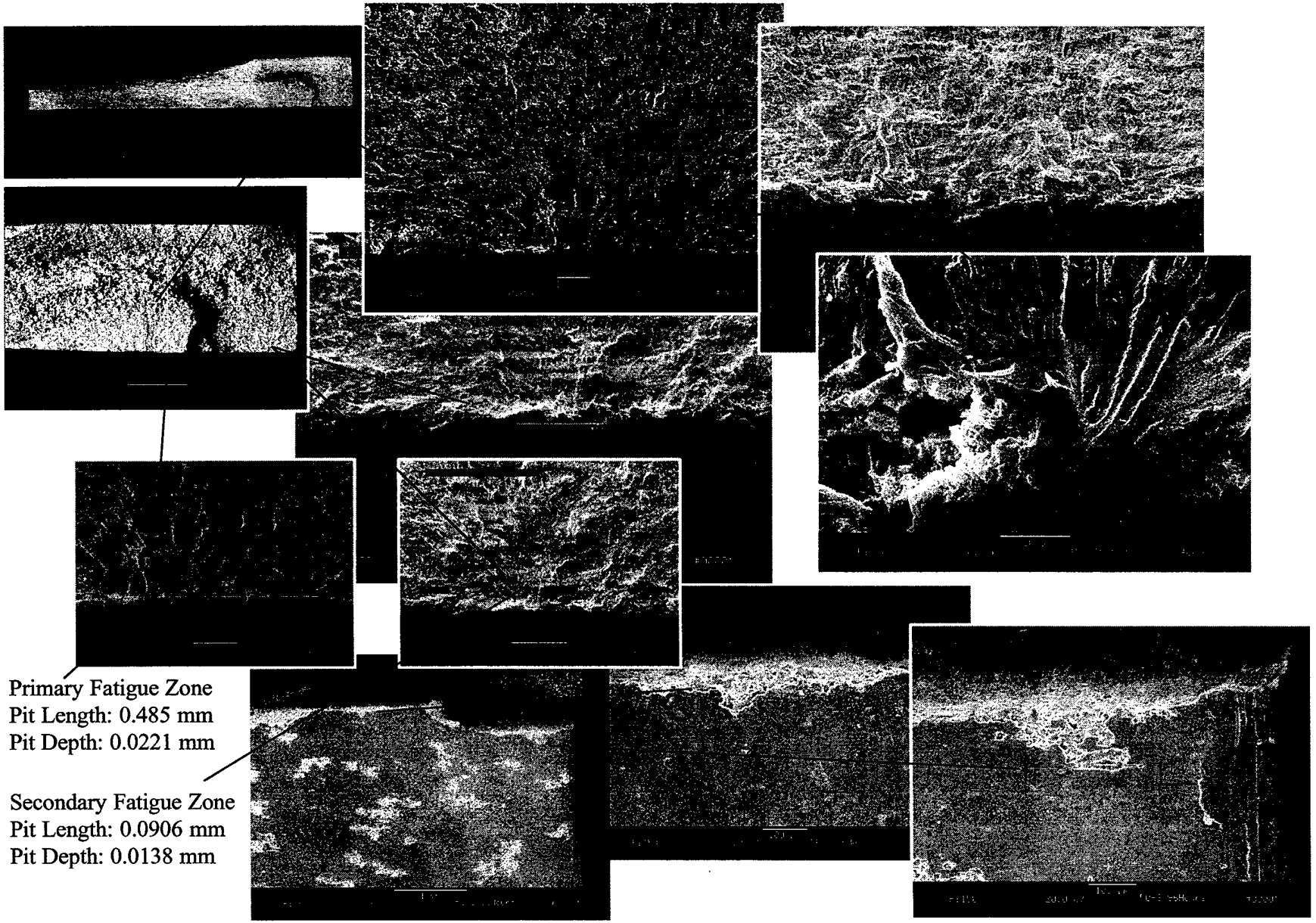

Figure A-35. Specimen 50-3

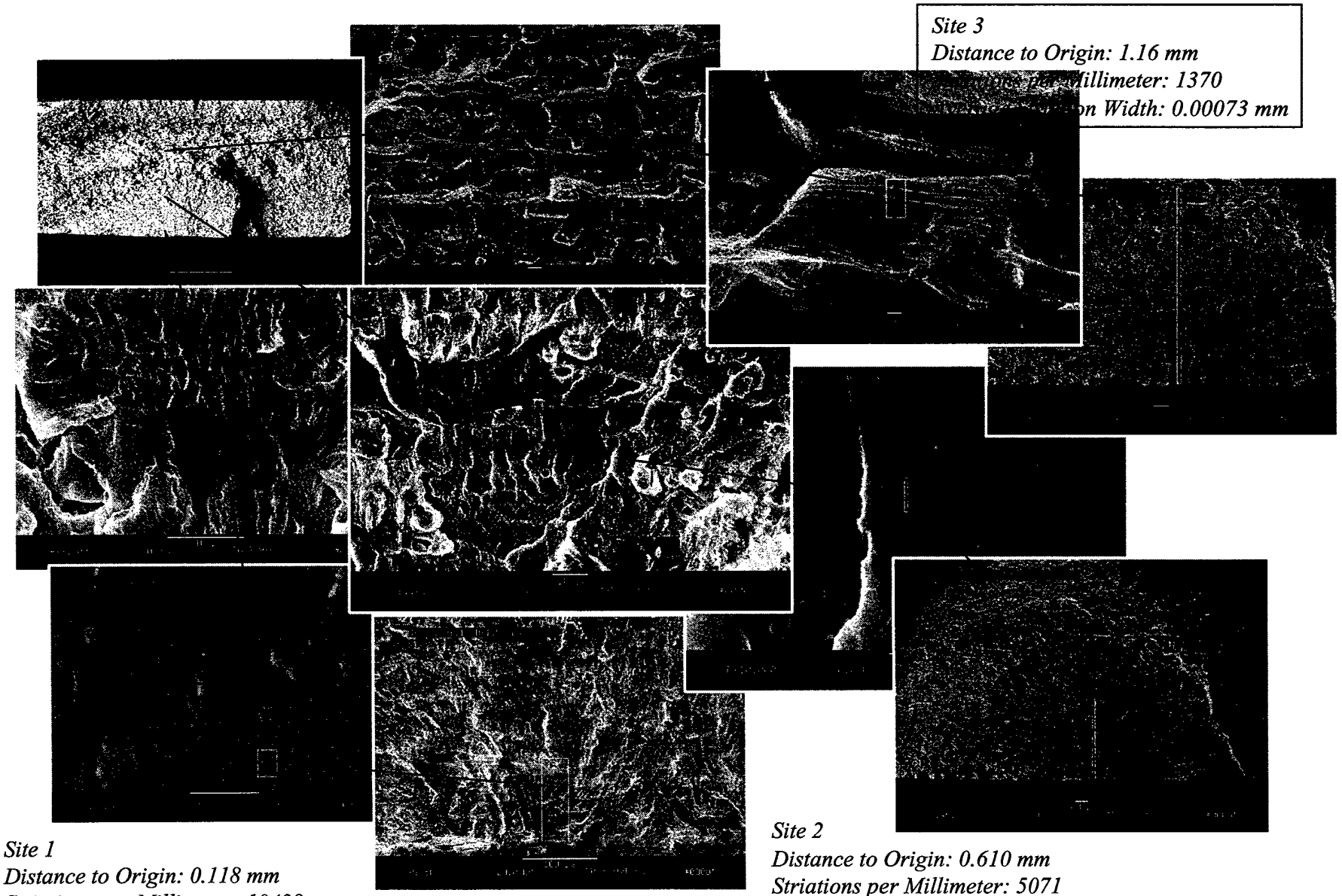

Site 1
Distance to Origin: 0.118 mm
Striations per Millimeter: 10438
Average Striation Width: 0.0000958mm

Site 2
Distance to Origin: 0.610 mm
Striations per Millimeter: 5071
Average Striation Width: 0.0001972 mm

Figure A-36. Specimen 50-3

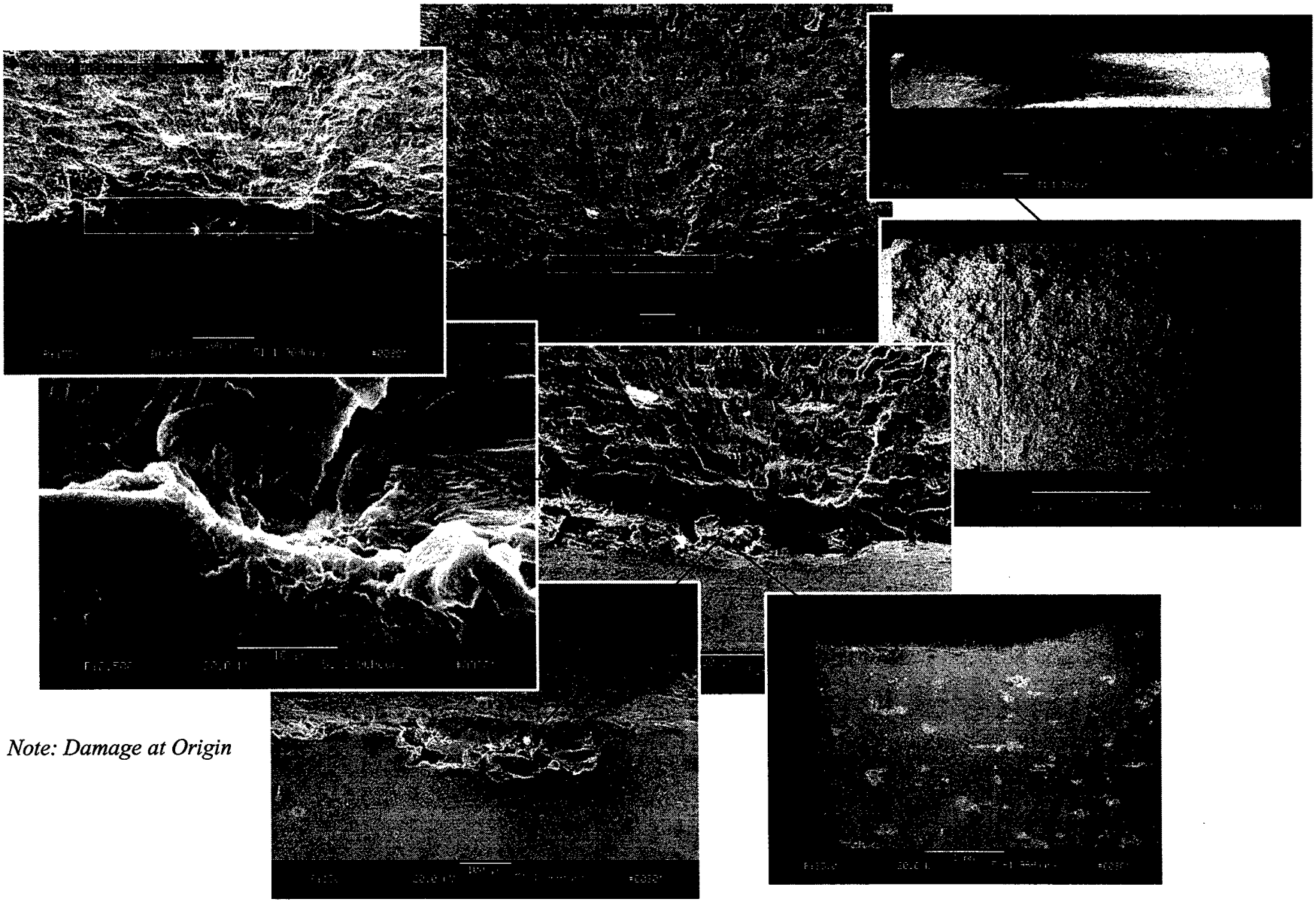

Note: Damage at Origin

Figure A-37. Specimen 51-1

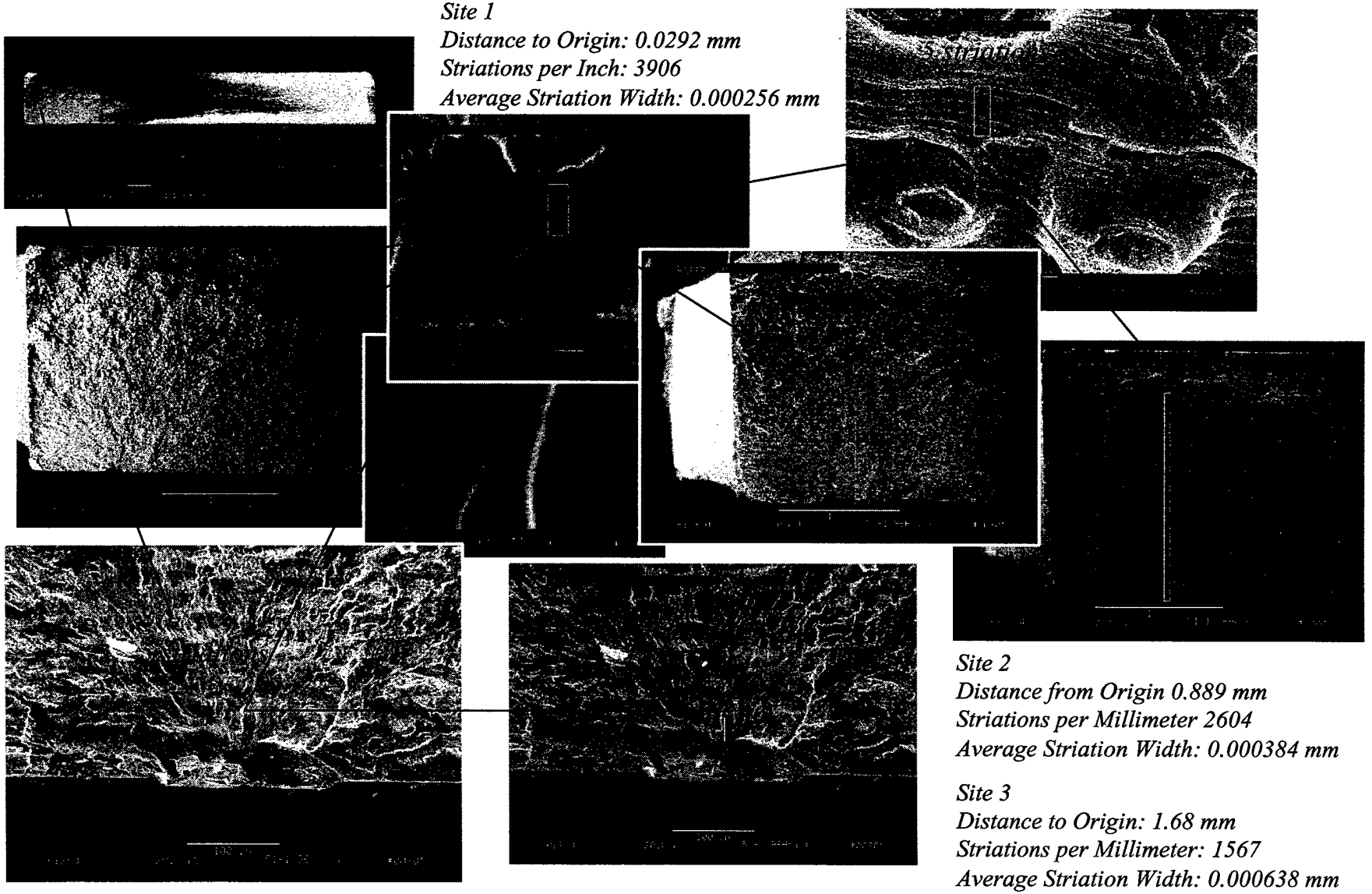

Site 1
Distance to Origin: 0.0292 mm
Striations per Inch: 3906
Average Striation Width: 0.000256 mm

Site 2
Distance from Origin 0.889 mm
Striations per Millimeter 2604
Average Striation Width: 0.000384 mm

Site 3
Distance to Origin: 1.68 mm
Striations per Millimeter: 1567
Average Striation Width: 0.000638 mm

Figure A-38. Specimen 51-1

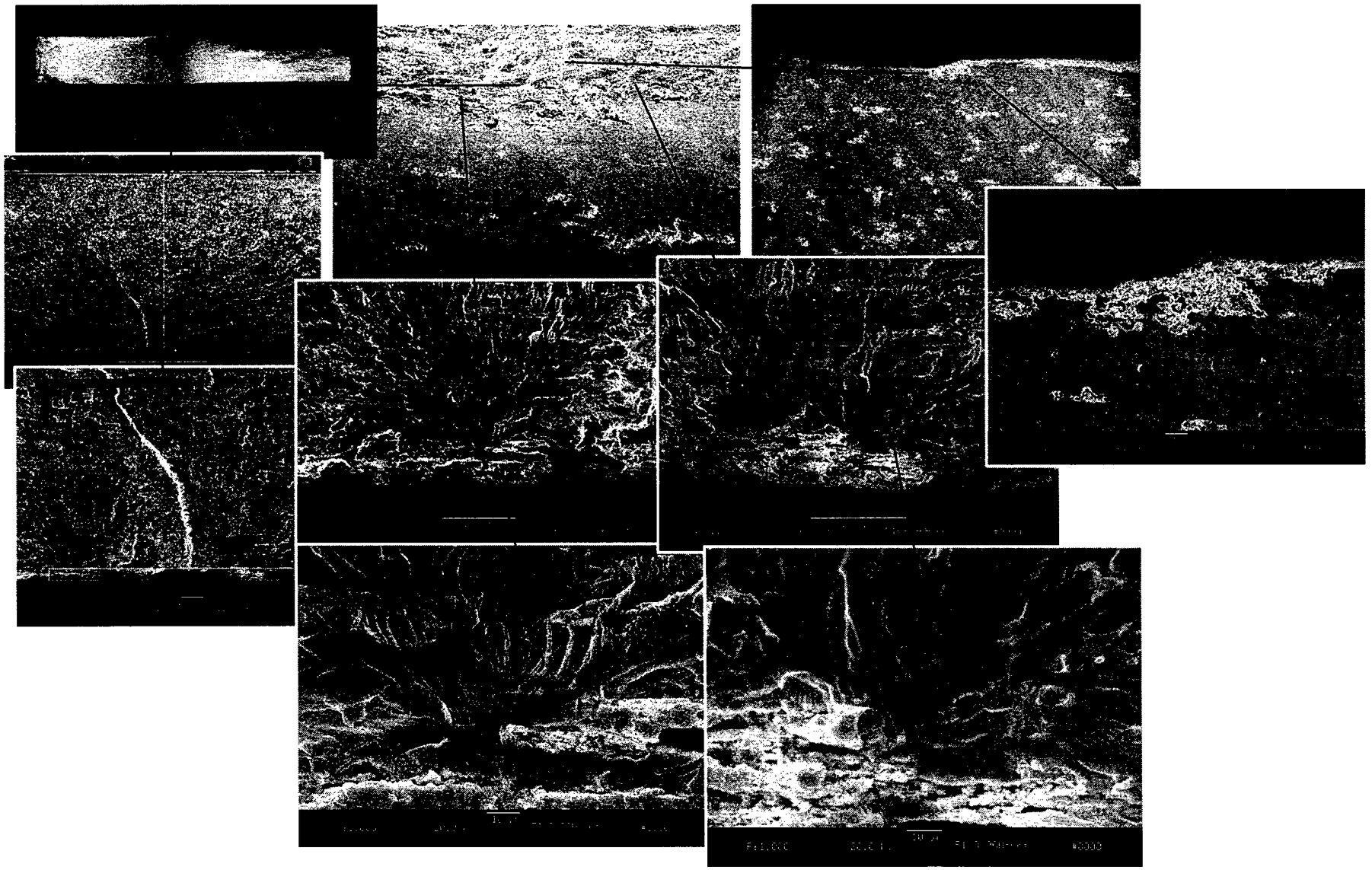

Figure A-39. Specimen 51-3

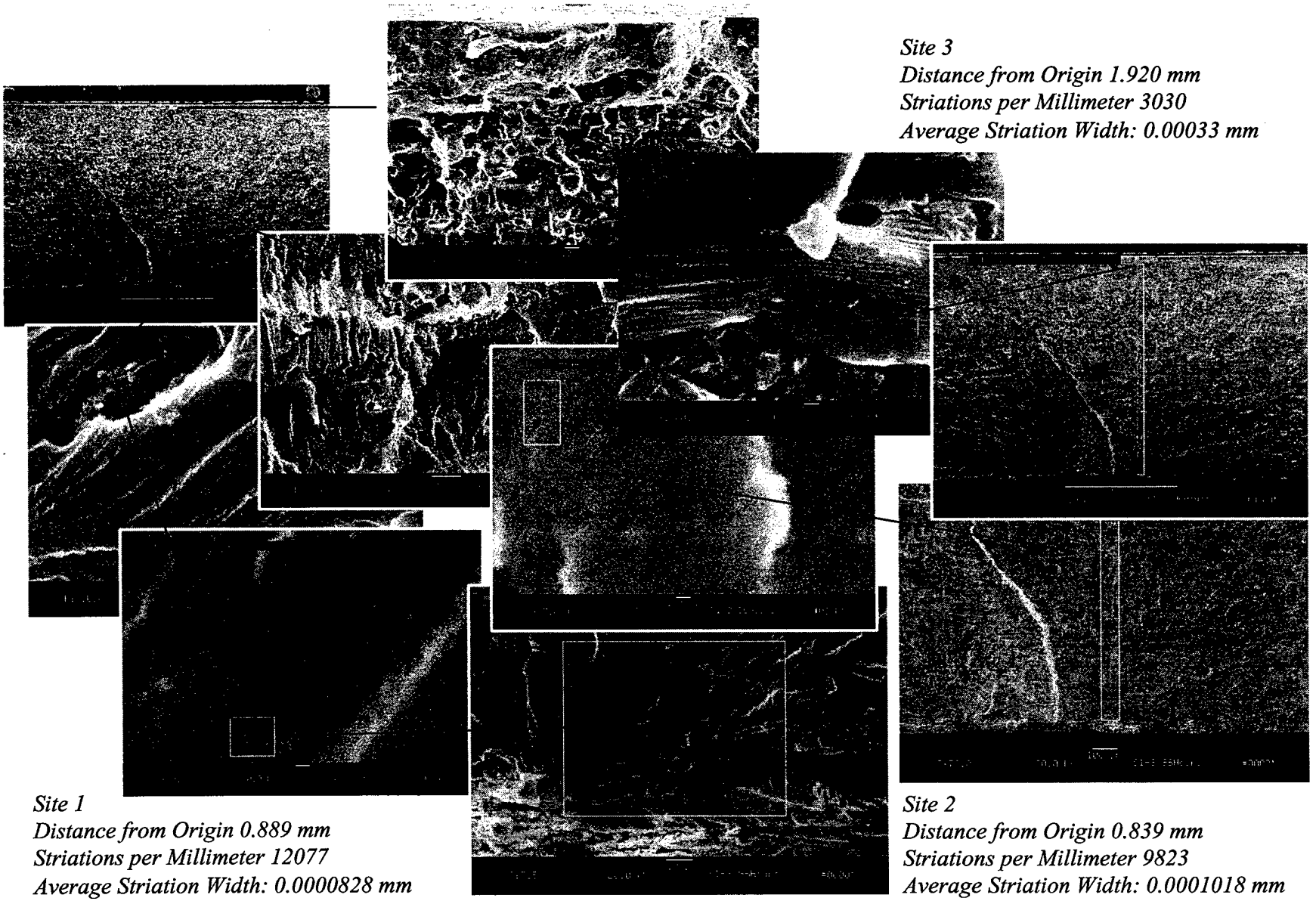

Site 3
Distance from Origin 1.920 mm
Striations per Millimeter 3030
Average Striation Width: 0.00033 mm

Site 1
Distance from Origin 0.889 mm
Striations per Millimeter 12077
Average Striation Width: 0.0000828 mm

Site 2
Distance from Origin 0.839 mm
Striations per Millimeter 9823
Average Striation Width: 0.0001018 mm

Figure A-40. Specimen 51-3

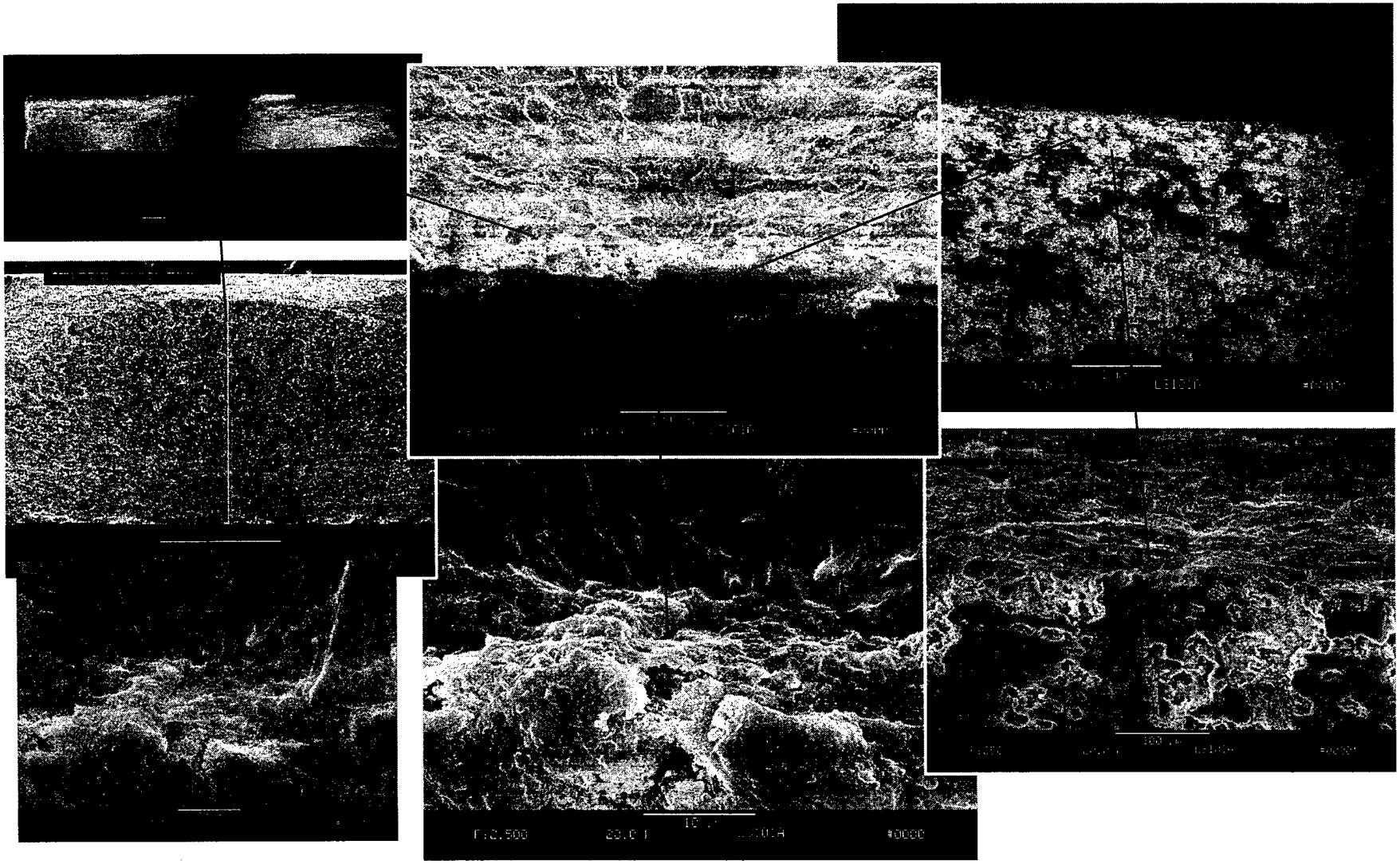

Figure A-41. Specimen 58-1

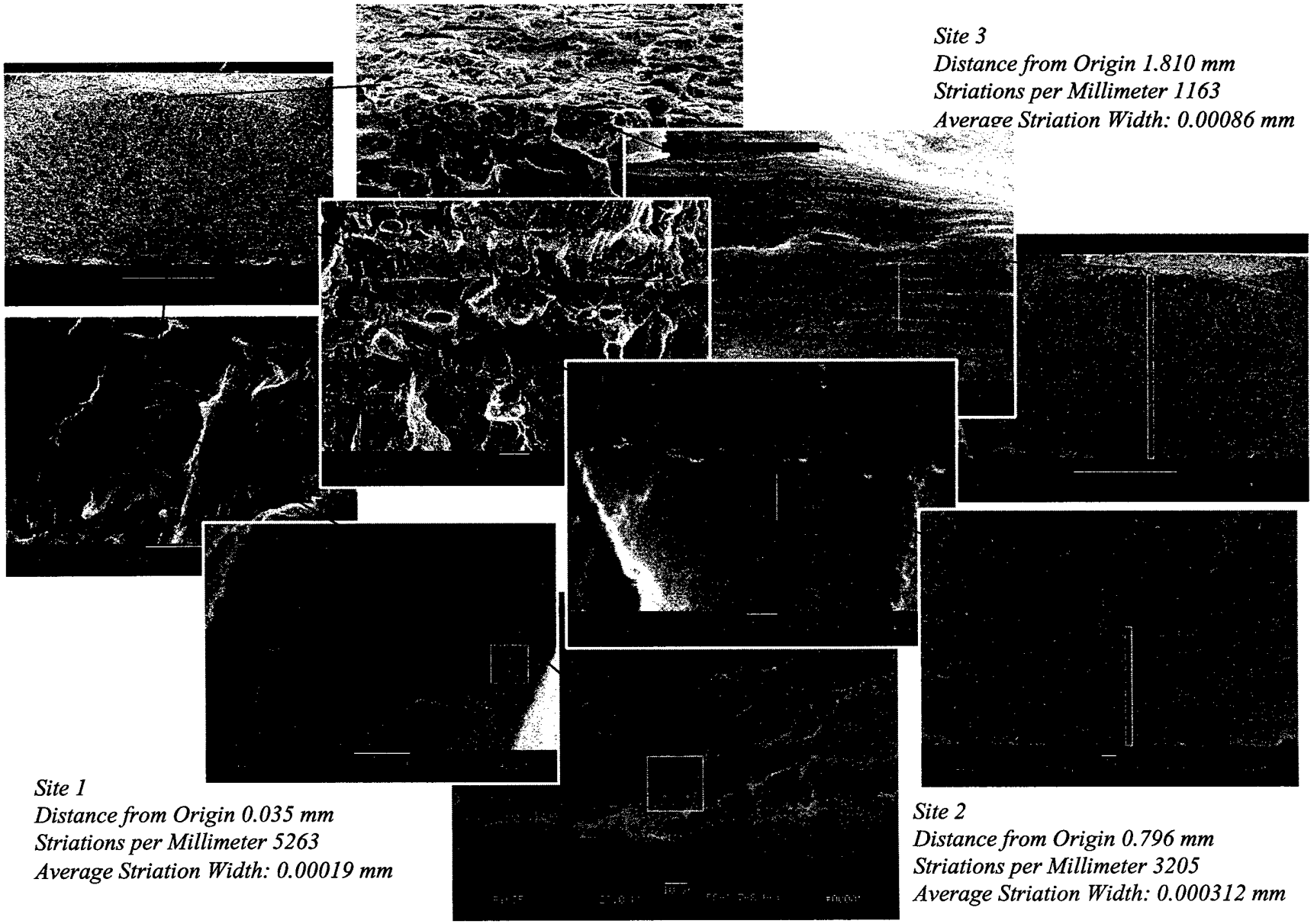

Site 3
Distance from Origin 1.810 mm
Striations per Millimeter 1163
Average Striation Width: 0.00086 mm

Site 1
Distance from Origin 0.035 mm
Striations per Millimeter 5263
Average Striation Width: 0.00019 mm

Site 2
Distance from Origin 0.796 mm
Striations per Millimeter 3205
Average Striation Width: 0.000312 mm

Figure A-42. Specimen 58-1

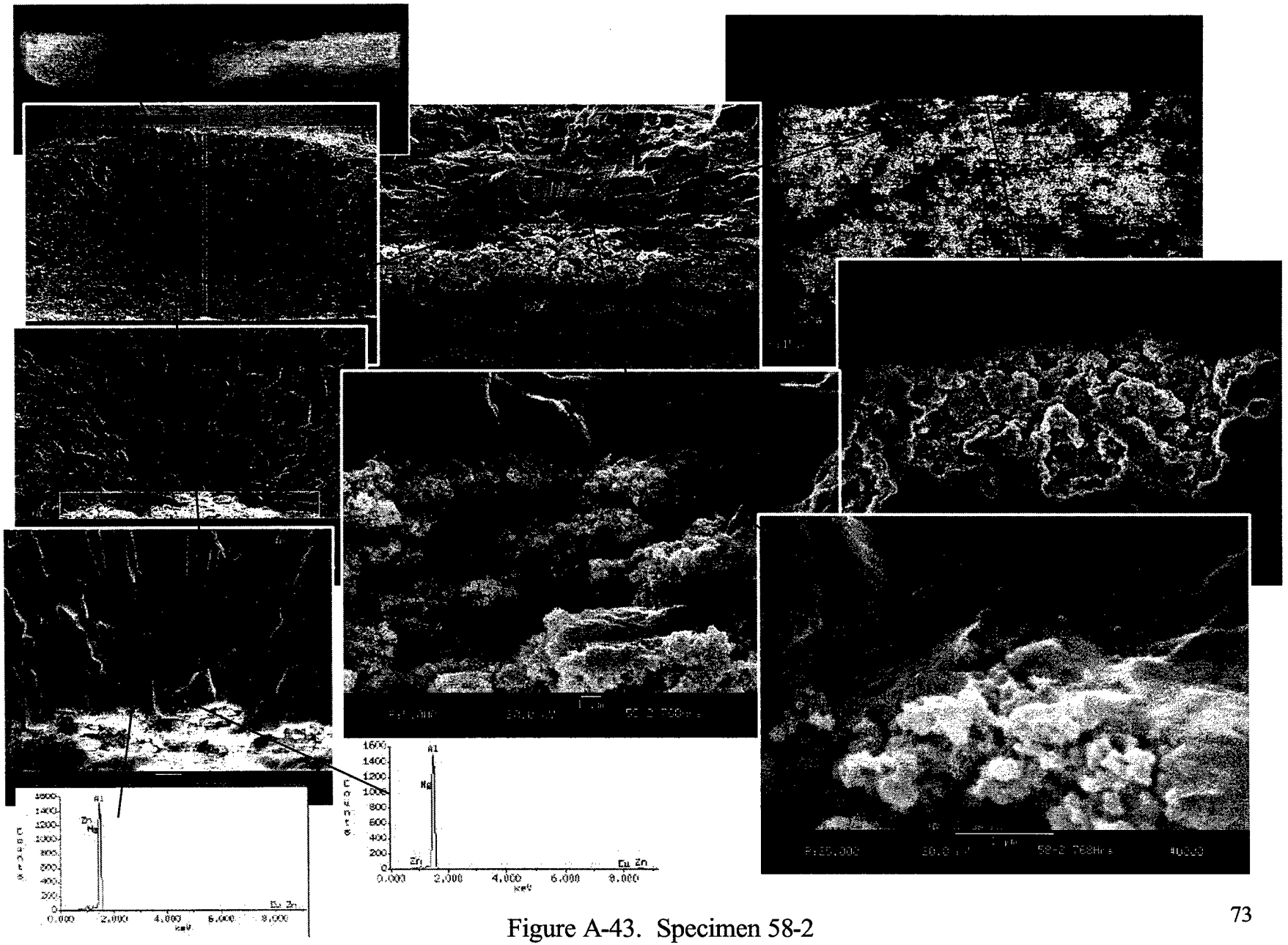

Figure A-43. Specimen 58-2

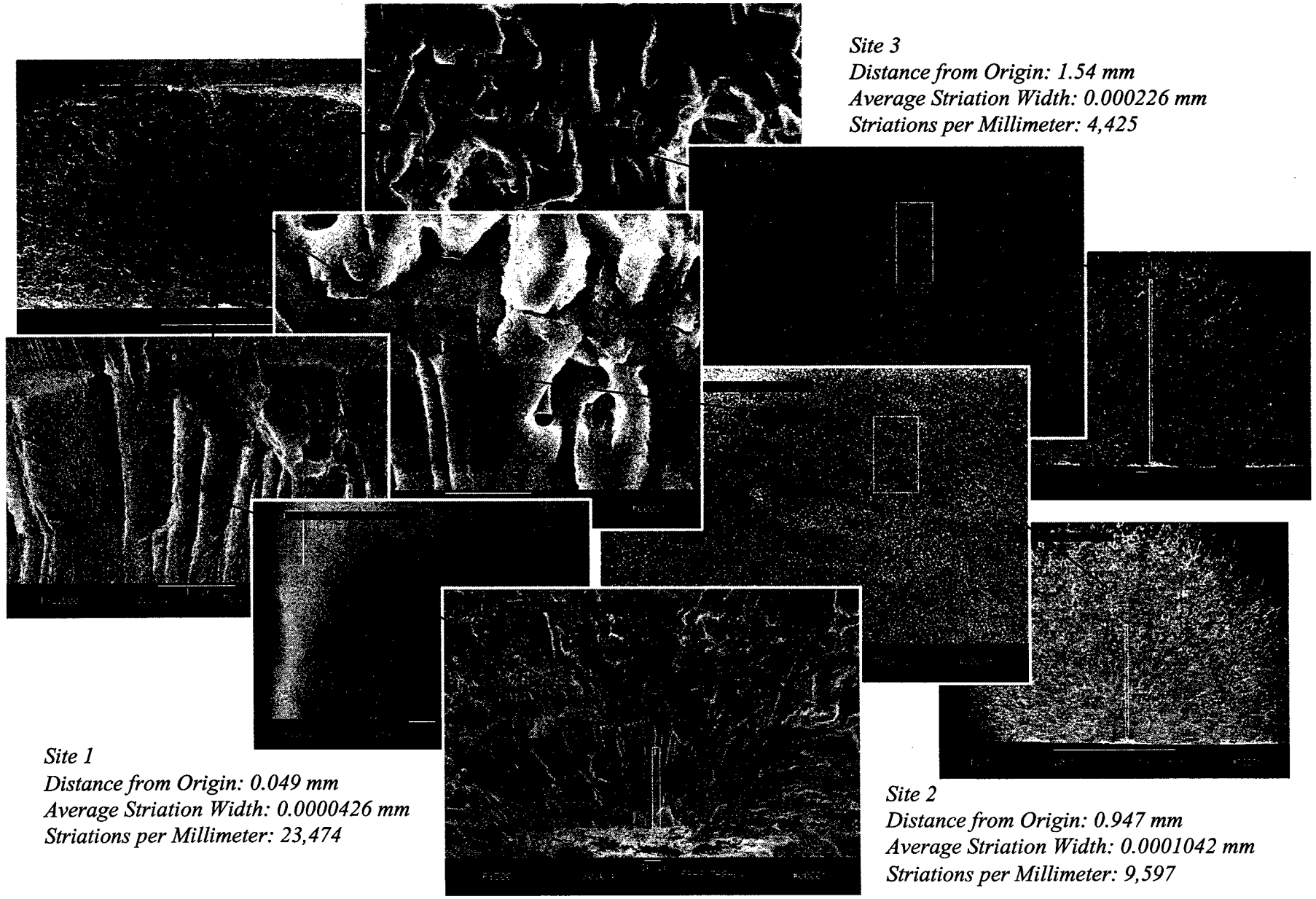

Site 3
Distance from Origin: 1.54 mm
Average Striation Width: 0.000226 mm
Striations per Millimeter: 4,425

Site 1
Distance from Origin: 0.049 mm
Average Striation Width: 0.0000426 mm
Striations per Millimeter: 23,474

Site 2
Distance from Origin: 0.947 mm
Average Striation Width: 0.0001042 mm
Striations per Millimeter: 9,597

Figure A-44. Specimen 58-2

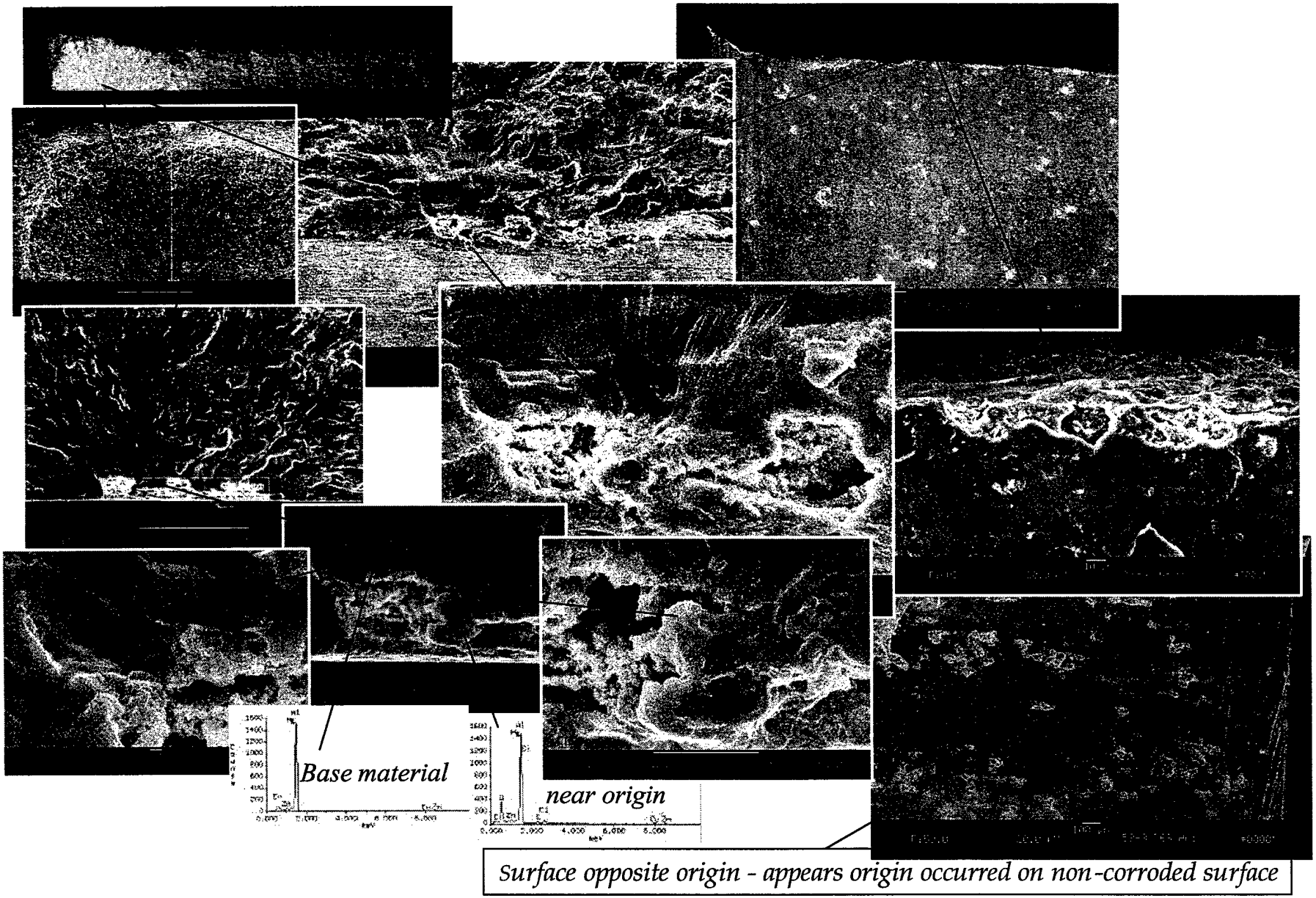

Figure A-45. Specimen 58-3

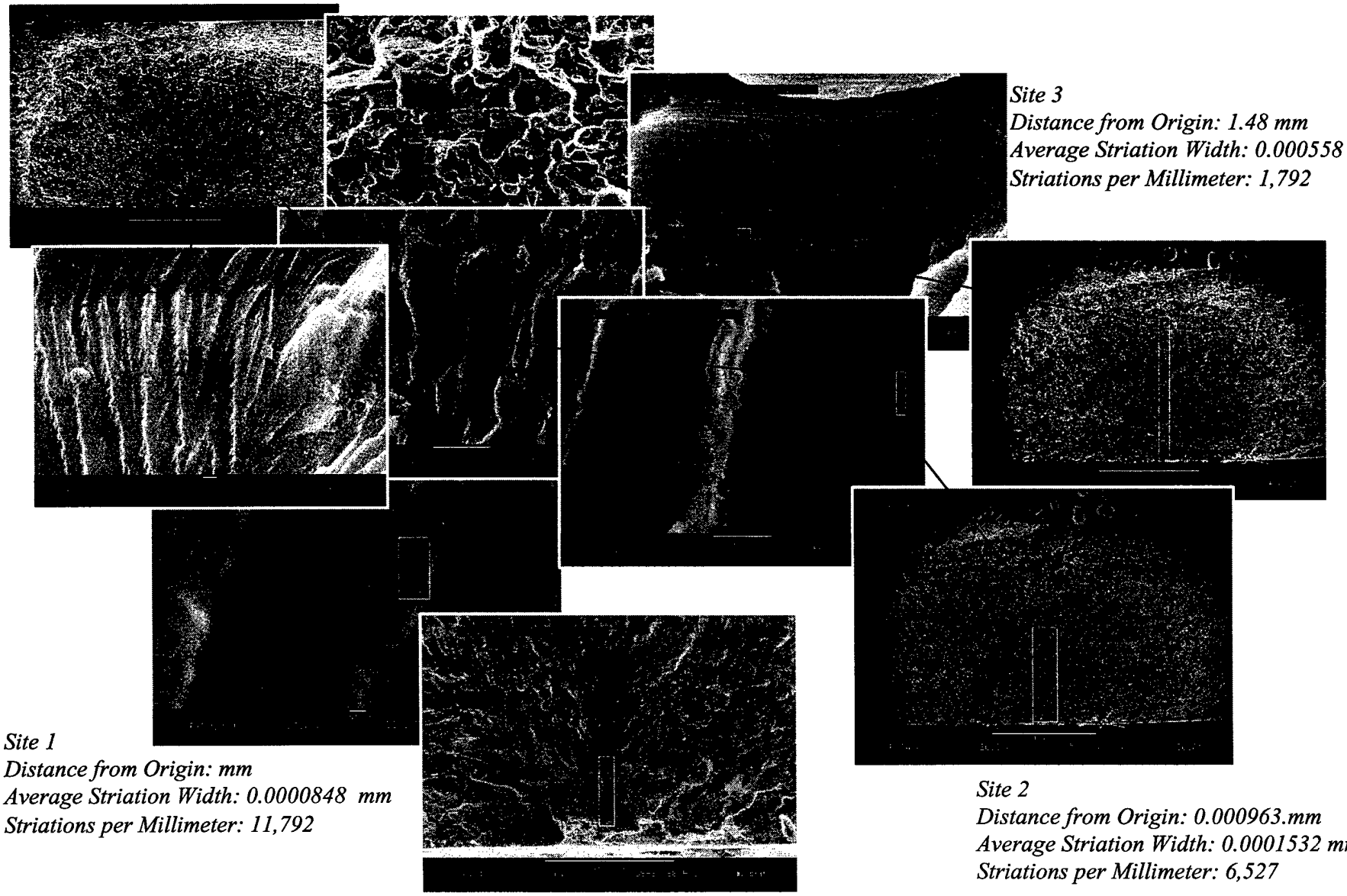

Site 3
Distance from Origin: 1.48 mm
Average Striation Width: 0.000558 mm
Striations per Millimeter: 1,792

Site 1
Distance from Origin: mm
Average Striation Width: 0.0000848 mm
Striations per Millimeter: 11,792

Site 2
Distance from Origin: 0.000963.mm
Average Striation Width: 0.0001532 mm
Striations per Millimeter: 6,527

Figure A-46. Specimen 58-3

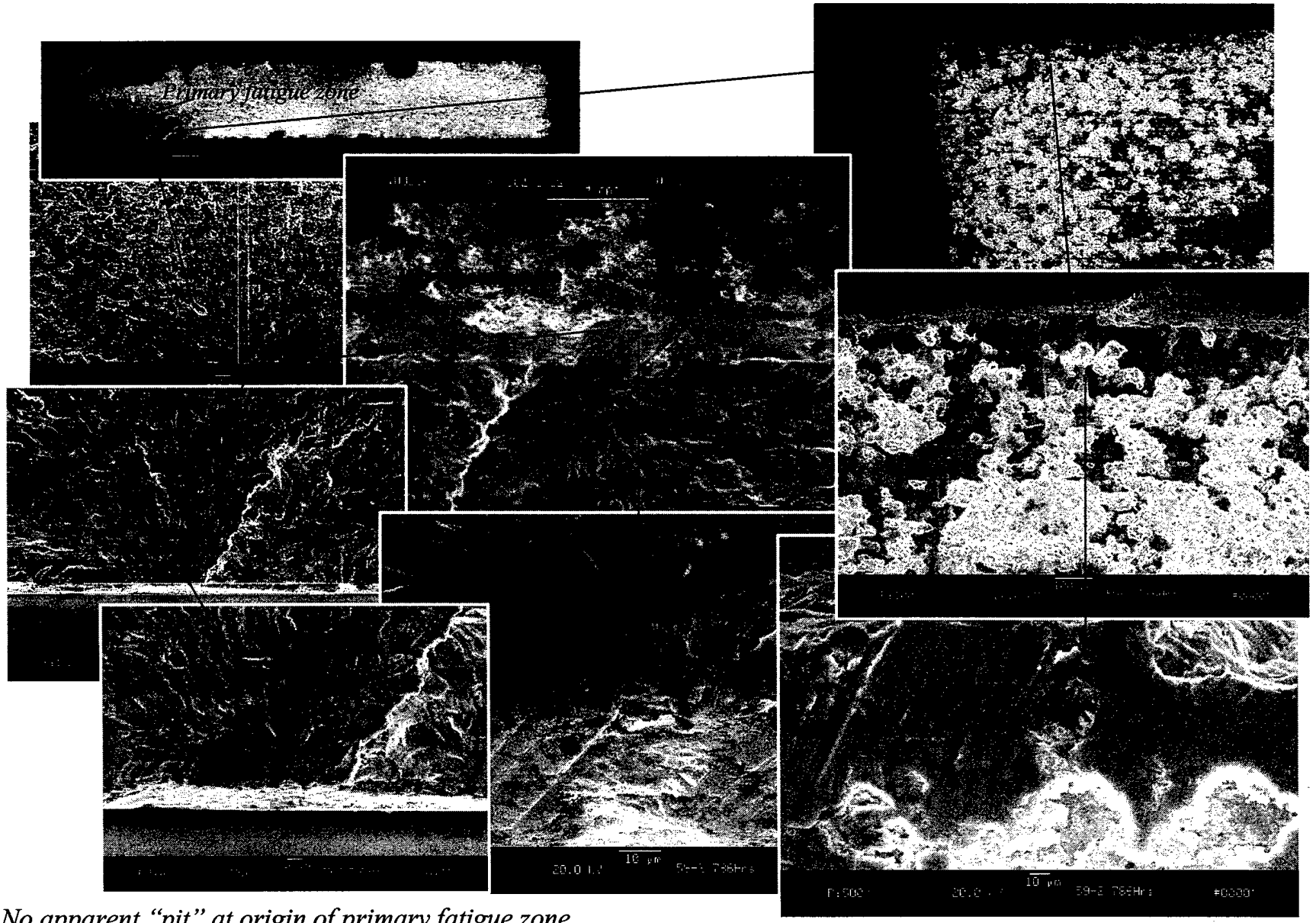

No apparent "pit" at origin of primary fatigue zone

Figure A-47. Specimen 59-2

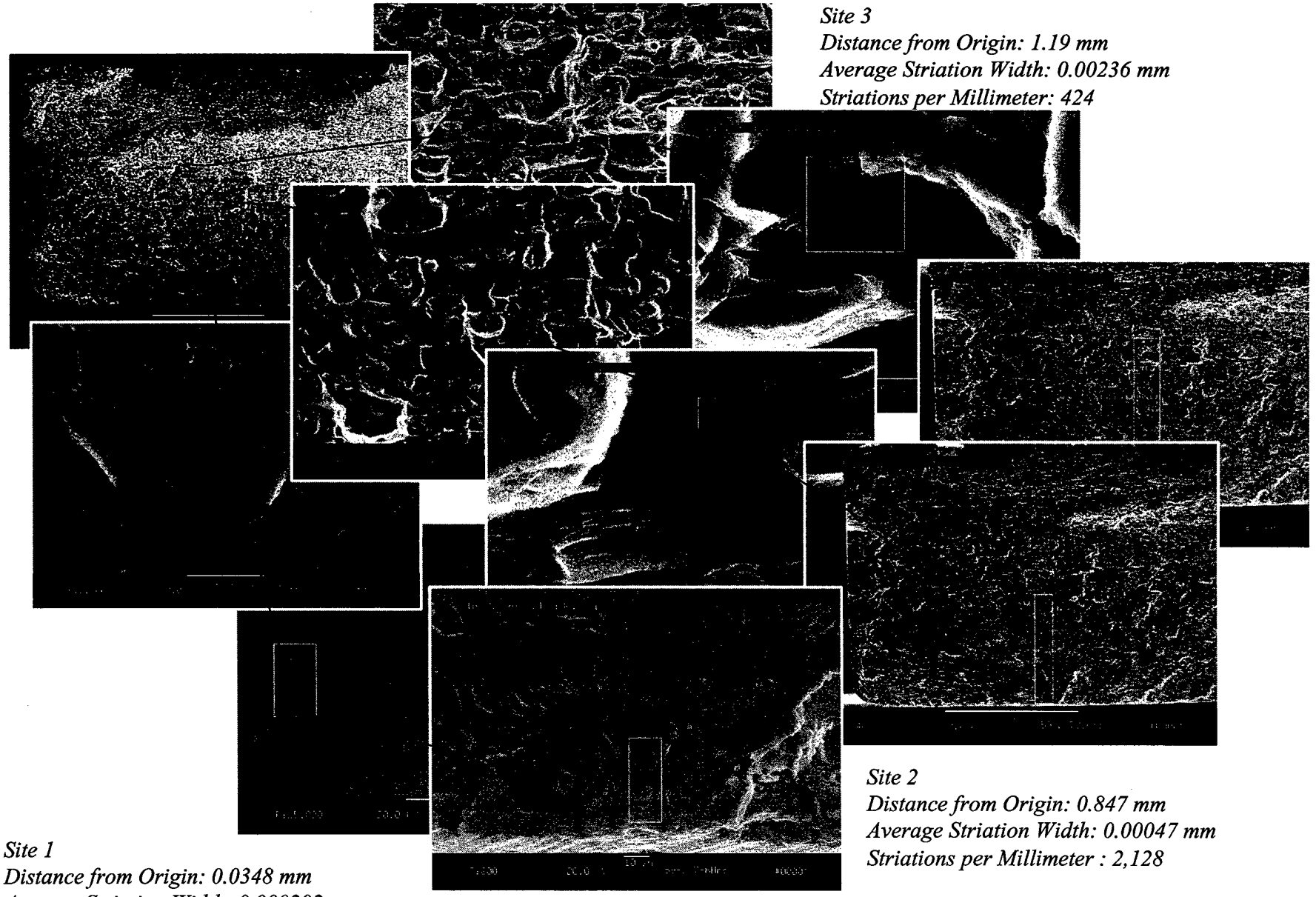

Site 3
Distance from Origin: 1.19 mm
Average Striation Width: 0.00236 mm
Striations per Millimeter: 424

Site 2
Distance from Origin: 0.847 mm
Average Striation Width: 0.00047 mm
Striations per Millimeter : 2,128

Site 1
Distance from Origin: 0.0348 mm
Average Striation Width: 0.000202 mm
Striations per Millimeter: 4,950

Figure A-48. Specimen 59-2

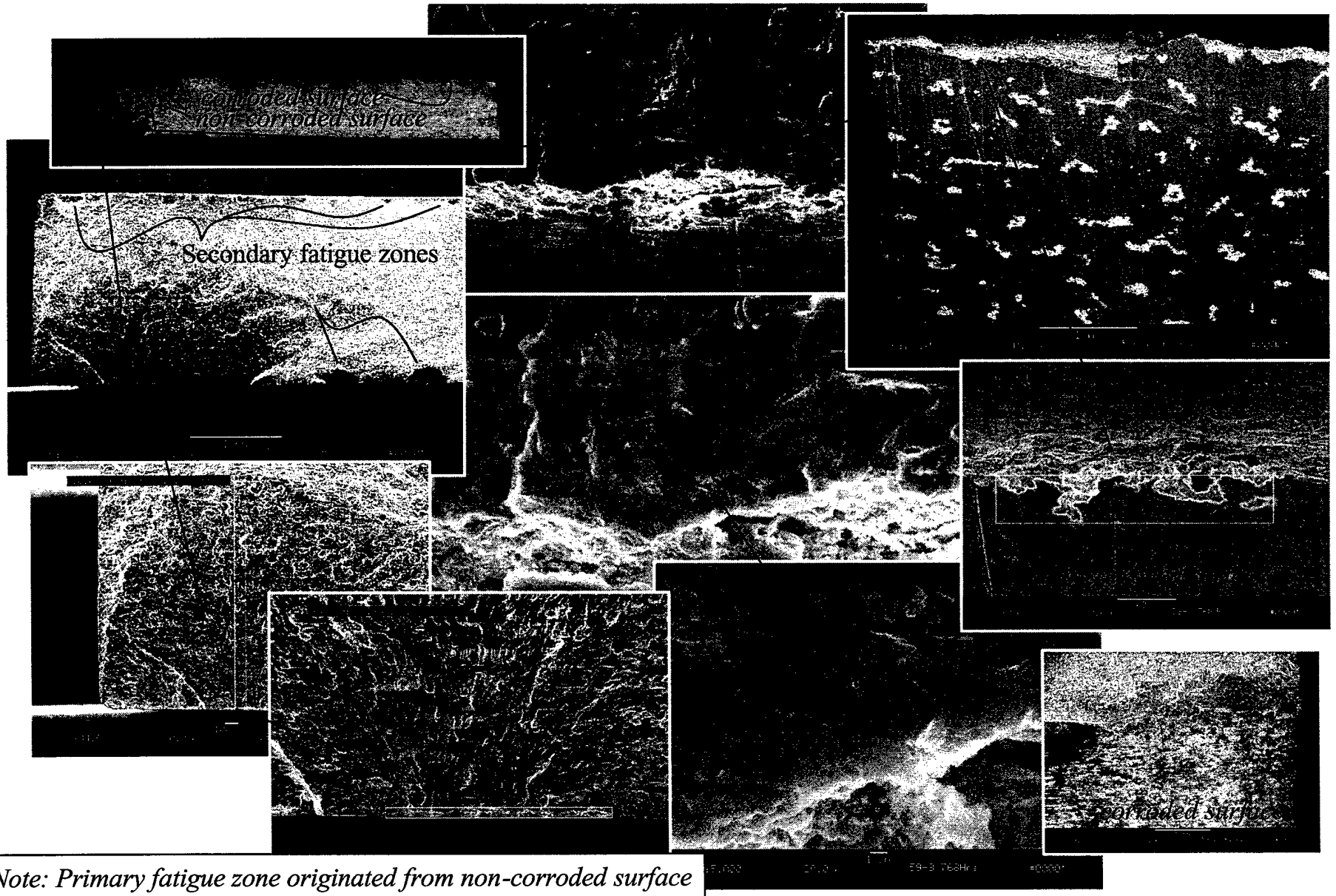

Note: Primary fatigue zone originated from non-corroded surface

Figure A-49. Specimen 59-3

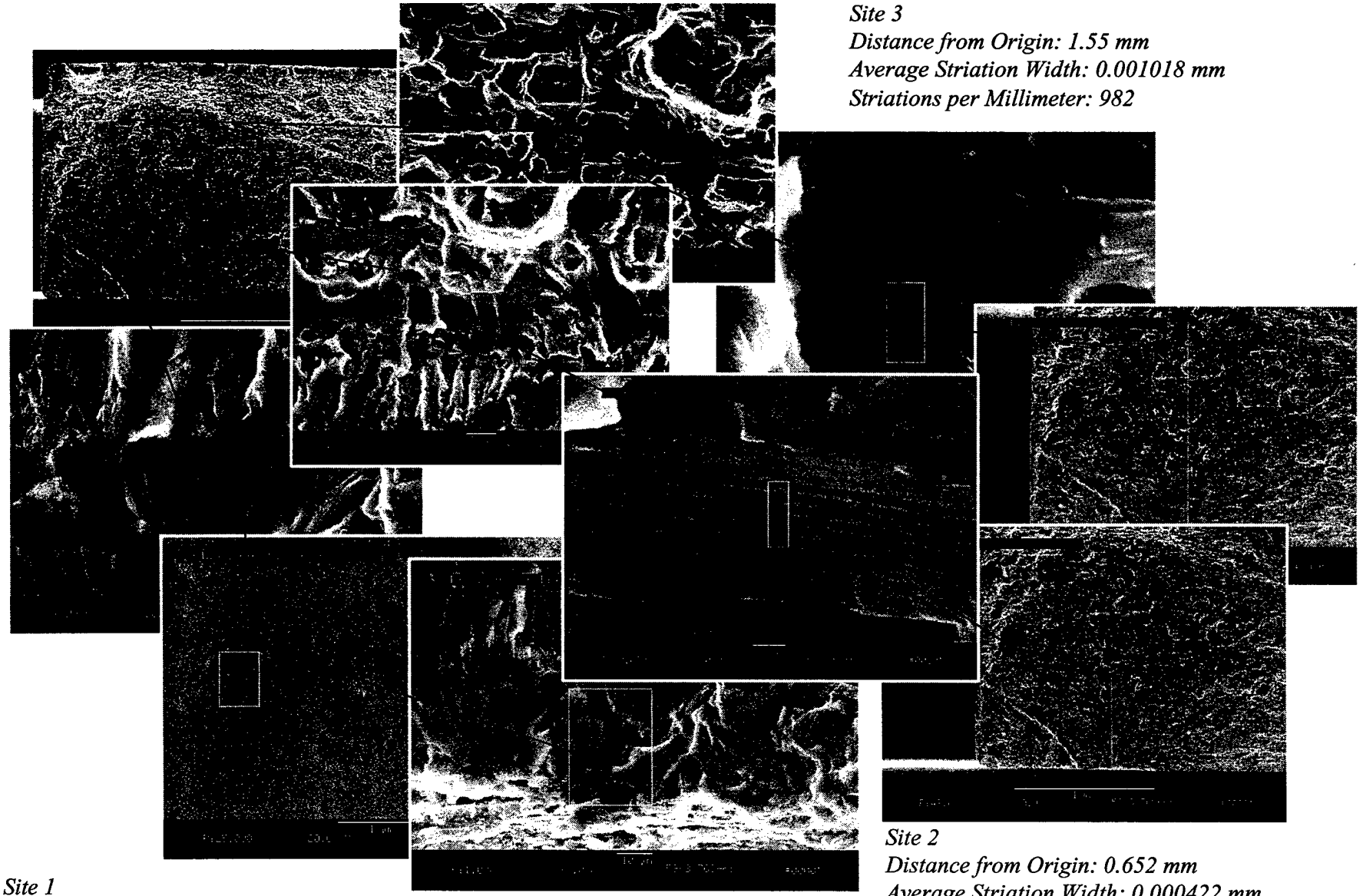

Site 3
Distance from Origin: 1.55 mm
Average Striation Width: 0.001018 mm
Striations per Millimeter: 982

Site 2
Distance from Origin: 0.652 mm
Average Striation Width: 0.000422 mm
Striations per Millimeter : 2,370

Site 1
Distance from Origin: 0.041 mm
Average Striation Width: 0.0001552 mm
Striations per Millimeter: 6,443

Figure A-50. Specimen 59-3

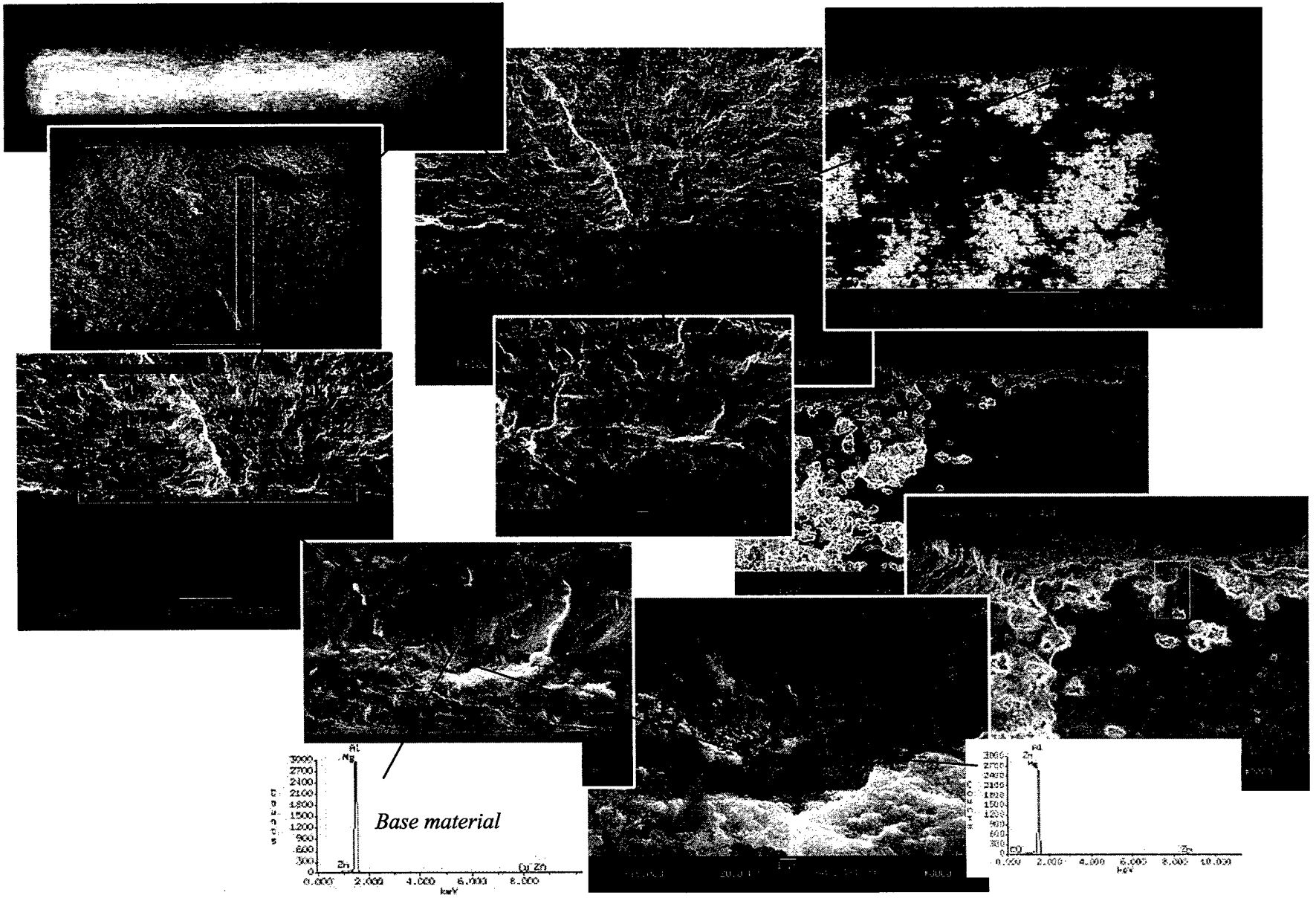

Figure A-51. Specimen 60-1

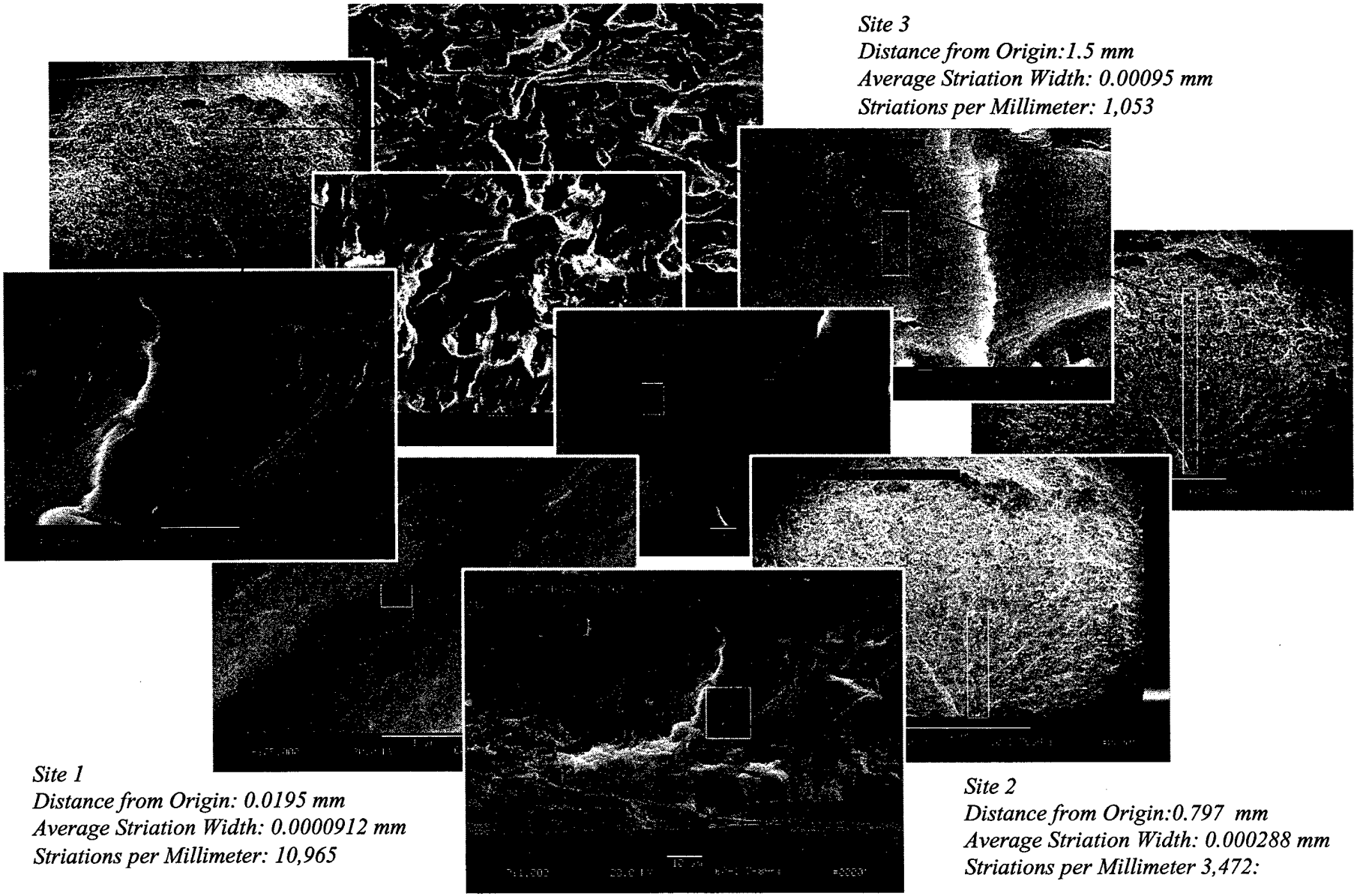

Site 3
Distance from Origin:1.5 mm
Average Striation Width: 0.00095 mm
Striations per Millimeter: 1,053

Site 1
Distance from Origin: 0.0195 mm
Average Striation Width: 0.0000912 mm
Striations per Millimeter: 10,965

Site 2
Distance from Origin:0.797 mm
Average Striation Width: 0.000288 mm
Striations per Millimeter 3,472:

Figure A-52. Specimen 60-1

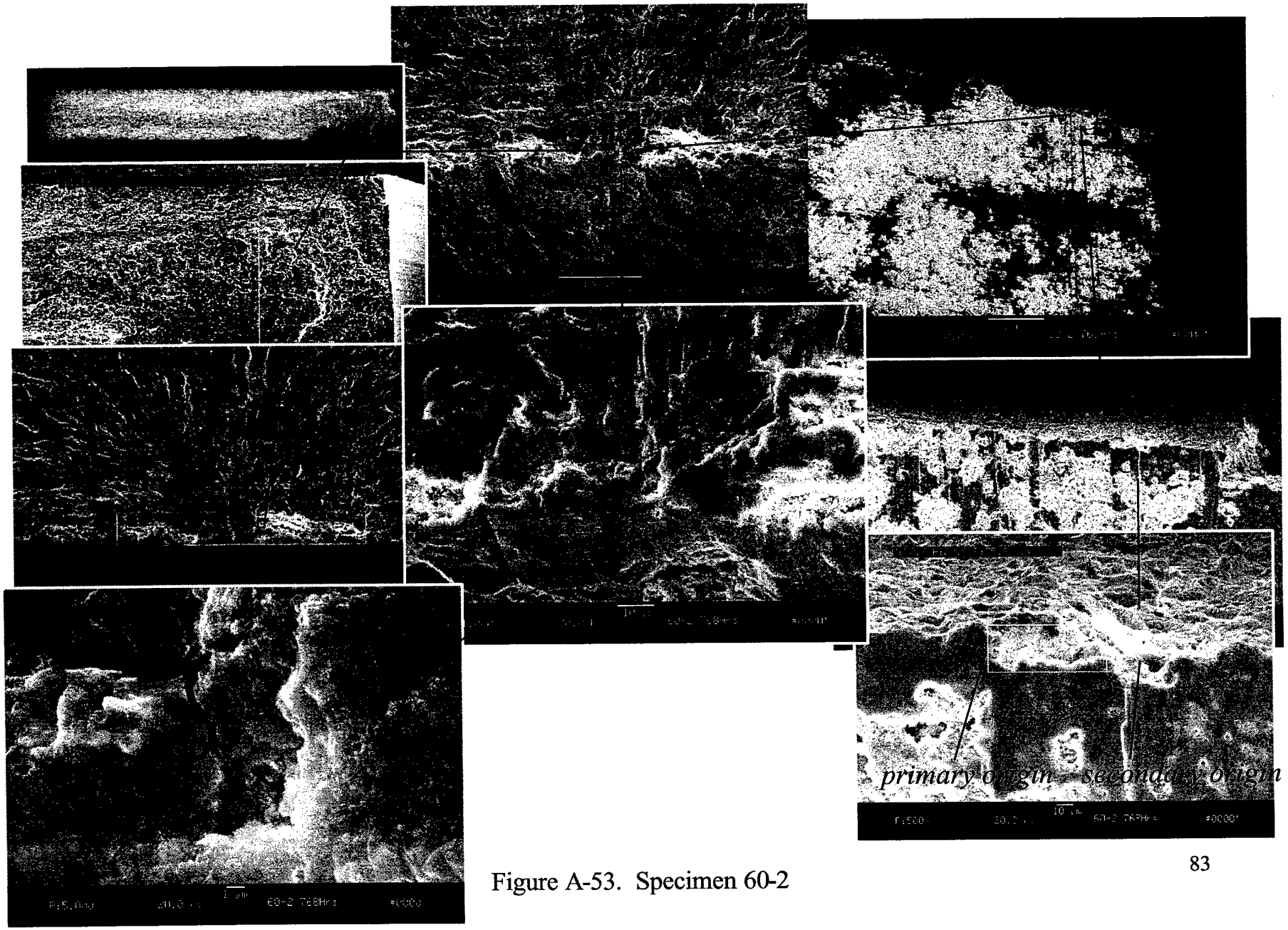

Figure A-53. Specimen 60-2

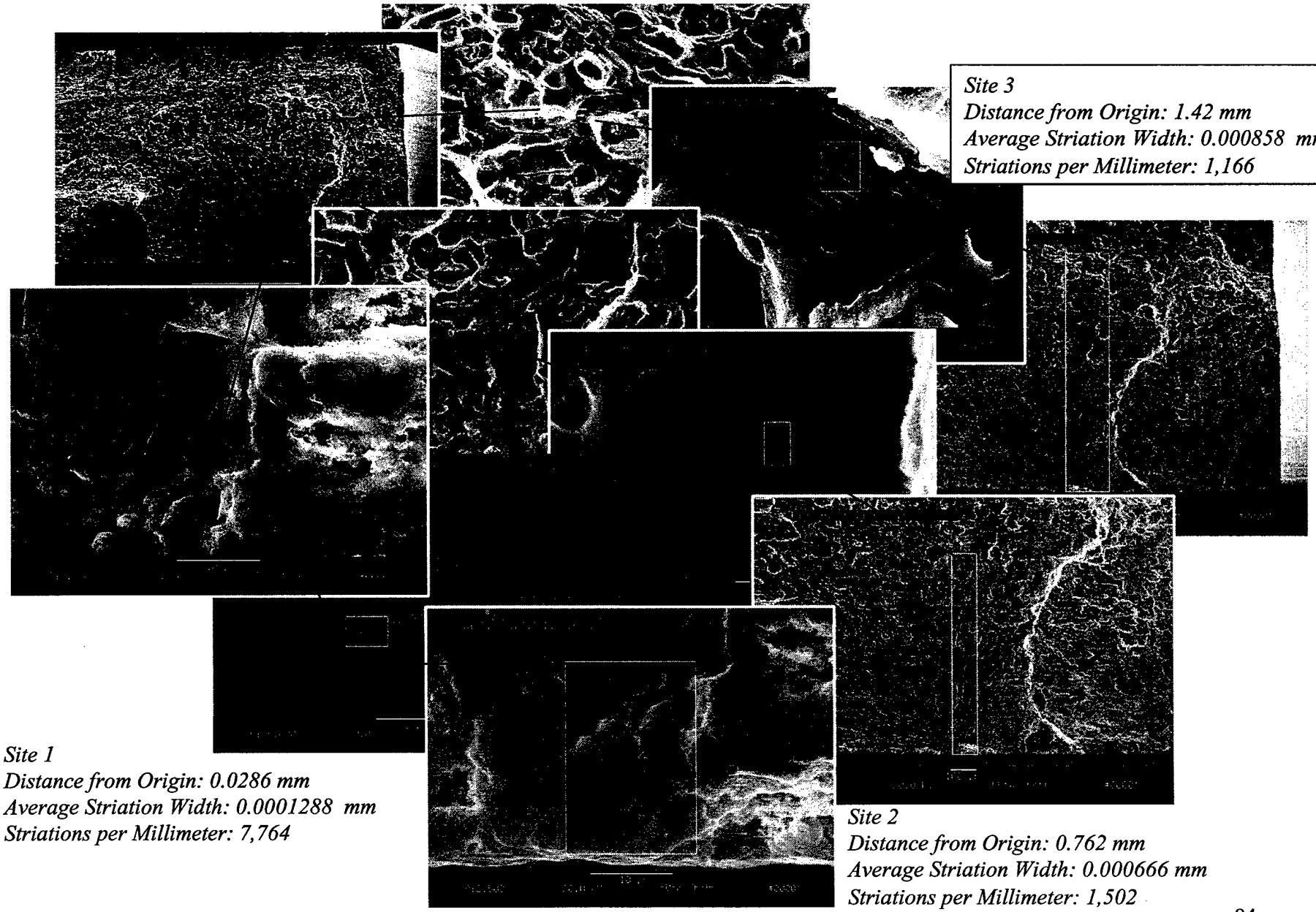

Site 3
Distance from Origin: 1.42 mm
Average Striation Width: 0.000858 mm
Striations per Millimeter: 1,166

Site 1
Distance from Origin: 0.0286 mm
Average Striation Width: 0.0001288 mm
Striations per Millimeter: 7,764

Site 2
Distance from Origin: 0.762 mm
Average Striation Width: 0.000666 mm
Striations per Millimeter: 1,502

Figure A-54. Specimen 60-2

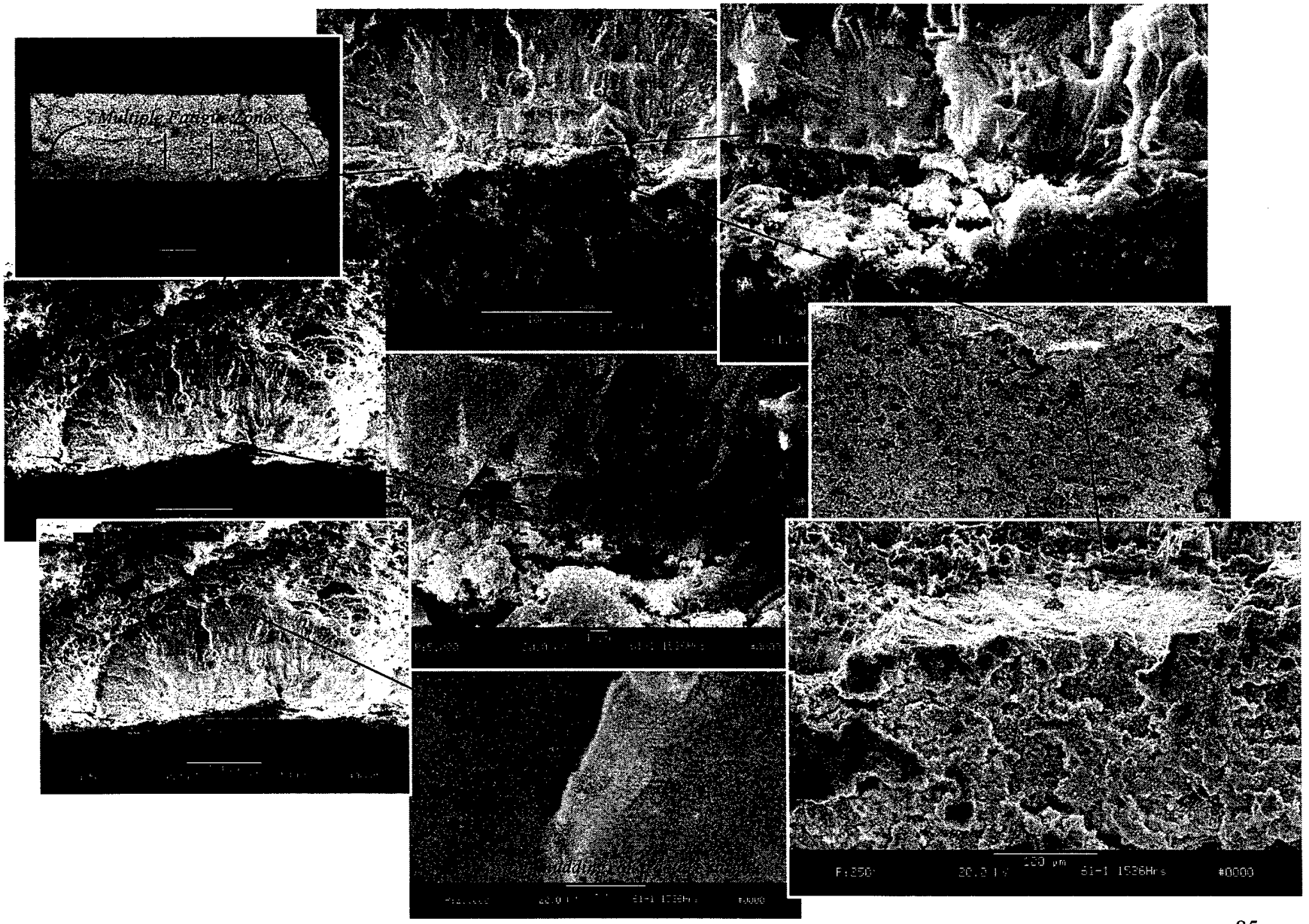

Figure A-55. Specimen 61-1

Very hard to read - much surface corrosion

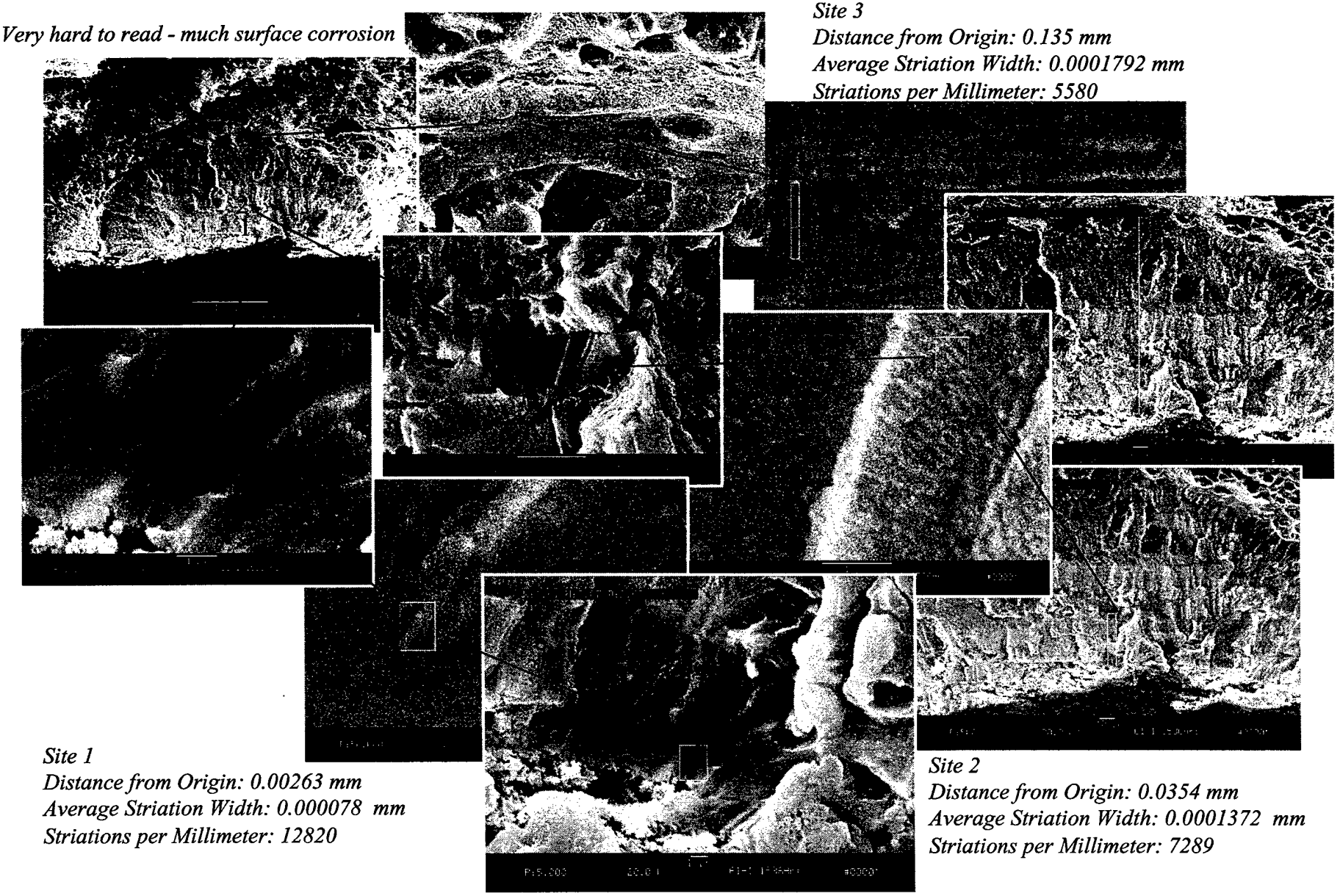

Site 3
Distance from Origin: 0.135 mm
Average Striation Width: 0.0001792 mm
Striations per Millimeter: 5580

Site 1
Distance from Origin: 0.00263 mm
Average Striation Width: 0.000078 mm
Striations per Millimeter: 12820

Site 2
Distance from Origin: 0.0354 mm
Average Striation Width: 0.0001372 mm
Striations per Millimeter: 7289

Figure A-56. Specimen 61-1

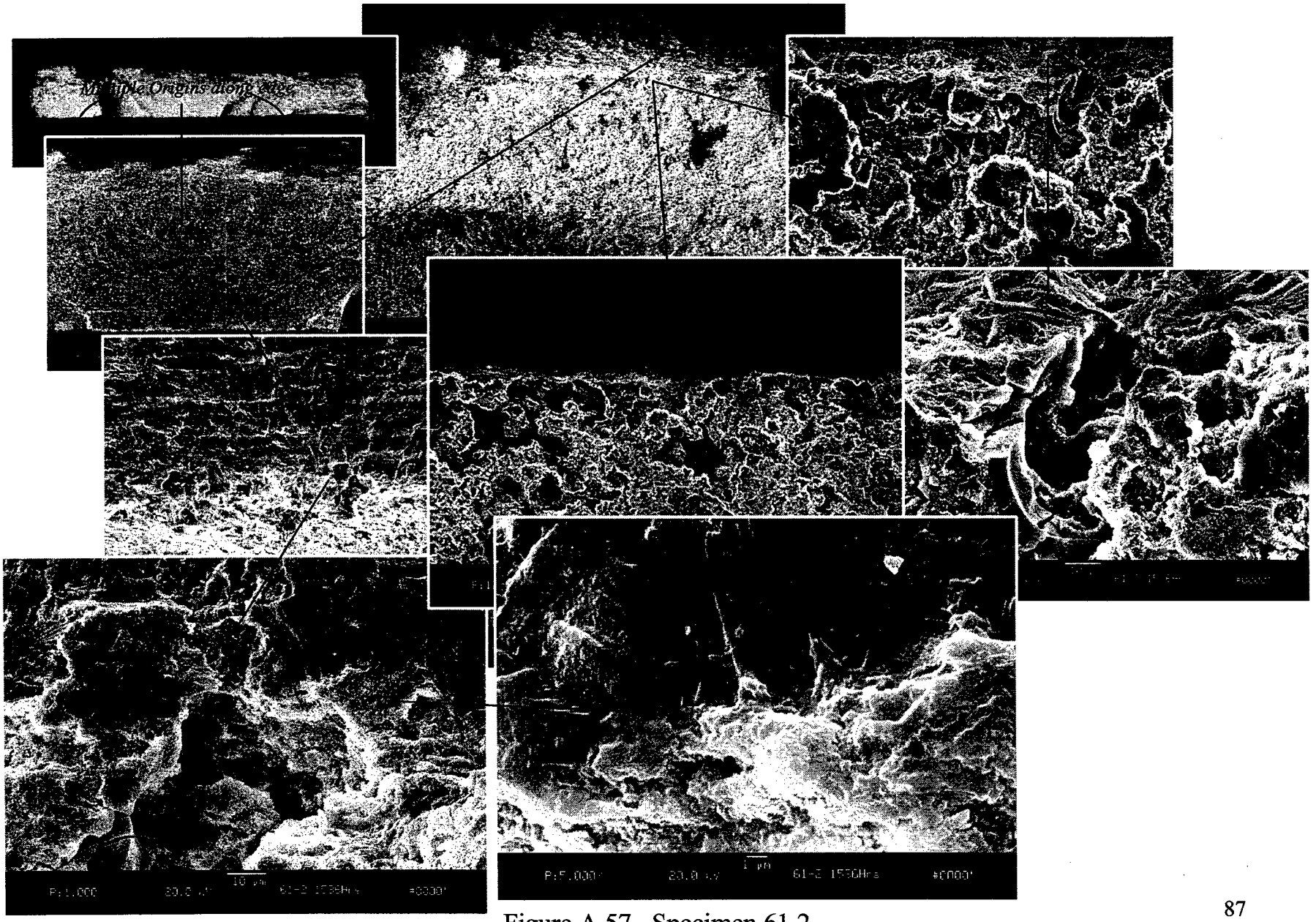

Figure A-57. Specimen 61-2

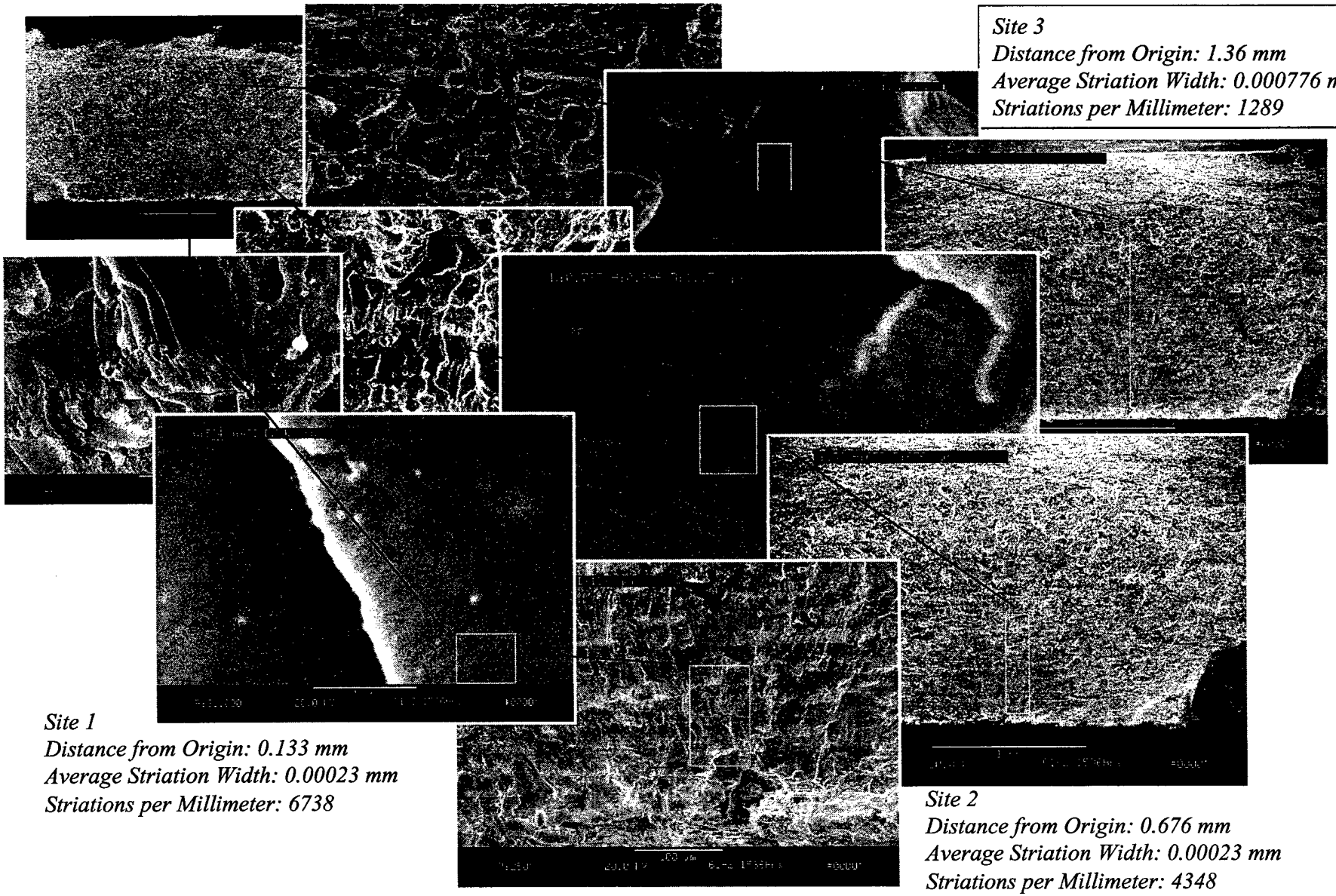

Site 3
Distance from Origin: 1.36 mm
Average Striation Width: 0.000776 mm
Striations per Millimeter: 1289

Site 1
Distance from Origin: 0.133 mm
Average Striation Width: 0.00023 mm
Striations per Millimeter: 6738

Site 2
Distance from Origin: 0.676 mm
Average Striation Width: 0.00023 mm
Striations per Millimeter: 4348

Figure A-58. Specimen 61-2

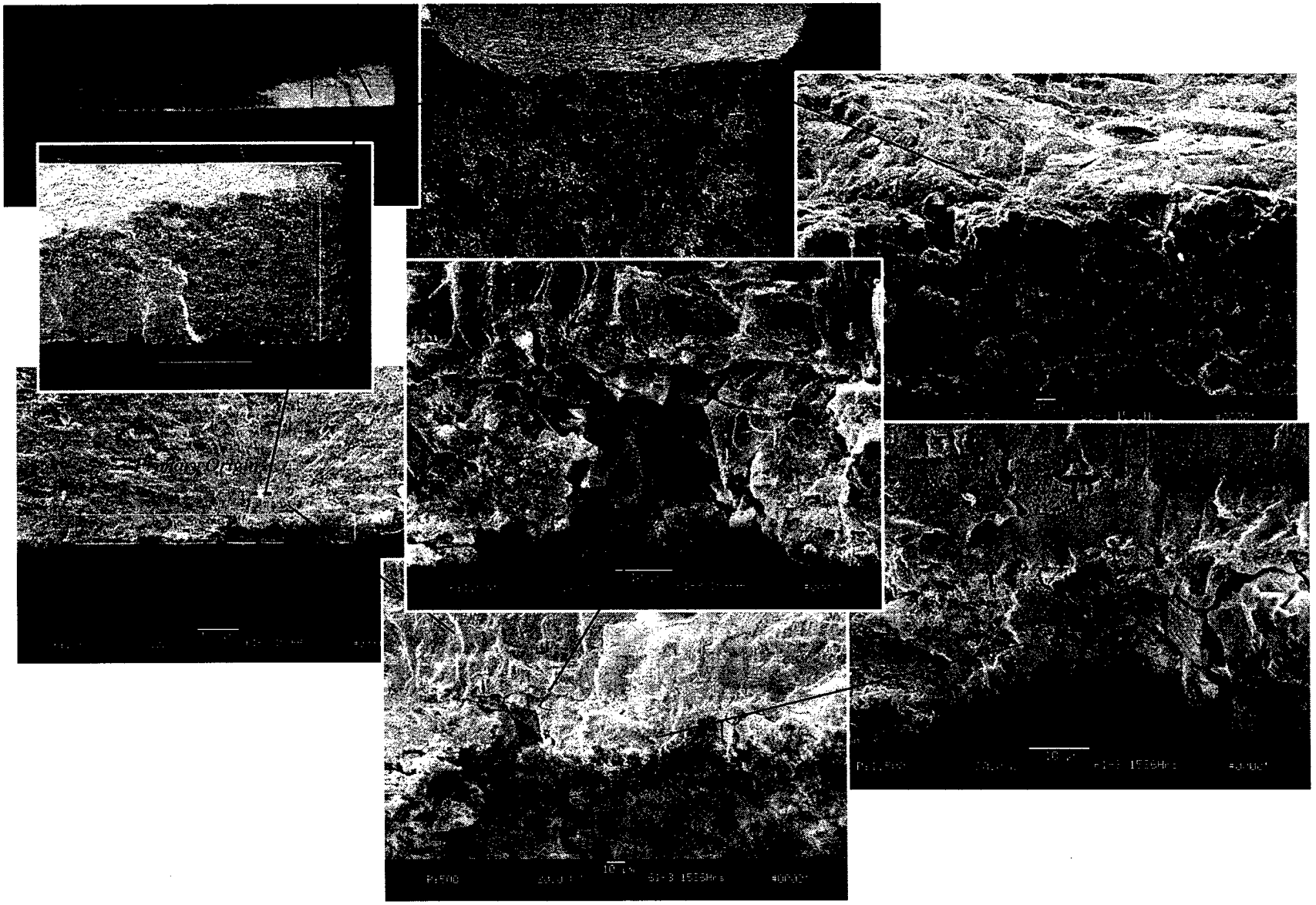

Figure A-59. Specimen 61-3

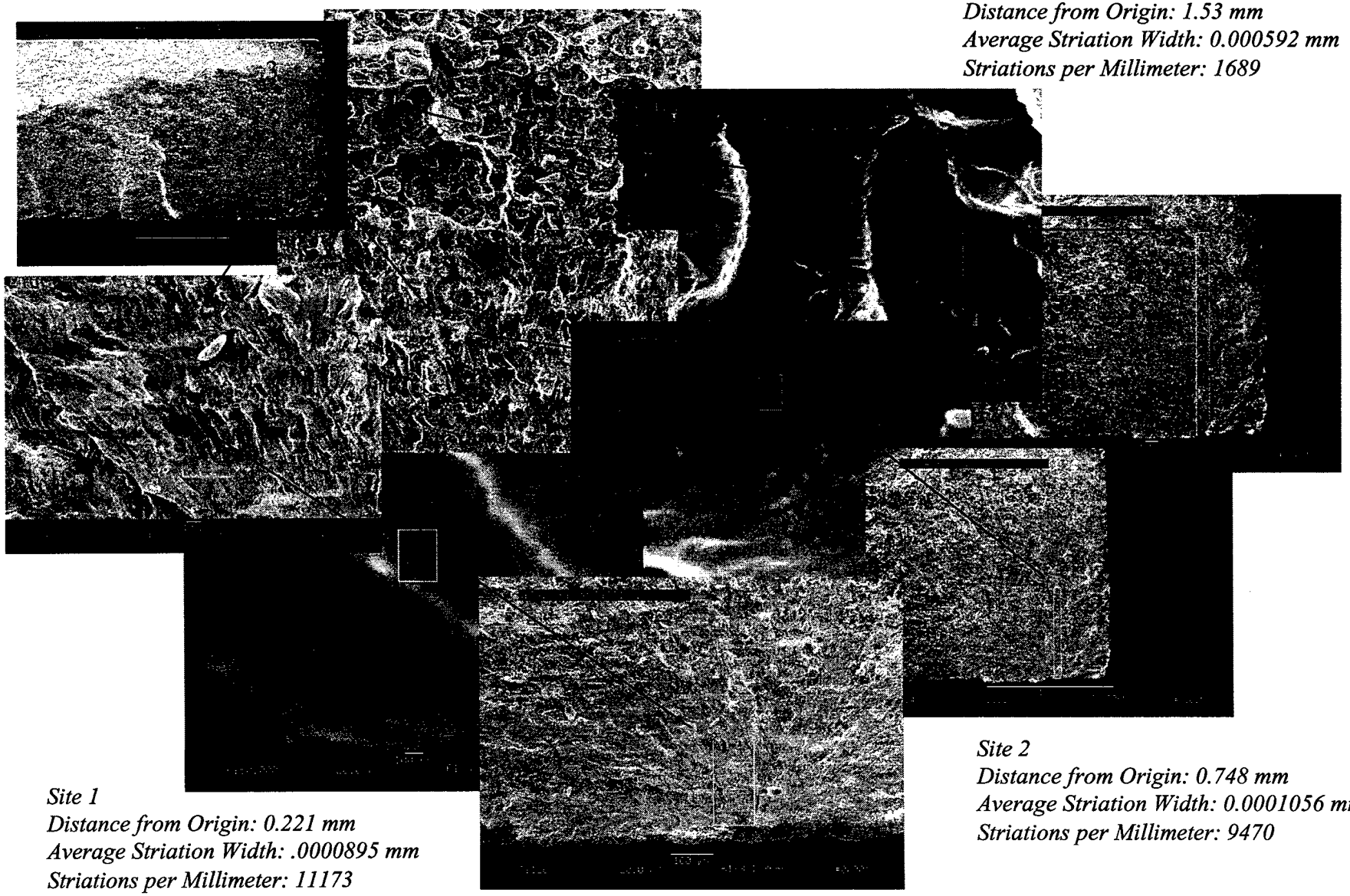

Site 3
Distance from Origin: 1.53 mm
Average Striation Width: 0.000592 mm
Striations per Millimeter: 1689

Site 1
Distance from Origin: 0.221 mm
Average Striation Width: .0000895 mm
Striations per Millimeter: 11173

Site 2
Distance from Origin: 0.748 mm
Average Striation Width: 0.0001056 mm
Striations per Millimeter: 9470

Figure A-60. Specimen 61-3

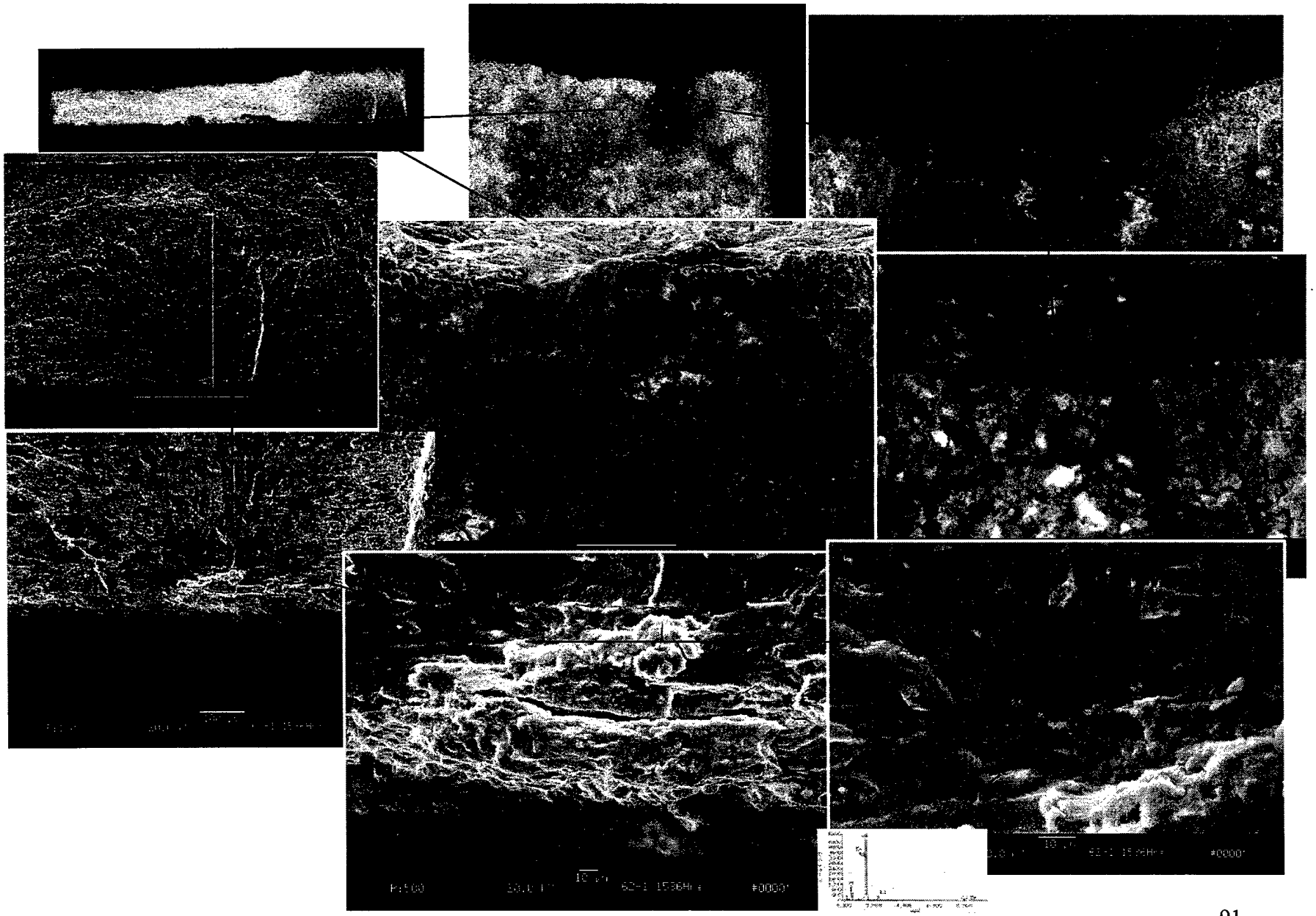

Figure A-61. Specimen 62-1

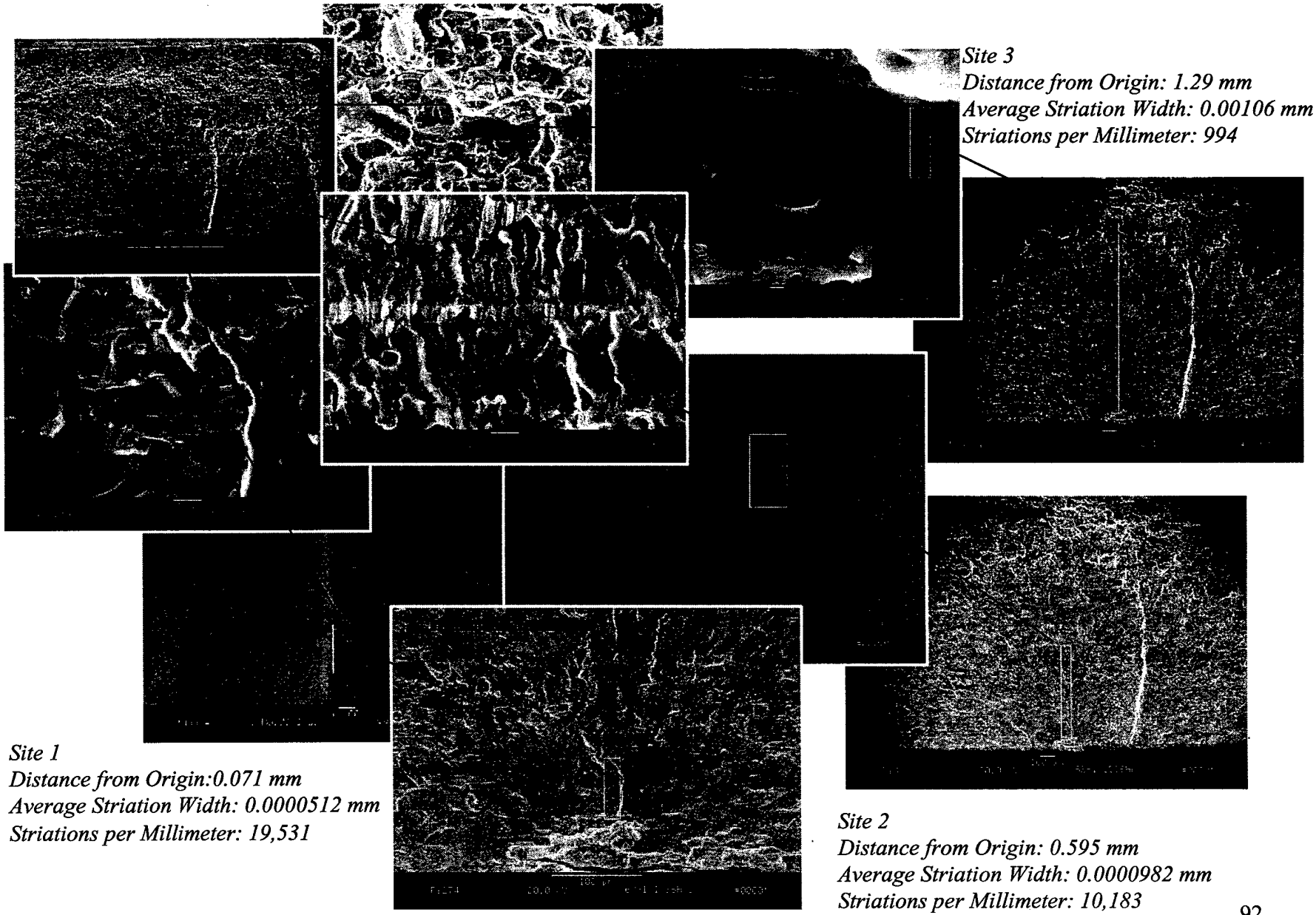

Site 3
Distance from Origin: 1.29 mm
Average Striation Width: 0.00106 mm
Striations per Millimeter: 994

Site 1
Distance from Origin:0.071 mm
Average Striation Width: 0.0000512 mm
Striations per Millimeter: 19,531

Site 2
Distance from Origin: 0.595 mm
Average Striation Width: 0.0000982 mm
Striations per Millimeter: 10,183

Figure A-62. Specimen 62-1

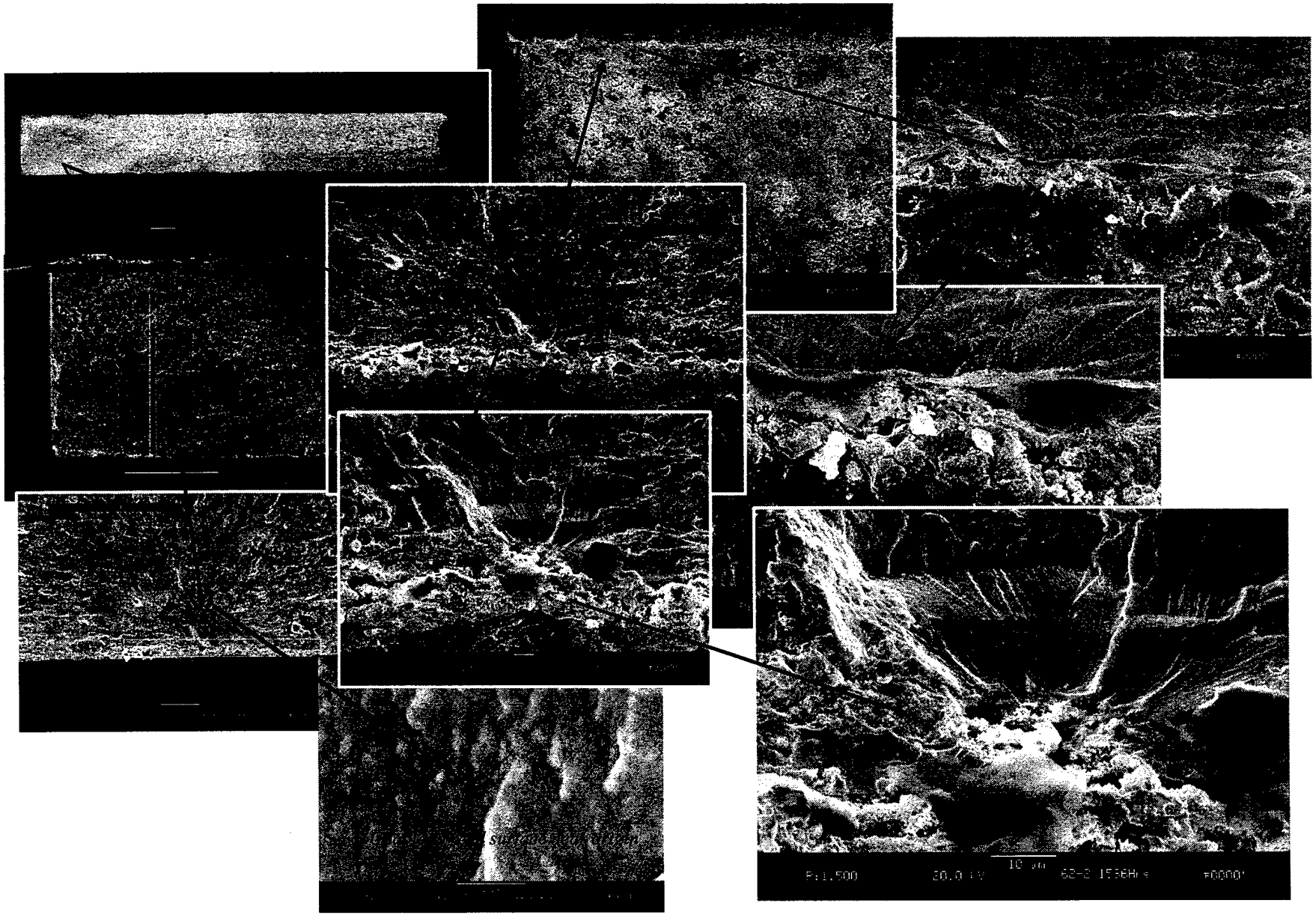

Figure A-63. Specimen 62-2

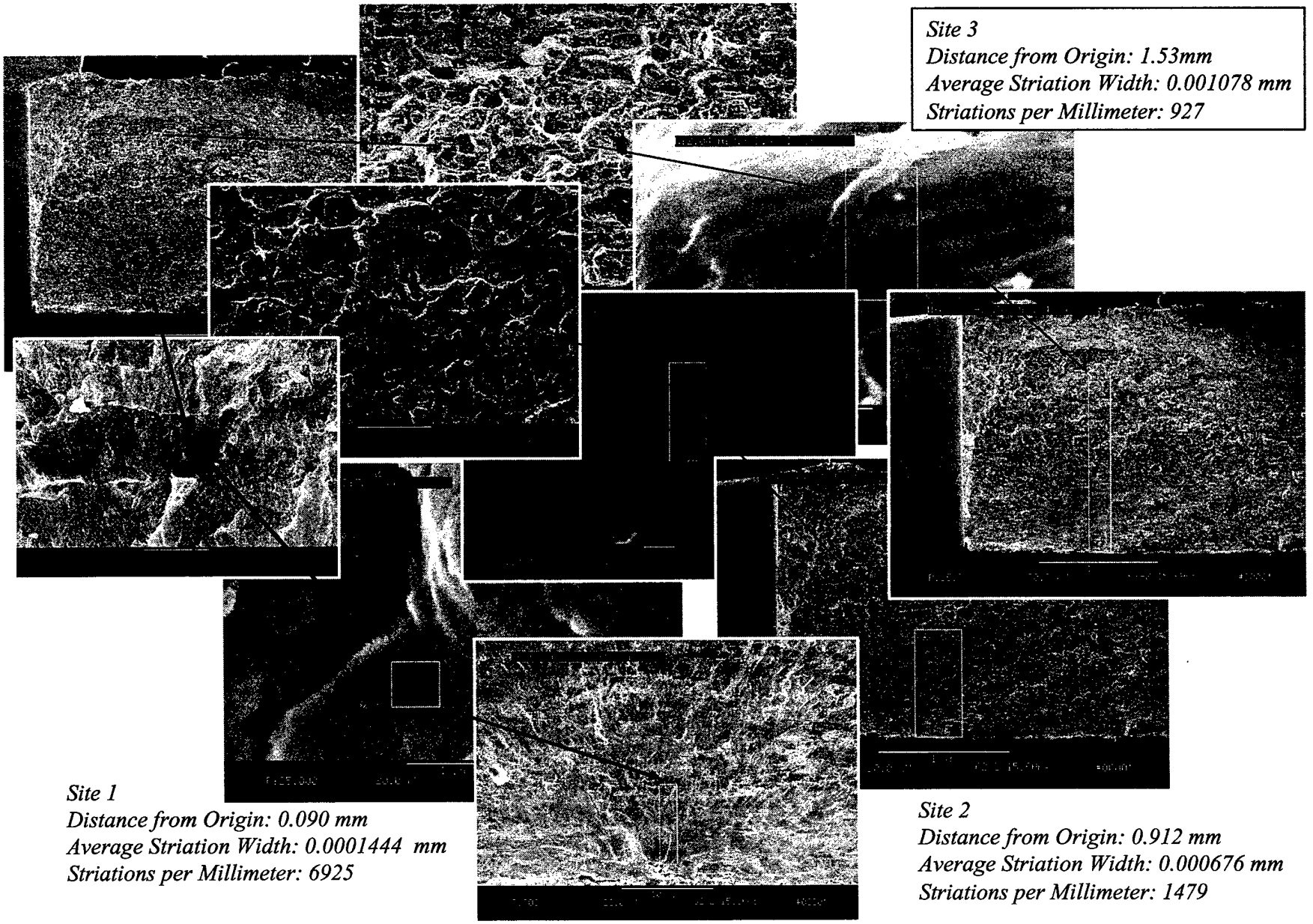

Site 3
Distance from Origin: 1.53mm
Average Striation Width: 0.001078 mm
Striations per Millimeter: 927

Site 1
Distance from Origin: 0.090 mm
Average Striation Width: 0.0001444 mm
Striations per Millimeter: 6925

Site 2
Distance from Origin: 0.912 mm
Average Striation Width: 0.000676 mm
Striations per Millimeter: 1479

Figure A-64. Specimen 62-2

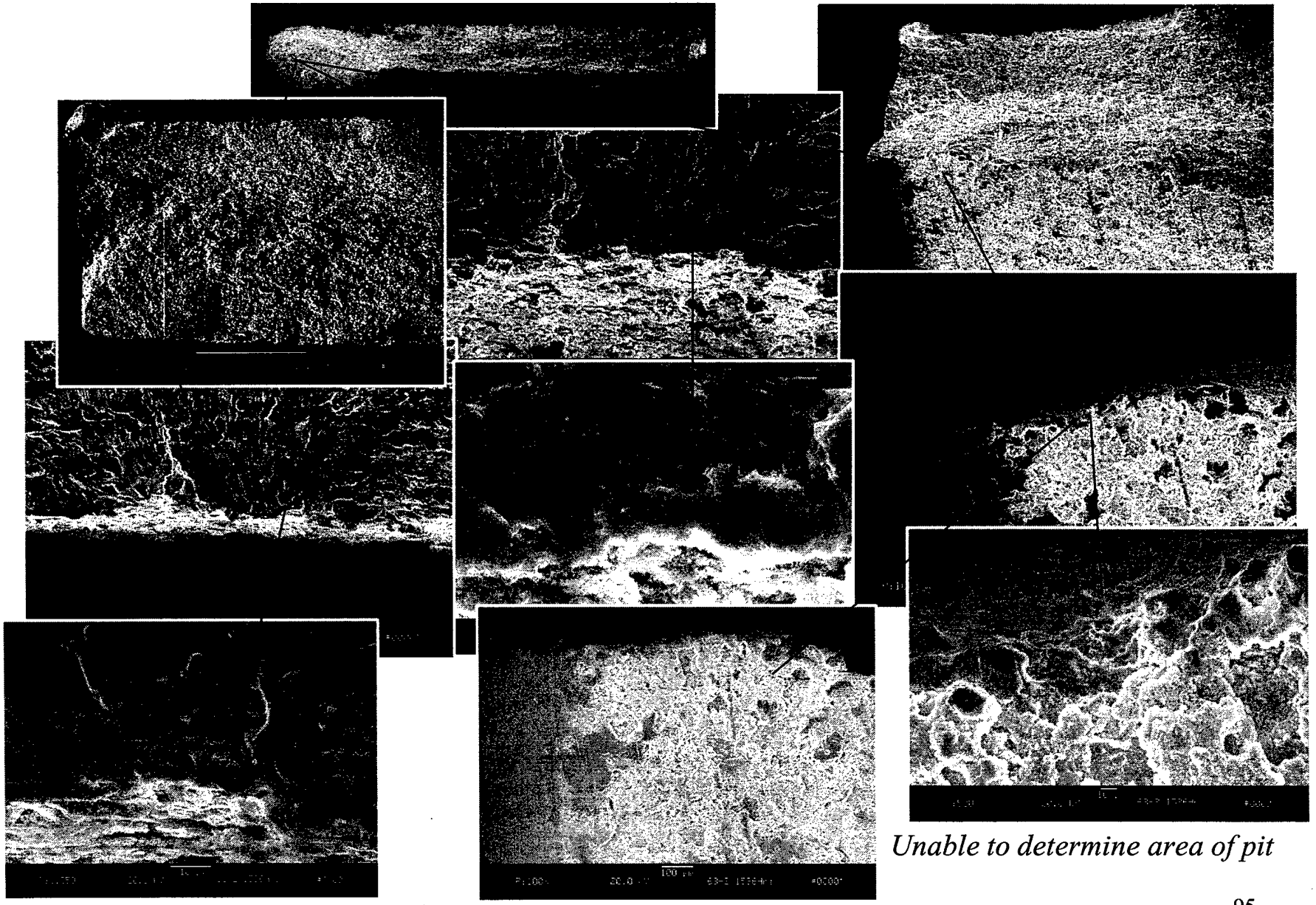

Unable to determine area of pit

Figure A-65. Specimen 63-2

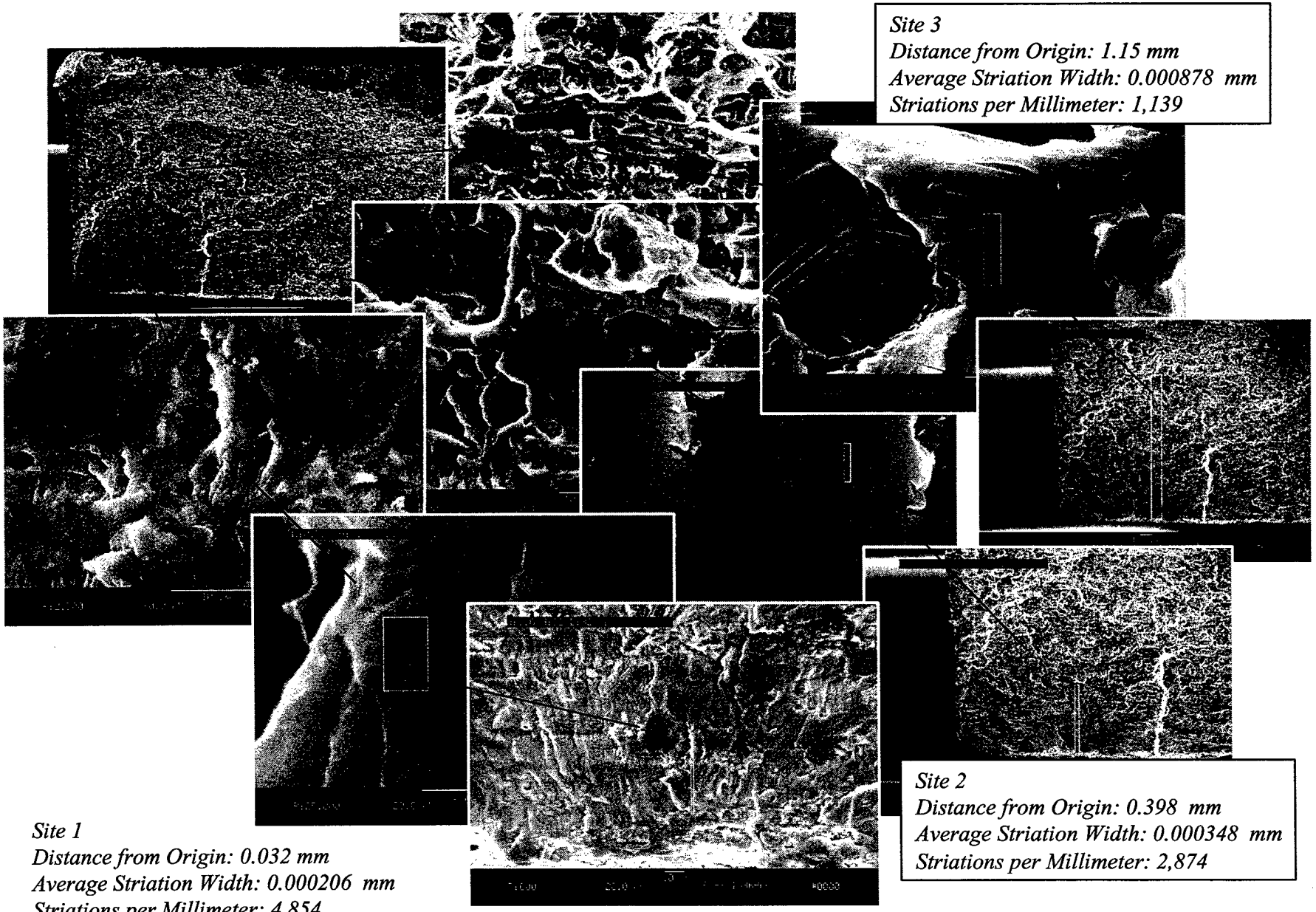

Site 3
Distance from Origin: 1.15 mm
Average Striation Width: 0.000878 mm
Striations per Millimeter: 1,139

Site 1
Distance from Origin: 0.032 mm
Average Striation Width: 0.000206 mm
Striations per Millimeter: 4,854

Site 2
Distance from Origin: 0.398 mm
Average Striation Width: 0.000348 mm
Striations per Millimeter: 2,874

Figure A-66. Specimen 63-2

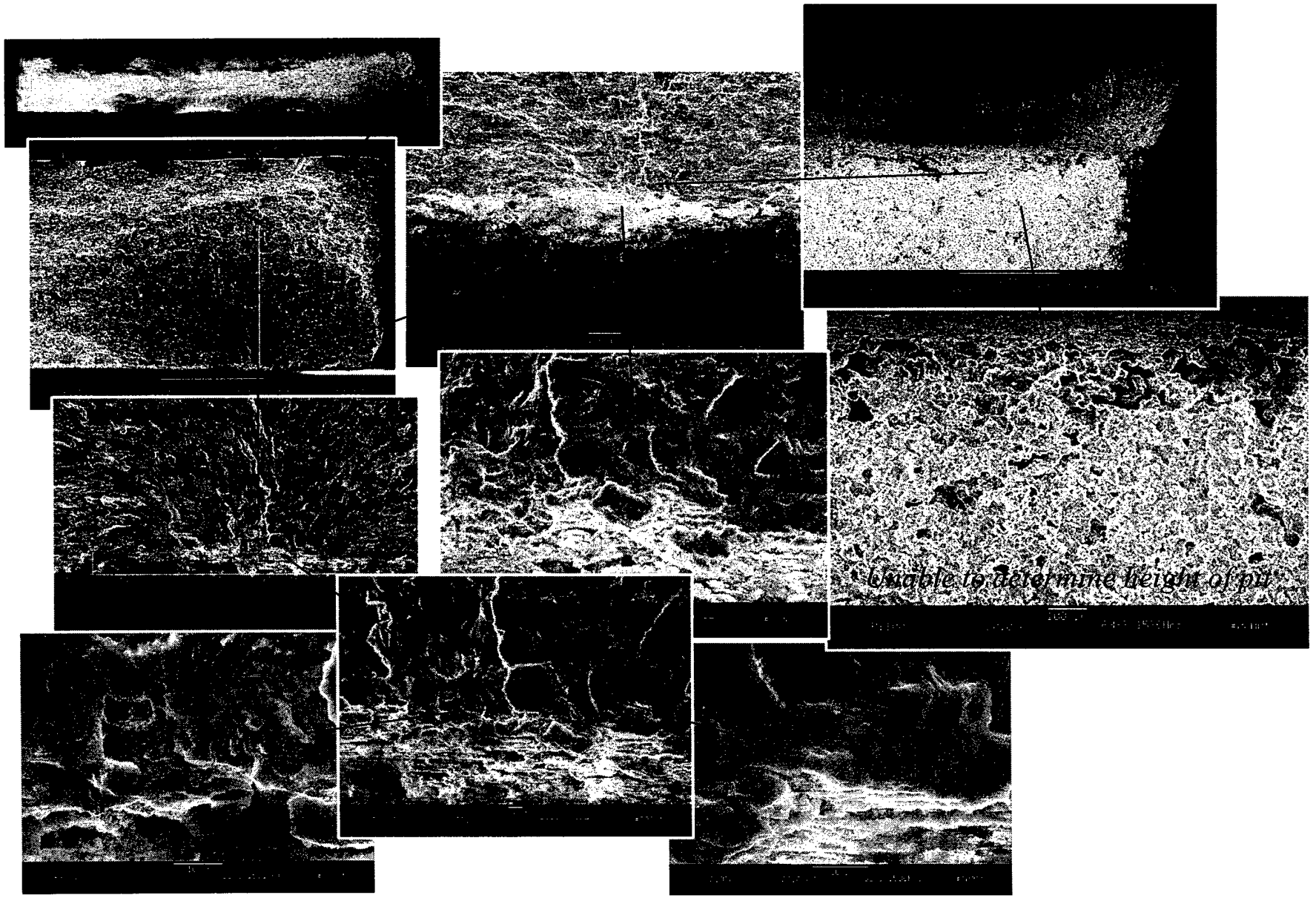

Figure A-67. Specimen 63-3

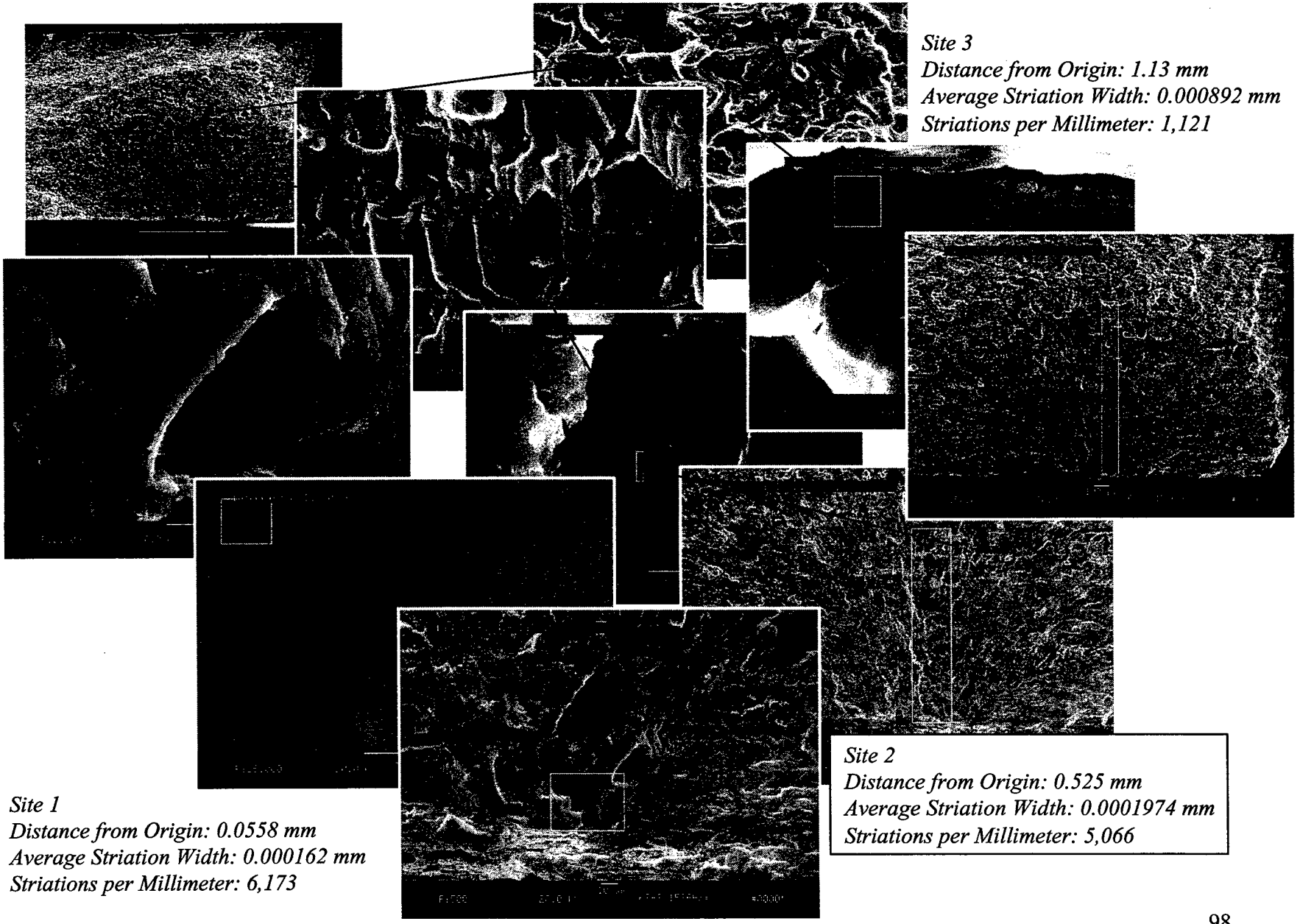

Site 3
Distance from Origin: 1.13 mm
Average Striation Width: 0.000892 mm
Striations per Millimeter: 1,121

Site 2
Distance from Origin: 0.525 mm
Average Striation Width: 0.0001974 mm
Striations per Millimeter: 5,066

Site 1
Distance from Origin: 0.0558 mm
Average Striation Width: 0.000162 mm
Striations per Millimeter: 6,173

Figure A-68. Specimen 63-3